



begutachtet durch

---

Prof. Dr. Gerhard Kahl

## DIPLOMARBEIT

---

# Thermodynamic properties of particles with heterogeneously patterned surfaces

---

Ausgeführt am Institut für Theoretische Physik  
der Technischen Universität Wien

unter der Anleitung von

Prof. Dr. Gerhard Kahl

Dr. Emanuela Bianchi

durch

Monika Stipsitz

Matrikelnummer: 0926973  
Kirchenweg 25, 3423 St. Andrä-Wördern

WIEN, May 7, 2015

---

Monika Stipsitz

## Zusammenfassung

Im Rahmen dieser Diplomarbeit wurden Kristalle aus sogenannten „patchy particles“ untersucht. Diese Bezeichnung stellt einen Sammelbegriff für Teilchen mit einer heterogenen Oberflächenbeschaffenheit dar; hier wechselwirken bestimmte Regionen der Oberfläche anders als andere Regionen. Wir untersuchen zwei Arten von „patchy particles“: einerseits Janus Teilchen, bei denen der Großteil der Oberfläche nicht wechselwirkend ist, während der Rest der Oberfläche, die „patches“, aufeinander anziehend wirken. Andererseits sogenannte „inverse patchy colloids“, die aus negativ geladenen Kolloiden und darauf adsorbierten positiv geladenen Regionen bestehen.

Durch diese stark anisotrope Wechselwirkung der Teilchen kann eine Vielzahl an interessanten Kristallen entstehen. Daher werden Partikel als mögliche Bausteine von neuartigen funktionalen Materialien gehandelt: durch die richtige Wahl der äußeren Bedingungen soll das Entstehen einer erwünschten Struktur möglich werden.

In dieser Arbeit wird der Einfluss von äußeren thermodynamischen Parametern (Druck, Temperatur, etc.) auf die bevorzugte kristalline Struktur eines Systems anisotroper Teilchen untersucht. Dafür wurde eine kürzlich entwickelte Methode verallgemeinert und auf eine Vielzahl an zwei- und drei-dimensionalen Strukturen angewandt. Dieses Konzept beruht auf einem störungstheoretischen Ansatz für die Wechselwirkung bei dem jedes Teilchen durch ein harmonisches Potential („Feder“) an seine Ruheposition gebunden ist. Da nicht nur die Positionen sondern auch die Orientierungen der Teilchen die Energie beeinflussen, enthält das Modell neben einer Federkraft, die die Translation der Teilchen beeinflusst auch eine harmonische Kraft zur Regulierung der Rotation der Teilchen in Bezug auf ihre Gleichgewichtsorientierung.

Mit Hilfe dieser Methode lassen sich relativ einfach und vor allem mit weniger Rechenaufwand als bei sonst üblichen Methoden die thermodynamischen Eigenschaften des Systems berechnen. Durch Vergleich der freien Energie und des Drucks für verschiedene Kristalle und bei verschiedenen Temperaturen können die bevorzugt angenommene Struktur und mögliche meta-stabile Morphologien bestimmt werden.

## Abstract

In this thesis we investigate structures formed by patchy particles using an extended version of the so-called self-consistent phonon (SCP) approach. Patchy particles are particles with a heterogeneous surface which show a highly anisotropic interaction and thus form a large number of interesting structures. They are considered as possible building entities for functional materials, which are expected to self-assemble into desired target structures controlled solely by an appropriate choice of the ambient parameters.

One step towards functional material is to know how a system of patchy particles will behave under changing external conditions (temperature, pressure, etc.). In this thesis we study this dependence by extending the SCP method and applying it to various two- and three- dimensional structures formed by ordered or randomly oriented particles at a wide range of temperatures and densities. Two different types of patchy particles are investigated: Janus particles where only a small portion of the surface is attractive while the other part is inert and inverse patchy particles which consist of a negatively charged colloid that adsorbed a number of positively charged patches.

The SCP method is based on a perturbation theory for the interactions; the particles of a candidate structure are linked to their equilibrium position via harmonic potentials ('springs'). Since the energy of a system of patchy particles depends strongly on the orientation of the particles, not only a spring constraining the translation of the particles but also a spring regulating the rotation around the equilibrium orientation is included.

The free energy and the pressure of the system follow from the thermodynamic integration of the interaction energy resulting from the translational and orientational deviations from the equilibrium state. Comparing these two values for different structures at different temperatures, the preferred crystal structure of a system and possible meta-stable structures can be determined.

# Contents

<b>1</b>	<b>Introduction</b>	<b>5</b>
<b>2</b>	<b>Models for patchy particles</b>	<b>7</b>
2.1	Janus particles . . . . .	7
2.2	Inverse patchy colloids . . . . .	8
<b>3</b>	<b>Self-consistent Phonon Approach (SCP) for orientationally dependent colloids</b>	<b>12</b>
<b>4</b>	<b>SCP for Janus particles in two dimensions</b>	<b>16</b>
4.1	Theory . . . . .	16
4.2	Results . . . . .	18
4.2.1	Zigzag structure . . . . .	20
4.2.2	Trimer structure . . . . .	27
4.3	Plastic crystals . . . . .	32
4.4	Phase diagram for two dimensional Janus crystals . . . . .	35
<b>5</b>	<b>SCP for inverse patchy colloids in two dimensions</b>	<b>37</b>
5.1	Ordered crystals . . . . .	37
5.2	Plastic crystals . . . . .	38
5.3	Results . . . . .	39
<b>6</b>	<b>SCP for inverse patchy colloids in three dimensions</b>	<b>52</b>
6.1	Plastic structure . . . . .	53
6.1.1	Results for fcc structure . . . . .	54
6.2	Angular SCP . . . . .	56
6.2.1	Fcc structure . . . . .	58
6.2.2	Layered structure . . . . .	63
<b>7</b>	<b>Conclusion</b>	<b>67</b>

# 1 Introduction

Patchy particles are mesoscopic particles ( $nm$  to  $\mu m$  large) usually dispersed in a microscopic solvent. They have a heterogeneous surface coverage, which leads to a strongly anisotropic interaction between the particles. The large interest in this kind of particles is due to the large number of structures into which the particles self-assemble.

Due to the rich phase behavior patchy particles attract attention as promising building blocks for functional materials. It is hoped that via modifying the external conditions (pressure, temperature, salinity, etc.) it can become possible to control the self-assembly of those particles and to produce desired structures without further intervention. Therefore it should be possible to construct structures on a much smaller scale than with conventional building methods. Possible fields of application of functional materials include among others drug delivery and photovoltaics.

For computer simulations models for the patchy particles are introduced to simplify the occurring interactions as much as possible while still keeping the rich self-assembly behavior. In this thesis, two different models are investigated; Janus particles and so-called inverse patchy colloids (IPCs).

The former are hard-sphere particles where only a portion of the surface is attractive while the rest of the surface is inert. Thus Janus particles have a quite simple potential which is a combination of a hard sphere and square-well potential with a simple step-like angular dependence. The interaction of IPCs are more complicated: they are hard-sphere particles where most of the surface is negatively charged. The rest of the surface is covered by positively charged patches.

Advances in the experimental methods already allow the synthesis of larger amounts of patchy particles with different properties. One of the most promising methods is the glancing-angle deposition technique [1], where the particles are arranged in a close-packed mono-layer. By deposition of gold vapor on to one hemisphere, Janus particles are created. The extension of the patch is controlled by the angle of incidence of the vapor beam. A similar method can be used for the formation of IPCs; where a number of positively charged patches are deposited on a negatively charged colloid while dispersed in a solution [2]. The extension of the patches can be controlled via the amount of salt in the solution.

Simultaneously to the experimental progress, techniques for the simulation of various kinds of patchy particles have evolved. The most straight-forward method to investigate the phase diagram of a given type of particle is through a Monte Carlo Simulation, where the trajectories of a large number of particles is investigated, until the system eventually reaches its equilibrium. Such a simulation has to be performed for each state point separately [3] which renders investigations rather expensive. Using Monte Carlo simulations methods exist that allow an accurate determination of the phase coexistence.

In this thesis, a different method to calculate the phase diagram is applied that might be computationally less involved than simulations. It is based on the Self-consistent phonon approach (SCP) as introduced by Fixman et al. in Ref. [4] for hard spheres and has been extended by Schweizer et al. for Janus particles [5]. In this approach it is assumed that the particles are linked to their equilibrium positions by harmonic potentials ('springs'). Since the interaction of the particles studied here is strongly direction dependent, not only their positions but also their rotations around their equilibrium orientations are constrained via a spring. Thus the free energy of a given system can be calculated by evaluating the energy of these oscillations in the given potential via a reference potential that is self-consistently mapped to the interaction potential.

For the approach ordered candidate structures are needed; we focus on structures which were already investigated in the literature [5, 6, 7]. Using the SCP approach the thermodynamic properties of various two- and three-dimensional structures formed by Janus particles and IPCs are

investigated. We obtain the free-energy and the pressure for the different structures for a wide range of temperatures and densities. Thus, where applicable, phase diagrams are constructed to identify the stable and meta-stable structures. Additionally, the oscillation frequencies corresponding to the harmonically constrained oscillations around the equilibrium position and orientation are obtained.

This thesis is organized in the following way: In Sec. 2 the two models for patchy particles are presented; Janus particles and IPCs. In Sec. 3 we derive the theory details following the self-consistent phonon approach (SCP) introduced in Ref. [5]. This is done for a general system of  $N$  particles which are interacting via an orientationally and spatially dependent potential. The formulas summarized in Sec. 3 are then applied to two-dimensional crystals formed by Janus particles (see Sec. 4) and the obtained results are compared to available results from literature [5]. The last two chapters are dedicated to the application of the SCP approach to IPCs forming two-dimensional (Sec. 5) and three-dimensional crystals (Sec. 6). This thesis report is concluded by a short summary containing also some ideas for future studies of the discussed procedure.

## 2 Models for patchy particles

In this thesis the SCP approach is used to calculate the thermodynamic properties of crystals formed by two different types of particles with heterogeneous surface interactions: (i) Janus particles with a very simple two-particle potential where only some regions of the surface attract each other while the rest of the surface is inert, and (ii) IPCs where only patches and patch-free regions attract each other while the patches and the patch-free zones repel each other, respectively.

### 2.1 Janus particles

Janus particles, named after the two-faced roman god Janus, have a surface with two distinct regions with different interaction properties. The Janus particles investigated in this thesis have a patch (specified by the opening angle  $\theta_0$  around the orientation vector  $\hat{\Omega}$ ) that attracts other patches (see Fig. 1). The rest of the surface does not interact with other particles. For Janus particles the particle diameter  $\sigma$  is used as unit of length.

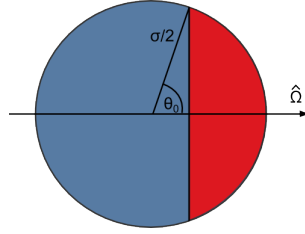


Figure 1: Schematic drawing of a Janus particle of diameter  $\sigma$ , showing one patch (in red) with opening angle  $\theta_0$  around the orientation vector  $\hat{\Omega}$ .

The Janus potential is a combination of a hard-sphere potential with a short ranged rotationally dependent part, namely

$$v_{ij}(r, \hat{\Omega}_i, \hat{\Omega}_j) = \begin{cases} +\infty & 0 < r < \sigma \\ -\epsilon \cdot v_\varphi(\hat{\mathbf{r}}_{ij}, \hat{\Omega}_i, \hat{\Omega}_j) & \sigma < r < \sigma + \delta \\ 0 & r < \sigma + \delta \end{cases} . \quad (1)$$

Here  $\hat{\Omega}_i$  is a normalized vector that specifies the orientation of particle  $i$  and  $r = |\mathbf{r}_i - \mathbf{r}_j|$  is the actual distance between particle  $i$  and  $j$ . The angular potential  $v_\varphi(\hat{\mathbf{r}}_{ij}, \hat{\Omega}_i, \hat{\Omega}_j)$  is a step-like function that is only non-zero if the two patches face each other,

$$v_\varphi(\hat{\mathbf{r}}_{ij}, \hat{\Omega}_i, \hat{\Omega}_j) = \begin{cases} 1 & \text{if } \hat{\Omega}_i \cdot \hat{\mathbf{r}}_{ij} > \cos(\theta_0) \text{ and } \hat{\Omega}_j \cdot \hat{\mathbf{r}}_{ji} > \cos(\theta_0) \\ 0 & \text{else} \end{cases} . \quad (2)$$

Thus particles are attracted to each other if they are located within a distance  $r$  smaller than their diameter plus the attraction range  $\delta$  and if their patches face each other. Note that the energy does not depend on the actual relative orientation between the particles, as long as they face each other. For a fixed distance the energy of a system of Janus colloids depends only on the number of bonds but not on the exact contact angle of the patches.

Janus particles are thus one of the simplest models for patchy particles; still they show a rich phase behavior due to the heterogeneous surface coverage.

## 2.2 Inverse patchy colloids

Inverse patchy colloids (IPCs) are heterogeneously charged particles which can e.g. emerge when positive polyelectrolyte stars absorb on a negatively charged, spherical colloid [8, 9]. Thus they show a strong anisotropy in their effective interaction: while the patches and patch-free zones repel each other respectively, an attraction occurs between the patches and patch-free zones. Due to the anisotropic surface a wide variety of self-assembled structures is expected.

In recent works (e.g. [10, 11]) the self-assembly of such particles was investigated using Monte Carlo simulations which attempt to find stable structures by minimizing the total energy of the system. In this thesis a different route of obtaining the phase diagram of crystalline structures formed by IPCs is explored. However, irrespective of the method used for the calculations, an effective way to calculate the interaction energy of a system of IPCs is needed. Two methods for the evaluation of the pair-energy exist: An analytic method based on the Debye-Hückel approximation and a coarse grained model introduced for the fast evaluation of the two-particle energy.

In the following these two methods are outlined exemplary for IPCs with two patches which are symmetric in size and charge.

### Analytic description

For the analytic calculation of the interaction energy of two IPCs, the colloids are modeled as impenetrable, hard spheres of radius  $\sigma$  with a negatively charged main body and positively charged patches. The particles are surrounded by a liquid dielectric solvent containing co- and counter-ions.

According to Gauss' law the potential induced by a charged sphere at a distance  $r$  to the center of the sphere is equal to the potential of a point charge which has exactly the charge contained in a similar sphere of radius  $r$ . The patch-free zone of the colloid can thus be replaced by a single charge  $Z_c$ , located at the center of the particle, the charged patches are replaced by point charges  $Z_p$  positioned at distances  $a$  from the center of the colloid (see Fig. 2).

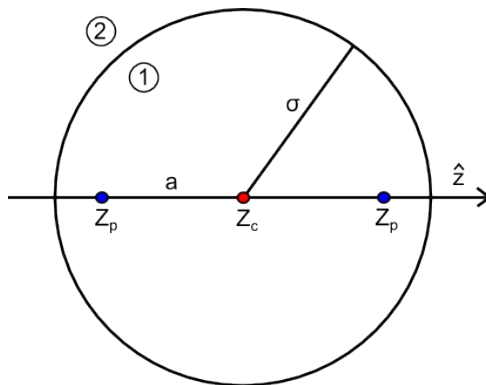


Figure 2: For the calculation of the pair energy using the Debye-Hückel approach an IPC with two identical patches is represented by three point charges: a point with charge  $Z_c$  located at the center of the particle and two points with charge  $Z_p$  at distances  $\pm a$  along the  $\hat{z}$ -axis. The potential created by this charge arrangement is separately constructed in the inner (labeled 1) and in the outer region (labeled 2).

In region 1 ( $r \leq a$ ) the potential is generated solely by the central and by the patch charges. The corresponding non-linear differential equation for the potential  $\Phi^{(1)}(r, \theta)$  for a colloid with



two patches positioned along the  $\hat{z}$ -axis (assuming azimuthal symmetry) is given by

$$\Delta\Phi^{(1)}(r, \theta) = -\frac{4\pi}{\epsilon} Z_p [\delta(\mathbf{r} - a\hat{\mathbf{z}}) + \delta(\mathbf{r} + a\hat{\mathbf{z}})] - \frac{4\pi}{\epsilon} Z_c \delta(\mathbf{r}). \quad (3)$$

Outside the particles (region 2) the co- and counter-ions of the surrounding solvent need to be taken into account. Here the Debye-Hückel approximation is used [12]: it assumes that the charge density of the surrounding ions can be described by a Boltzmann statistics. Additionally, it is assumed that the ionic density is sufficiently small so that a linearized equation for the potential contains all relevant details; thus one arrives at

$$\Delta\Phi^{(2)}(r, \theta) = \kappa^2 \cdot \Phi^2(r, \theta), \quad (4)$$

where  $\kappa$  denotes the inverse Debye screening length that depends on the number densities  $\rho_i^0$  and on the corresponding valences of the co- and counter-ions denoted by  $Z_i^0$ ,  $\kappa = \sqrt{\frac{4\pi q_e^2}{\epsilon k_B T} \sum_i \rho_i^0 Z_i^0}$ .

Expanding the potential inside and outside of the sphere in Legendre polynomials and enforcing the usual boundary conditions at the surface, the full potential can be obtained. For the pair-energy of two colloids the potential of one particle is evaluated at the positions of the point charges of the other colloid and vice versa. The pair energy is given by the symmetrized pair energies of the two particles.

### Coarse grained description

Since energy calculations via the above Debye-Hückel approximation are too expensive for extensive self-assembly studies a simpler way of calculating the energy is needed. In Ref. [13] a coarse grained model is introduced where the colloid is again modeled as a sphere of radius  $\sigma$ , while the patches are modeled as spheres of radius  $\rho$ , located at distances  $e$  from the center of the particle (see Fig. 3). Note, that the radius of an IPC is called  $\sigma$  while for Janus particles  $\sigma$  denotes the particle diameter. However, in both cases the particle diameter is used as unit of length.

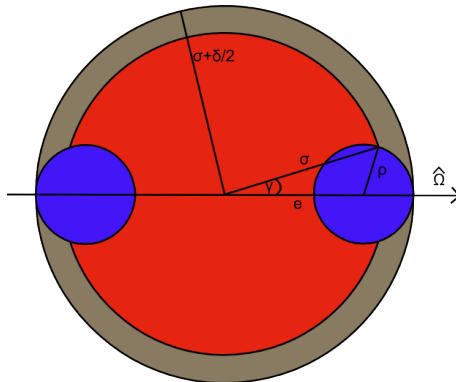


Figure 3: Schematic drawing of an IPC within the coarse-grained model: the central sphere of radius  $\sigma$  is decorated by two spherical patches of radius  $\rho$  (corresponding to an opening angle of  $\gamma$ ) at  $\pm e$  outside of the center along the  $\hat{\Omega}$ -axis. The interaction region is given by the gray sphere of radius  $\sigma + \delta/2$  where  $\delta$  is the interaction range.

The interaction of two IPCs is modeled via an interaction sphere of radius  $\sigma + \delta/2$ , located at the center of the particle. The opening angle  $\gamma$  of the patch of an IPC is given by the eccentricity parameter  $e$  and the patch radius  $\rho$  via

$$\cos \gamma = \frac{\sigma^2 + e^2 - \rho^2}{2\sigma e}. \quad (5)$$

The number of parameters  $(e, \rho, \delta, \gamma)$  is reduced by a geometric relation between those quantities, namely

$$\delta = 2(e + \rho) - 2\sigma. \quad (6)$$

Thus, for a fixed interaction range  $\delta$  the extension  $\gamma$  of the patches defines the geometry of the IPC.

The pair-potential of two IPCs (with indices  $i$  and  $j$ ) within the coarse grained model is a combination of a hard sphere potential with a distance and the orientation dependent part within the interaction range,

$$V(r_{ij}, \theta_i, \theta_j, \theta_{ij}) = \begin{cases} \infty & \text{if } r_{ij} < 2\sigma \\ U(r_{ij}, \theta_i, \theta_j, \theta_{ij}) & \text{if } 2\sigma \leq r_{ij} \leq 2\sigma + \delta \\ 0 & \text{if } 2\sigma + \delta < r_{ij} \end{cases}. \quad (7)$$

The potential  $U(r_{ij}, \theta_i, \theta_j, \theta_{ij})$  depends on the distance between particle  $i$  and particle  $j$ ,  $r_{ij}$ , the orientation of the patches,  $\theta_i$  and  $\theta_j$ , and on the relative orientation of the two particles,  $\theta_{ij}$ . For the calculation of the interaction potential  $U$  only the overlap volumes  $\Omega_{\alpha\beta}$  of a sphere of type  $\alpha$  with a sphere of type  $\beta$  needs to be evaluated: here  $\alpha$  and  $\beta$  denote either the big sphere ('B') with radius  $r_B = \sigma + \delta/2$  corresponding to the body of the particle or the small sphere ('S') representing one of the patches with radius  $r_S = \rho$ . This geometric overlap volumes  $\Omega_{\alpha\beta}$  are normalized by the reference volume  $\Omega_R = \frac{4\pi\sigma^3}{3}$  of the central sphere,

$$w_{\alpha\beta} = \Omega_{\alpha\beta}/\Omega_R. \quad (8)$$

The energy of two IPCs within the interaction range  $2\sigma \leq r_{ij} \leq 2\sigma + \delta$  is then defined via a sum of overlap volumes  $w_{\alpha\beta}$  weighted by respective energy factors  $u_{\alpha\beta}$  which are as yet undefined, namely

$$U(r_{ij}, \theta_i, \theta_j, \theta_{ij}) = w_{BB}u_{BB} + w_{BS}u_{BS} + w_{SS}u_{SS}, \quad (9)$$

with

$$\Omega_{BB} = \Omega_{B_i B_j} \quad (10)$$

$$\Omega_{BS} = \Omega_{B_i S_j^1} + \Omega_{B_i S_j^2} + \Omega_{B_j S_i^1} + \Omega_{B_j S_i^2} \quad (11)$$

$$\Omega_{SS} = \Omega_{S_i^1 S_j^1} + \Omega_{S_i^1 S_j^2} + \Omega_{S_i^2 S_j^1} + \Omega_{S_i^2 S_j^2}. \quad (12)$$

The energy factors  $u_{\alpha\beta}$  of Equ. (9) are set using the potential calculated via the Debye-Hückel approach. For this mapping between the Debye-Hückel and the coarse grained model, reference configurations of two IPCs at contact ( $r_{ij} = 2\sigma$ ) are used. For an IPC with two symmetrical patches three reference configurations are sufficient to fix those parameters: an equatorial-equatorial configuration where the patch-free zones of two IPCs overlap, an equatorial-polar configuration where the energy is given by the overlap of the patch-free zone with one of the patches and a polar-polar configuration where two patches overlap. For an illustration of the reference configurations see Fig. 4.

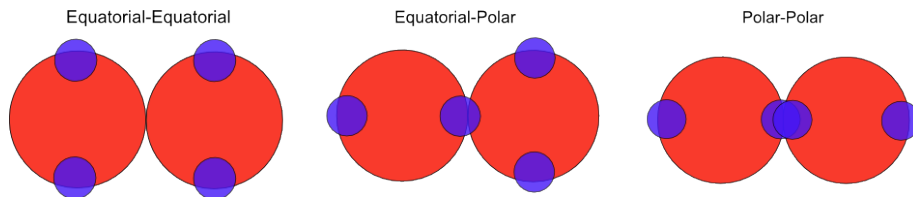


Figure 4: The reference configurations used for the mapping between the energy calculated using the Debye-Hückel approach and the coarse-grained model. For an IPC with two symmetrical patches three reference configurations are sufficient, namely an equatorial-equatorial (left), an equatorial-polar (middle) and a polar-polar configuration (right).

For the mapping of the energy the mapping procedure called 'max' in Ref. [13] is used: here the absolute maximum values of the energies of the reference configurations obtained via the Debye-Hückel approach and the coarse grained model are set equal. Thus the energy contribution stemming from an overlap of the form 'BB' and 'SS' is repulsive while an overlap of the form 'BS' results in an attractive contribution to the pair-energy.

In summary the potential calculated via the coarse grained model represents interactions of a real IPC in a very reliable way while reducing the computational effort decisively. The symmetry of an IPC is preserved and the heterogeneous surface coverage resulting in a rich phase behavior is represented.

### 3 Self-consistent Phonon Approach (SCP) for orientationally dependent colloids

The Self-consistent Phonon Approach (SCP) is a mean field type theory used for the calculation of the free energy of systems where thermodynamic integration schemes to obtain the thermodynamic potentials (e. g. free energy) are not easily achieved. To avoid in these approaches a direct integration over the complete potential, a reference potential is introduced for which integrations can be performed in an easier way; in contrast to the full potential this reference potential depends only on the translational and rotational deviations from the equilibrium positions and orientations of the particles. This potential is then fitted to the full potential by solving a self-consistency equation for the yet-open parameters. It is now used instead of the full potential for the calculation of the free energy.

In this Section we will give an outline of the SCP procedure adapted to a system of  $N$  particles which are interacting via an orientationally dependent potential. Since the potential is left for the moment as general as possible, the formulas derived in this Section can be applied to both Janus particles and IPCs (see Sec. 4 and Sec. 5).

The SCP approach was first introduced by M. Fixman in Ref. [4] for a system of hard spheres located in a constrained face-centered cubic where each atom is constrained within its Wigner-Seitz cell. These constraints are mathematically realized via wall-potentials  $v_i$  that are added to the potential of the system; thus the total potential energy of a system of  $N$  particles is given by

$$V_S(|\mathbf{r}_i - \mathbf{r}_j|, \boldsymbol{\Omega}_i, \boldsymbol{\Omega}_j) = \frac{1}{2} \sum_{i \neq j} \sum_{j=1}^N v_{ij}(|\mathbf{r}_i - \mathbf{r}_j|, \boldsymbol{\Omega}_i, \boldsymbol{\Omega}_j) + \sum_{i=1}^N v_i. \quad (13)$$

Here  $v_{ij}(|\mathbf{r}_i - \mathbf{r}_j|, \boldsymbol{\Omega}_i, \boldsymbol{\Omega}_j)$  denotes the two-particle interaction between particle  $i$  and  $j$  located at positions  $\mathbf{r}_i$  and  $\mathbf{r}_j$  and orientations  $\boldsymbol{\Omega}_i$  and  $\boldsymbol{\Omega}_j$ , respectively. The wall-potential  $v_i$  of particle  $i$  is different from system to system (see Sec. 4 and 5). It contains a translational part that vanishes if particle  $i$  is located within its Wigner-Seitz cell and infinite otherwise. For colloids with orientational dependent interactions a second wall-potential is needed, that constrains the particle rotation.

Instead of using the full potential for the calculation of the partition function, a reference potential is introduced within the SCP approach. Since its purpose is primarily to simplify the integration of the potential, Fixman proposed to use a simple harmonic potential for the translational deviations  $\mathbf{w}_i$  from the equilibrium positions  $\mathbf{R}_i$  of the particles [4]. This approach can be generalized to include rotational deviations  $\theta_i$  from the equilibrium orientations  $\boldsymbol{\Phi}_i$  as well, as has been done in [14, 5], namely

$$V_H(\mathbf{w}_i, \theta_i) = \sum_{i=1}^N t w_i^2 + \sum_{i=1}^N q \theta_i^2, \quad (14)$$

where  $t$  and  $q$  are spring constants which need to be determined in the following.

Using this reference potential the canonical partition function of the system,  $Q_S$ , can be transformed in the following way:

$$\begin{aligned} Q_S &= \int e^{-V_S(|\mathbf{r}_i - \mathbf{r}_j|, \boldsymbol{\Omega}_i, \boldsymbol{\Omega}_j)} d\{w_i\} d\{\theta_i\} \\ &= \frac{\int e^{-V_S(|\mathbf{r}_i - \mathbf{r}_j|, \boldsymbol{\Omega}_i, \boldsymbol{\Omega}_j) + V_H(\mathbf{w}_i, \theta_i)} \cdot e^{-V_H(\mathbf{w}_i, \theta_i)} d\{w_i\} d\{\theta_i\}}{\int e^{-V_H(\mathbf{w}_i, \theta_i)} d\{w_i\} d\{\theta_i\}} \cdot \int e^{-V_H(\mathbf{w}_i, \theta_i)} d\{w_i\} d\{\theta_i\} \\ &= \langle B \rangle \cdot Q_1, \end{aligned} \quad (15)$$

where  $B(\mathbf{R}_i, \mathbf{w}_i, \mathbf{r}_j, \Phi_i, \theta_i, \Omega_j) = \exp(-V_S(|\mathbf{r}_i - \mathbf{r}_j|, \Omega_i, \Omega_j) + V_H(\mathbf{w}_i, \theta_i))$ ;  $\langle \cdot \rangle$  is denoting an averaging procedure using the weight  $\exp(-V_H)$ . Equ. (15) is a general result for a system with an arbitrary number of degrees of freedom and thus an arbitrary number of directions for the deviations  $w_i$  and  $\theta_i$ . In Equ. (15) integrations over all occurring deviations are denoted by  $d\{w_i\}d\{\theta_i\}$ ; this notation includes also a Jacobian determinant, if applicable.

Since both the full potential as well as the reference potential can be written as a sum over one-particle contributions,  $B(\mathbf{R}_i, \mathbf{w}_i, \mathbf{r}_j, \Phi_i, \theta_i, \Omega_j)$  can be expressed as a product of one-particle quantities  $B_i(\mathbf{R}_i, \mathbf{w}_i, \mathbf{r}_j, \Phi_i, \theta_i, \theta_j)$ . At this point the first approximation is made as the coupling between the different  $B_i(\mathbf{R}_i, \mathbf{w}_i, \mathbf{r}_j, \Phi_i, \theta_i, \theta_j)$  factors is neglected,

$$\langle B(\mathbf{R}_i, \mathbf{w}_i, \mathbf{r}_j, \Phi_i, \theta_i, \Omega_j) \rangle = \left\langle \prod_i B_i \right\rangle \approx \prod_i \langle B_i \rangle (\mathbf{R}_i, \mathbf{w}_i, \Phi_i, \theta_i) = \prod_i \langle \exp(tw_i^2 + q\theta_i^2 - v_i - V_i) \rangle, \quad (16)$$

where  $V_i(\mathbf{r}_i, \Omega_i) = \frac{1}{2} \sum_{j \neq i} v_{ij}(|\mathbf{r}_i - \mathbf{r}_j|, \Omega_i, \Omega_j)$ .

This approximation might lead to errors for strongly position dependent potentials, e.g. for step potentials. The main aim of the SCP approach is however not a perfect result but an approximation which makes phase diagram calculations feasible.

In order to obtain the self-consistency equation for the spring constants  $t$  and  $q$  we expand the  $V_i(\mathbf{r}_i, \Omega_i)$  in a Taylor expansion in the deviations  $\mathbf{w}_i$  and  $\theta_i$ , where only the zeroth order term,  $v_e$ , is retained. For detailed calculations see e.g. [15]. We obtain

$$\exp\left(-\frac{1}{2}v_{ij}\right) \approx 1 + h(\mathbf{W}_i - \mathbf{w}_i, \theta_i), \quad (17)$$

where  $\mathbf{W}_i := \mathbf{W}_{ij} = \mathbf{R}_j - \mathbf{R}_i + \mathbf{w}_j$ ;  $\mathbf{R}_i$  and  $\mathbf{R}_j$  are the equilibrium positions of particle  $i$  and  $j$ , respectively. The actual calculation of the function  $h$  is done via

$$h(\mathbf{W}_i - \mathbf{w}_i, \theta_i) = \left\langle \exp\left(-\frac{1}{2}v_{ij}\right) \right\rangle_j - 1. \quad (18)$$

In the averaging procedure denoted by  $\langle \cdot \rangle_j$  the dependence of the potential  $v_{ij}(|\mathbf{r}_i - \mathbf{r}_j|, \Omega_i, \Omega_j)$  on the deviations  $\mathbf{w}_j$  and  $\theta_j$  of particle  $j$  are eliminated. In practice this is done by choosing a unit cell which contains all the necessary information to periodically build the whole crystal structure. To obtain the mean-field potential of the structure, the two-particle potential is averaged over all possible movements of the particle located in the center of the unit cell (labeled 'j' in Equ. (18)).

The approximated two-particle potential for particle  $i$  is thus

$$\frac{1}{2} \sum_{i \neq j} v_{ij} \approx v_e = - \sum_{i \neq j} \ln(1 + h(\mathbf{W}_i - \mathbf{w}_i, \theta_i)). \quad (19)$$

$v_e$  is now Taylor expanded in terms of the deviations  $\mathbf{w}_i$  and  $\theta_i$  to obtain an equation that has a similar form as Equ. (14),

$$v_e(\mathbf{w}_i, \theta_i) \approx \varepsilon + \gamma w_i^2 + \beta \theta_i^2, \quad (20)$$

where the coefficients  $\varepsilon$ ,  $\beta$  and  $\gamma$  are given by

$$\varepsilon(t, q) = - \sum_i \ln[1 + h(\mathbf{W}_i, 0)] \quad (21)$$

$$\gamma(t, q) = - \frac{1}{2d_t} \sum_i \nabla_{w_i} \nabla_{w_i} \ln[1 + h(\mathbf{W}_i - \mathbf{w}_i, \theta_i)]|_{\mathbf{w}_i=0, \theta_i=0} \quad (22)$$

$$\beta(t, q) = - \frac{1}{2d_r} \sum_i \partial_{\theta_i} \partial_{\theta_i} \ln[1 + h(\mathbf{W}_i - \mathbf{w}_i, \theta_i)]|_{\mathbf{w}_i=0, \theta_i=0}; \quad (23)$$

$d_t$  and  $d_r$  are the number of translational and rotational freedoms, respectively. The sums are carried out over the nearest neighbors of the central particle.

The self-consistency equation for  $t$  is then obtained by evaluating the mean squared displacement  $\langle w_i^2 \rangle$  using the expression for the potential in Eqs. (20) and (14),

$$\begin{aligned} \langle w_i^2 \rangle &= \frac{\int w_i^2 \exp(-V_H) d\{w_i\} d\{\theta_i\}}{\int \exp(-V_H) d\{w_i\} d\{\theta_i\}} = \frac{d_t}{2t} \\ &= \frac{\int_{\nu} \int_{\phi_0} w_i^2 \exp(-v_e) d\{w_i\} d\{\theta_i\}}{\int_{\nu} \int_{\phi_0} \exp(-v_e) d\{w_i\} d\{\theta_i\}}, \end{aligned} \quad (24)$$

where the integrals in Eq. (24) are evaluated over the Wigner-Seitz cell  $\nu$ . The angular integral is bounded by the wall-potential angle  $\phi_0$ , which gives the maximal rotation of the central particle that does not change the characteristics of the structure with respect to the equilibrium orientation. Thus,  $\phi_0$  depends on the equilibrium positions and orientations of all the particles in the unit cell as well as on the form of the interaction potential.

The self-consistency equation for the angular spring constant  $q$  follows in an analogous way:

$$\begin{aligned} \langle \theta_i^2 \rangle &= \frac{\int \theta_i^2 \exp(-V_H) d\{w_i\} d\{\theta_i\}}{\int \exp(-V_H) d\{w_i\} d\{\theta_i\}} = \frac{d_r}{2t} \\ &= \frac{\int_{\phi_0} \theta_i^2 \exp(-v_e) d\{w_i\} d\{\theta_i\}}{\int_{\phi_0} \exp(-v_e) d\{w_i\} d\{\theta_i\}}. \end{aligned} \quad (25)$$

The SCP approach can now be applied in the following way: First the  $h$ -function is calculated via Equ. (18) with some start values for  $t$  and  $q$ . Then the  $h$ -function is used to calculate  $\varepsilon$ ,  $\gamma$  and  $\beta$  from Equ. (21). The new values for the spring constants  $t$  and  $q$  follow from the non-linear, coupled self-consistency equations (24) and (25). This procedure is iterated until convergence in  $t$  and  $q$  is reached.

The partition function of the system of  $N$  particles can now be written in terms of the approximated potential  $v_e$ , which is a mean-field quantity, as

$$\begin{aligned} Q_S &= \prod_{i=1}^N \int_{\nu} d\{w_i\} d\{\theta_i\} \exp(-v_e(w_i, \theta_i)) \\ &= \left( \int_{\nu} d\{w_i\} d\{\theta_i\} \exp(-v_e(w_i, \theta_i)) \right)^N. \end{aligned} \quad (26)$$

Since the coefficients  $\varepsilon$ ,  $\beta$  and  $\gamma$  do not depend on the deviations  $\mathbf{w}_i$  and  $\theta_i$  themselves, the free energy  $f$  per particle is easily obtained from the converged spring constants (using Equ. (21), Equ. (22) and Equ. (23)) via

$$f = -\frac{\ln(Q_S)}{N} = -\ln \left( e^{-\varepsilon} \cdot \int d\{w_i\} e^{-\gamma w_i^2} \cdot \int d\{\theta_i\} e^{-\beta \theta_i^2} \right). \quad (27)$$

The free energy per particle can now be written as a sum of a static part,  $f_{\text{static}}$ , a translational part,  $f_{\text{trans}}$ , and a rotational part,  $f_{\text{rot}}$ , which are defined as

$$f_{\text{static}} = \varepsilon(t, q) \quad (28)$$

$$f_{\text{trans}} = -\ln \left( \int_{\nu} \exp(-\gamma(t, q) w_i^2) d\{w_i\} \right) \quad (29)$$

$$f_{\text{rot}} = -\ln \left( \int_{\phi_0} \exp(-\beta(t, q) \theta_i^2) d\{\theta_i\} \right) \quad (30)$$

$$f = f_{\text{static}} + f_{\text{trans}} + f_{\text{rot}}. \quad (31)$$

Due to the constraining wall potentials the integrals of Eqs. (29) and (30) are bounded by the Wigner Seitz cell  $\nu$  and the constraining angle  $\phi_0$ .

## 4 SCP for Janus particles in two dimensions

### 4.1 Theory

In this Section the SCP approach is applied to Janus particles following the procedure discussed in [5]. In the following we will restrict ourselves to two-dimensional structures formed by Janus colloids with an opening angle of  $\theta_0 = 65^\circ$  around the orientational vector  $\hat{\boldsymbol{\Omega}}$  (see Fig. 1).

We have first considered in this thesis Janus particles as they have already been investigated in Ref. [5]; this contribution provides reference data which helped to check our implementation of the SCP approach. In addition, Janus colloids interact via a simpler orientational potential than IPCs.

The Janus potential is a combination of a hard-sphere potential with a short ranged rotationally dependent part (see Sec. 2.1). For a fixed distance the energy of a system of Janus particles depends only on the number of bonds but not on the exact contact angle of the patches. The freedom of movement of the Janus particles can be restricted by adding a rotationally constraining factor  $\phi_i$  to the potential representing the crystal structure. Thus the total potential energy becomes

$$V_S(|\mathbf{r}_i - \mathbf{r}_j|, \boldsymbol{\Omega}_i, \boldsymbol{\Omega}_j) = \frac{1}{2} \sum_{i \neq j}^N \sum_j v_{ij}(|\mathbf{r}_i - \mathbf{r}_j|, \boldsymbol{\Omega}_i, \boldsymbol{\Omega}_j) + \sum_{i=1}^N v_i + \sum_{i=1}^N \phi_i. \quad (32)$$

The wall-potential  $\phi_i$  of the  $i$ -th particle is determined by the crystal structure: it is infinite if the particle's orientation has a deviation of more than  $\pm\phi_0$  from its equilibrium orientation and vanishes otherwise. The characteristic angle  $\phi_0$  is defined by the structure so that by a rotation of  $\pm\phi_0$  no new bonds can be formed and no bonds existing at equilibrium are broken.

For a lattice of  $N$  Janus particles the energy depends on the translational deviations  $\mathbf{w}_i$  and on the orientational deviation  $\theta_i$  of the  $i$ -th particle from the equilibrium location  $\mathbf{R}_i$  and the equilibrium orientation  $\boldsymbol{\Omega}_i$ . The reference potential is chosen in the following form [5]

$$V_H(\mathbf{w}_i, \theta_i) = \sum_{i=1}^N t \mathbf{w}_i^2 + \sum_{i=1}^N q \theta_i^2. \quad (33)$$

The spring constants,  $t$  and  $q$ , are scalars for which self-consistency equations are derived in the following. For some structures it might be appropriate to allow different spring constants parametrizing oscillations in different directions. This is for instance the case for elongated unit cells (see Sec. 6). However, in this Section we will only study structures based on the hexagonal close-packing of spheres where the distances between the particles are of comparable lengths in all directions.

Following the procedure discussed in Sec. 3 the  $h$ -function is calculated. This has already been presented in Ref. [5], however, since many parts of the  $h$ -function also occur for the potential of IPCs, the main steps of the calculation are repeated here. Starting with the definition of  $h(\mathbf{w}_i, \theta_i)$  in Equ. (18), the potential is averaged over the movements of the central particle  $c$  of the unit cell,

$$h(\mathbf{w}_i, \theta_i) = \frac{\int d\{w_c\} \int d\theta_c [e^{-\frac{1}{2}v_{ic}(r_{ci}, \boldsymbol{\Omega}_i, \boldsymbol{\Omega}_c)} - 1] e^{-q\theta_c^2} e^{-t\mathbf{w}_c^2}}{\int d\{w_c\} \int d\theta_c e^{-q\theta_c^2} e^{-t\mathbf{w}_c^2}}. \quad (34)$$

The potential depends on the actual distance  $r$  of the particles  $c$  and  $i$ , where

$$\mathbf{r}_{ci} = \mathbf{r}_c - \mathbf{r}_i = \mathbf{R}_c + \mathbf{w}_c - \mathbf{R}_i - \mathbf{w}_i = \mathbf{W} + \mathbf{w}_c. \quad (35)$$



We first solve the integral in the denominator using polar coordinates for the translational part,

$$\begin{aligned}\mathcal{N} &= \int_{\mathbb{R}} d\{w_c\} \int_{-\pi}^{\pi} d\theta_c e^{-q\theta_c^2} e^{-tw_c^2} \\ &= \int_0^{\infty} e^{-tw_c^2} w_c dw_c \int_0^{2\pi} d\varphi \cdot 2 \int_0^{\pi} e^{-q\theta_c^2} d\theta_c.\end{aligned}\quad (36)$$

Using the transformations  $u = tw_c^2$  and  $v = \sqrt{q}\theta_c$  we obtain

$$\mathcal{N} = \left(\frac{\pi}{t}\right) \left(\sqrt{\frac{\pi}{q}} \operatorname{erf}(\sqrt{q}\pi)\right), \quad (37)$$

where the error function is defined as  $\operatorname{erf}(x) = \frac{2}{\sqrt{\pi}} \int_0^x e^{-v^2} dv$ .

For the integral in the nominator of Equ. (34) the deviations  $\mathbf{w}_c$  can be rewritten as  $\mathbf{w}_c = \mathbf{r} - \mathbf{W}$  and the integral can be transformed into an integral over the actual distance vector  $\mathbf{r}$  between the particles (with  $|\mathbf{r}| = r$ ),

$$h(\mathbf{w}_i, \theta_i) = \frac{1}{\mathcal{N}} \int d\{\mathbf{r}\} \int d\theta_c [e^{-\frac{1}{2}v_{ic}(|\mathbf{r}|, \hat{\Omega}_i, \hat{\Omega}_c)} - 1] e^{-q\theta_c^2} e^{-t[\mathbf{r} - \mathbf{W}]^2}. \quad (38)$$

Introducing polar coordinates so that  $[\mathbf{r} - \mathbf{W}]^2 = r^2 + W^2 - 2rW \cos \varphi$  and using the radial dependence of the pair potential  $v_{ij}(r, \hat{\Omega}_i, \hat{\Omega}_j)$  from Equ. (1) we obtain

$$\begin{aligned}h(\mathbf{w}_i, \theta_i) &= \frac{1}{\mathcal{N}} \int_0^{\sigma} dr r \int_0^{2\pi} d\varphi \int_{-\pi}^{\pi} d\theta_c (-1) e^{-q\theta_c^2} e^{-t(r^2+W^2)} e^{2trW \cos \varphi} + \\ &+ \frac{1}{\mathcal{N}} \int_{\sigma}^{\sigma+\delta} dr r \int_0^{2\pi} d\varphi \int_{-\pi}^{\pi} d\theta_c [e^{\frac{1}{2}\varepsilon v_{\varphi}} - 1] e^{-q\theta_c^2} e^{-t(r^2+W^2)} e^{2trW \cos \varphi}\end{aligned}\quad (39)$$

In the first term of Equ. (39) the rotational integral cancels with the rotational part of the normalization factor. The integral over  $\varphi$  can be identified as a modified Bessel function of the first kind  $I_0(x)$  which is defined as [16]

$$I_0(x) = \frac{1}{2\pi} \int_0^{2\pi} d\varphi e^{x \cos \varphi}. \quad (40)$$

Thus the first term can be written as

$$h_{\text{HS}}(W) = -2t \int_0^{\sigma} du u e^{-t(u^2+W^2)} I_0(2tuW). \quad (41)$$

This contribution also occurs for a system of simple hard spheres and is therefore called  $h_{\text{HS}}(W)$ . In the second term of Equ. (39) the rotational and translational parts factorize. The integral becomes

$$h(\mathbf{w}_i, \theta_i) = h_{\text{HS}}(W) + h_{\text{SW}}(W) \cdot J(\theta_i), \quad (42)$$

with the square-well contribution  $h_{\text{SW}}(W)$

$$h_{\text{SW}}(W) = 2t \int_{\sigma}^{\sigma+\delta} du u e^{-t(u^2+W^2)} I_0(2tuW), \quad (43)$$

$$J(\theta_i) = \begin{cases} (e^{\varepsilon/2} - 1) \left[ \frac{\text{erf}(-\sqrt{q}(\theta_i - 2\phi_0)) + \text{erf}(\sqrt{q}(\theta_i + 2\phi_0))}{2\text{erf}(\sqrt{q}\pi)} \right] & \text{if bond exists} \\ 0 & \text{else} \end{cases}. \quad (44)$$

$J(\theta_i)$  is only non-zero if a bond between particle  $i$  and the central particle exists.

The self-consistency equations for the spring constants  $t$  and  $q$  follow from the Eqs. (24) and (25). For the evaluation of  $\langle \mathbf{w}_i^2 \rangle$  the Wigner-Seitz cell  $\nu$  is approximated by a disk of radius  $a$  with the same area as the actual Wigner-Seitz cell area, thus  $a = \sqrt{\sqrt{3}/(2\pi)} \cdot R$ , where  $R$  is the distance between the centers of two particles in equilibrium. The self-consistency equation (24) for  $t$  becomes then

$$\begin{aligned} \frac{d_t}{2t} &= \frac{\int_{\nu} w_i^2 e^{-\gamma w_i^2} d\{w_i\}}{\int_{\nu} e^{-\gamma w_i^2} d\{w_i\}} = \frac{\int_0^{\gamma a^2} \frac{x}{2\gamma^2} e^{-x} dx}{\int_0^{\gamma a^2} \frac{1}{2\gamma} e^{-x} dx} \\ &= \frac{\exp(-\gamma a^2) \cdot (\gamma a^2 + 1) - 1}{\gamma \cdot \exp(-\gamma a^2 - 1)}. \end{aligned} \quad (45)$$

The self-consistency equation (25) can be transformed into

$$\frac{d_r}{2q} \approx \frac{\sqrt{\pi} \text{erf}(\sqrt{\beta} \phi_0) - 2 \exp(-\beta \phi_0^2) \sqrt{\beta} \phi_0}{2\beta \sqrt{\pi} \text{erf}(\sqrt{\beta} \phi_0)}, \quad (46)$$

In Equ. (46) it was assumed that  $\pi \gg \phi_0$ .

The free energy per particle  $f$  can be evaluated starting from Eqs. (28)-(31). The static contribution  $f_{\text{static}}$  is given by the coefficient  $\varepsilon$  as obtained via the self-consistent procedure. Approximating the Wigner-Seitz cell as a disk with radius  $a$ , the translational contribution  $f_{\text{trans}}$  can be written as

$$\begin{aligned} f_{\text{trans}} &= -\ln \left( 2\pi \int_0^a e^{-\gamma w^2} w dw \right) \\ &= -\ln \left( \frac{\pi}{\gamma} (1 - e^{-\gamma a^2}) \right). \end{aligned} \quad (47)$$

The rotational free energy per particle  $f_{\text{rot}}$  for ordered crystals formed by Janus particles becomes

$$\begin{aligned} f_{\text{rot}} &= -\ln \left( \int_{-\phi_0}^{\phi_0} e^{-\beta \theta_i^2} d\theta_i \right) \\ &= -\ln \left( \sqrt{\frac{\pi}{\beta}} \text{erf}(\sqrt{\beta} \phi_0) \right). \end{aligned} \quad (48)$$

## 4.2 Results

In a first step we tried to reproduce the results published in [5] for Janus particles thus checking for possible errors in our implementation. The investigated crystal structures are two-dimensional hexagonal structures consisting of Janus colloids with patch angles of  $\theta_0 = 65^\circ$  with

different orientational order. The simplest structure is a plastic phase where the patches are orientated randomly. The two ordered structures, namely a zigzag phase forming three bonds per particle and a trimer phase where each particle forms two bonds, are shown in Fig. 5. The spatial attraction range of the square well of Equ. (1) is set to  $\delta = 0.05$  (in units of the diameter  $\sigma$ ).

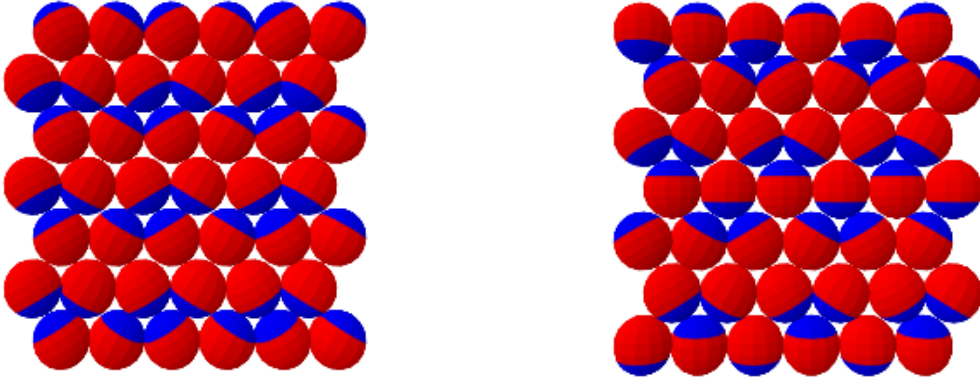


Figure 5: Two-dimensional ordered structures formed by Janus colloids: The zigzag crystal (left) which shows three bonds per particle and the trimer phase (right) where two bonds per particle are formed.

The expressions for  $h_{\text{hs}}(W)$  (Equ. (41)) and  $h_{\text{sw}}(W)$  (Equ. (43)) have to be calculated numerically. In most cases the spring constant  $t$  turns out to be very large ( $t \approx 1200\sigma^{-1}$ ). For these cases the Bessel function  $I_0$  can be approximated by an expansion for large arguments (for details see [16], p. 376),

$$I_0(x) \approx \frac{e^x}{\sqrt{2\pi x}} \left( 1 - \frac{0.125}{x} + \frac{4.5}{(8x)^2} + \frac{37.5}{(8x)^3} \right). \quad (49)$$

Although the integration range for  $h_{\text{hs}}(W)$  starts at  $u = 0$  where the large argument expansion is not valid, the contributions with larger  $u$  dominate as long as  $t$  is sufficiently large so that the error of the approximation can be safely neglected. This is true for the high density phases in Fig. 14, where  $t \approx 1200\sigma^{-1}$ . However, even for low density phases where we typically find  $t \approx 5\sigma^{-1}$ , the error is still quite small.

The  $h$ -function is now calculated for each pair of particle  $i(\neq c)$  contained in the unit cell and the central particle. The self-consistency equations for the spring constants  $t$  and  $q$  from Eqs. (45) and (46) were iterated until the mean squared displacements  $\langle w^2 \rangle$  and  $\langle \theta^2 \rangle$  vary by less than  $10^{-9}$  in relative units.

Using the converged spring constants the free energy per particle  $f$  is easily obtained using Equ. (28). The pressure can now be calculated via

$$p = - \left( \frac{\partial f}{\partial V} \right)_{|T} = - \frac{1}{2\sqrt{3}(r+x/2)} \left( \frac{\partial f}{\partial x} \right)_{|T} \quad (50)$$

$$= \eta^2 \frac{\pi}{4} \left( \frac{\partial f}{\partial \eta} \right)_{|T} \quad (51)$$

where  $V$  is the area of the Wigner-Seitz cell. The numerical derivative with respect to  $x$  is performed by slightly varying the distance between the particles from  $r$  to  $r+x$  so that the

pressure can be calculated using Equ. (50). Introducing the packing fraction  $\eta = \frac{\pi}{4}\rho\sigma^2$ , where  $\rho$  is the density, Equ. (51) can be used. Following the definition of the pressure in [5] the reduced pressure is defined as

$$p^* = p \cdot \frac{4}{\pi}. \quad (52)$$

#### 4.2.1 Zigzag structure

The zigzag crystal consists of a hexagonal structure of Janus particles where the patches are aligned in a zigzag ordering. The unit cell used for the SCP calculation is shown in Fig. 6 in the left panel; the central and right panel illustrate the angle  $\phi_0$  at which the wall potential restricts the rotation of the central particle.

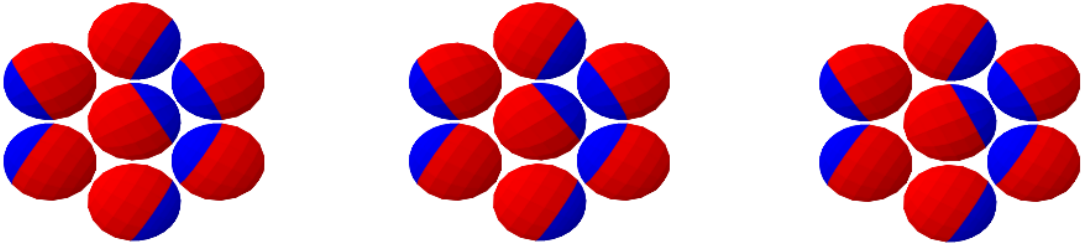


Figure 6: Unit cell of the zigzag structure formed by Janus particles at equilibrium (left). A wall potential  $\phi_0$  is introduced to restrict the rotation of the central particle of the structure. This angle is given by the maximal rotation of the central particle from its equilibrium orientation for which no existing bonds are broken or additional ones are formed with respect to the equilibrium orientation. The panel in the middle shows the structure if the central particle is rotated by this maximal rotation angle of  $\phi_0 = 5^\circ$  to the left, the corresponding rotation to the right is shown in the right panel.

For this structure the increment  $x$  for the numerical evaluation of the pressure via Equ. (50) was set to  $x = 0.0007$  since the pressure at this value is numerically stable while still giving the smoothest curves compared with other values for the increment; details are shown in Fig. 7.

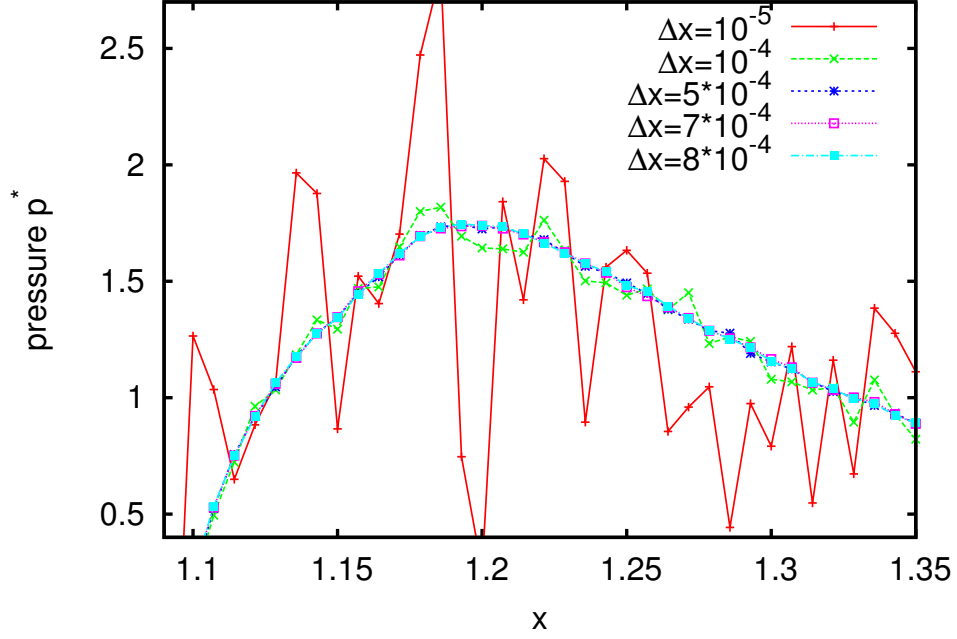


Figure 7: Reduced pressure  $p^*$  over distance  $x$  between the particles at  $T^* = 0.2$  for different increments  $\Delta x$  (as labeled) for the numerical calculation of the pressure via Equ. (50) for the zigzag structure. The smoothest curve is found at  $\Delta x = 7 \cdot 10^{-4}$ .

Since we perform our calculations in the canonical ensemble it is not possible to directly impose the pressure; instead the system has to be treated at a certain density and then the corresponding pressure can be determined via Equ. (50). Subsequently the distance between the particles (and hence the density) is changed and the calculation repeated until the desired pressure is obtained. A successful realization of this procedure does however depend on the starting distance of the particles. This can be seen in Fig. 8 where the reduced pressure  $p^*$  is plotted over the distance  $x$  of the particles in the zigzag structure for different reduced temperatures  $T^*$ .

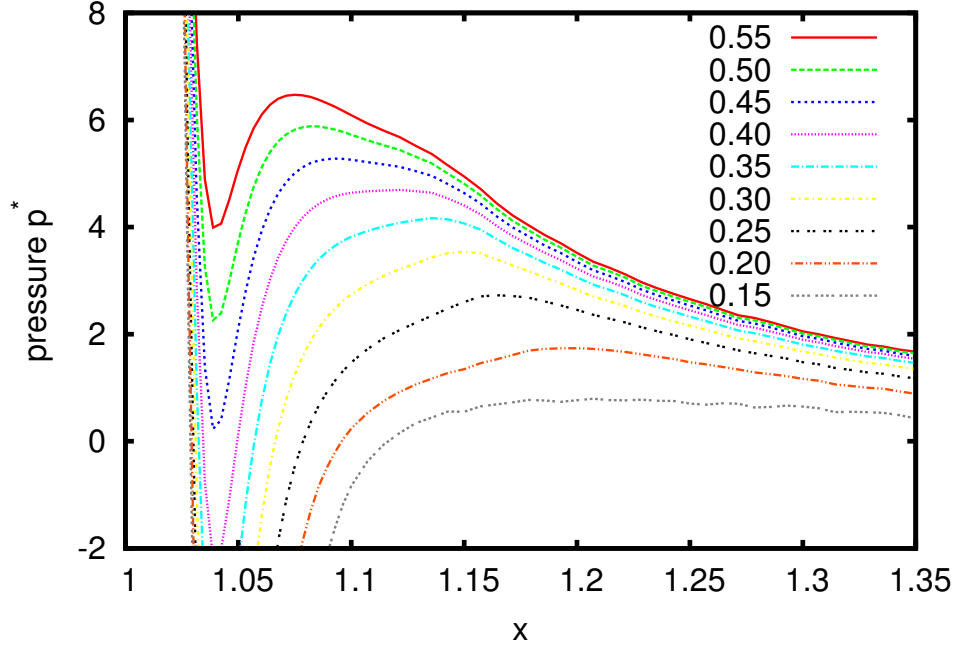


Figure 8: Reduced pressure  $p^*$  over the distance  $x$  between the particles in the zigzag structure. The different lines correspond to different values of the reduced temperatures  $T^*$  (as labeled).

For pressure  $p^* = 2$ , for example, it seems that for  $0.25 \leq T^* \leq 0.45$  three different solutions occur. However, only two of these solutions are physical because the free energy should be strictly convex as a function of the volume, this means that the compressibility  $\kappa_T$  is always positive [17],

$$\frac{1}{\kappa_T} \propto \left( \frac{\partial^2 f}{\partial V^2} \right)_{|T} \geq 0, \quad (53)$$

or similarly

$$\left( \frac{\partial p}{\partial V} \right)_{|T} \leq 0. \quad (54)$$

For  $1.04 \lesssim x \lesssim 1.1$  this is not the case, so that only two physical solutions for  $p^* = 2$  remain. In the non-physical range the free energy has a negative curvature, see Fig. 9, while it is physical everywhere else.

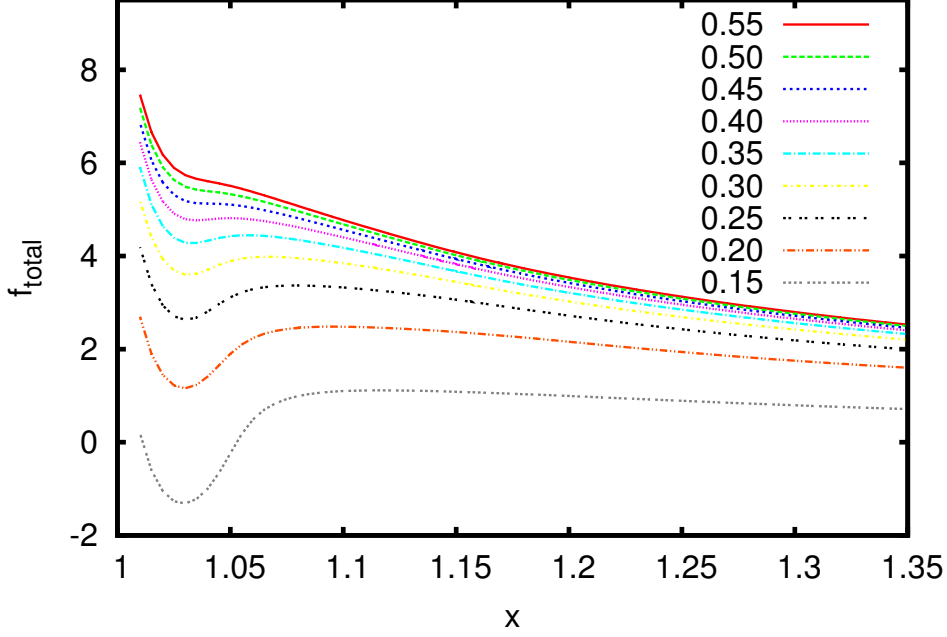


Figure 9: Total free energy per particle,  $f_{\text{total}}$ , over the distance  $x$  between the particle centers in a zigzag structure for different reduced temperatures  $T^*$  (as labeled).

At the first solution the particles are very densely packed, the distances between the particles are only a few percent larger than the densest possible packing. At the other solution the distances between the particle centers are about  $1.3\sigma$ . If the pressure search is started with a high density structure the high density solution is found; for a low-density starting structure the low-density solution is obtained. For temperatures higher than  $T^* \approx 0.45$  only low density crystals are formed, and for temperatures below  $T^* \approx 0.25$  only the dense packed solution exists at  $p^* \geq 2$ .

When the pressure is fixed to a value lower than  $p^* \approx 7$  the free energy changes discontinuously from the low density to the high density state as the temperature decreases. The actual position of this transition does, however, depend on the starting value of the density of the pressure search. In the region between the positions of the discontinuity obtained with a low and a high starting density the structure is meta-stable (see Sec. 4.4). In Fig. 10 the static contribution to the free energy,  $f_{\text{static}}$ , found for high and low starting densities at low reduced pressures  $p^*$  is shown.

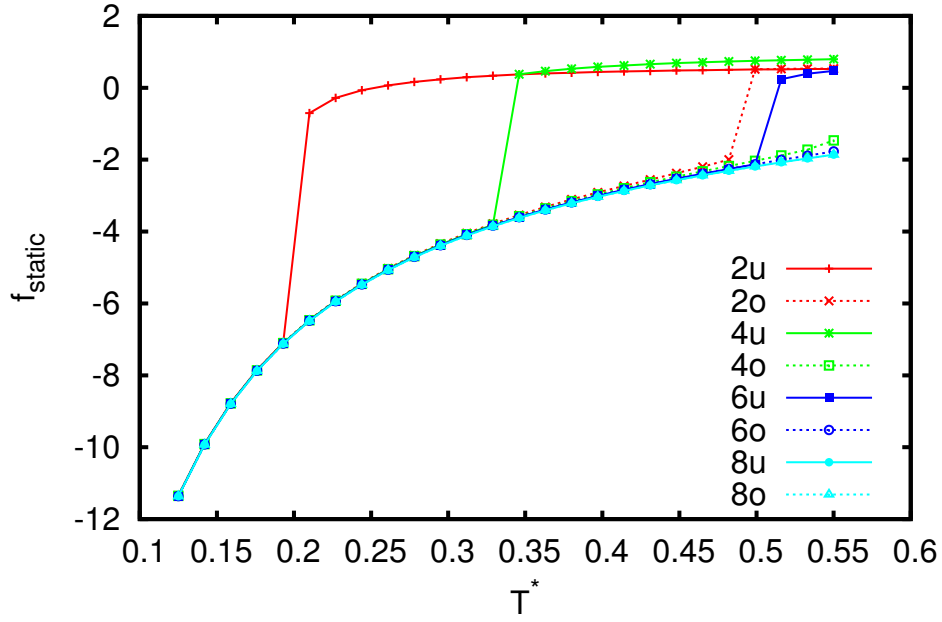


Figure 10: Static free energy per particle,  $f_{\text{static}}$ , over the reduced temperature  $T^*$  in a zigzag structure for low fixed pressures  $p^*$  (as labeled). 'u' denotes the high density, 'o' the low density starting configuration.

For larger pressures only the high density solution exists which becomes continuously less dense as the temperature increases, see Fig. 11.

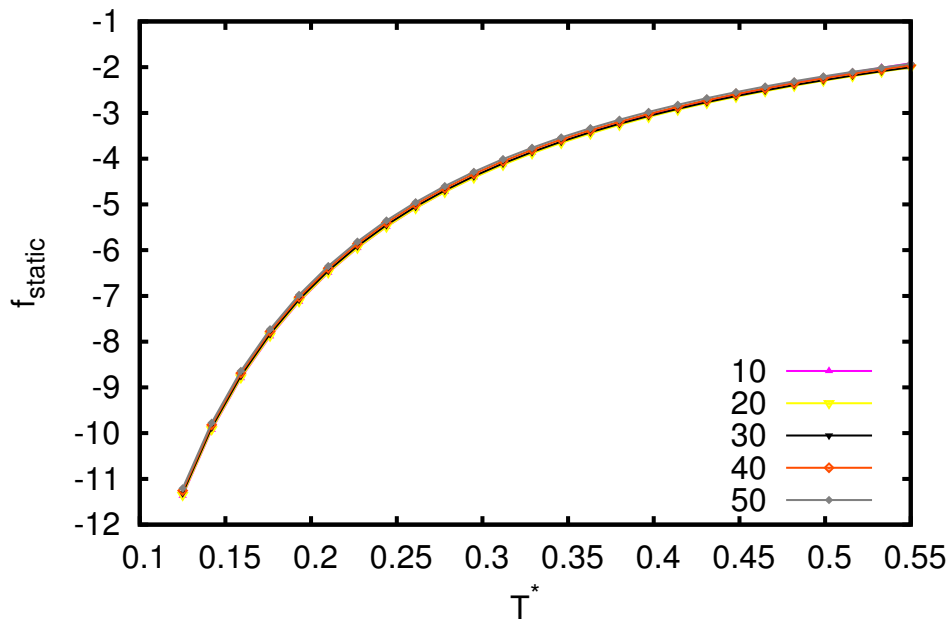


Figure 11: Static free energy per particle,  $f_{\text{static}}$ , over the reduced temperature  $T^*$  in a zigzag structure for high fixed pressures  $p^*$  (as labeled). The solution is independent of the density of the starting configuration.

Note that this discontinuity occurs also in the translational and rotational part of the free energy



(Figs. 12 and 13), it is however very small in  $f_{\text{rot}}$ .

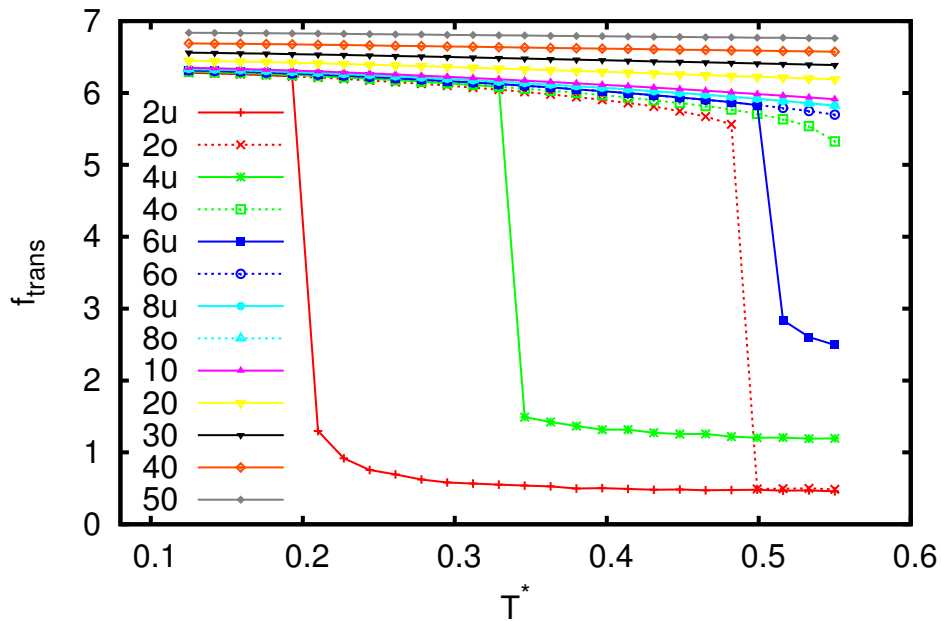


Figure 12: Translational part of the free energy per particle,  $f_{\text{trans}}$ , over the reduced temperature  $T^*$  in a zigzag structure for different pressures  $p^*$  (as labeled). 'u' denotes the high density, 'o' the low density starting configuration.

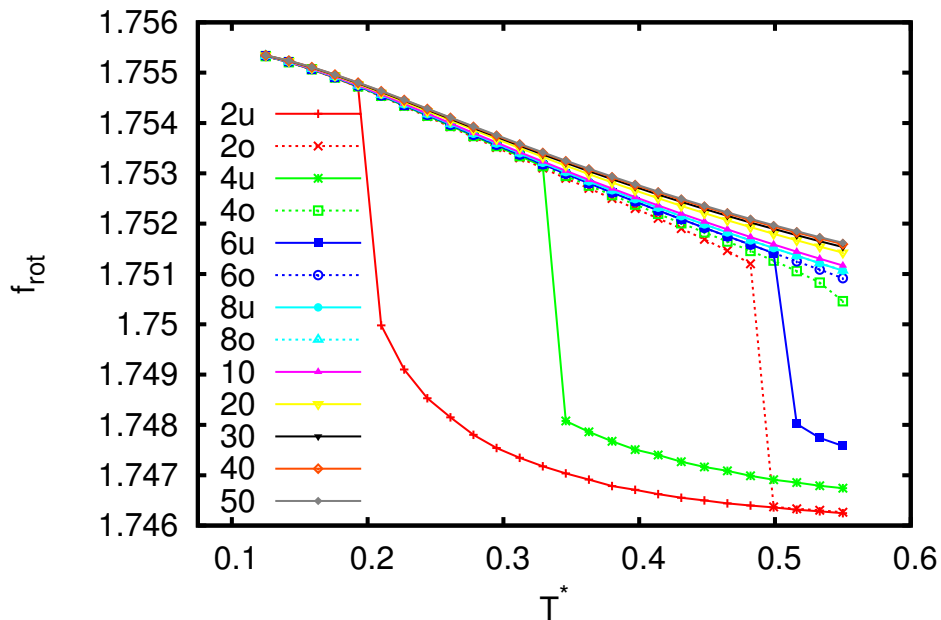


Figure 13: Rotational part of the free energy per particle,  $f_{\text{rot}}$ , over the reduced temperature  $T^*$  in a zigzag structure for different pressures  $p^*$  (as labeled). 'u' denotes the high density, 'o' the low density starting configuration.

Of course, the distance between the particles does mainly affect the translational deviations; both the spring constant  $t$  (right panel of Fig. 14) and  $\langle w^2 \rangle$  (left panel of Fig. 14) show

discontinuities for small fixed pressures. For higher pressures the spring constant  $t$  is shifted to larger values.

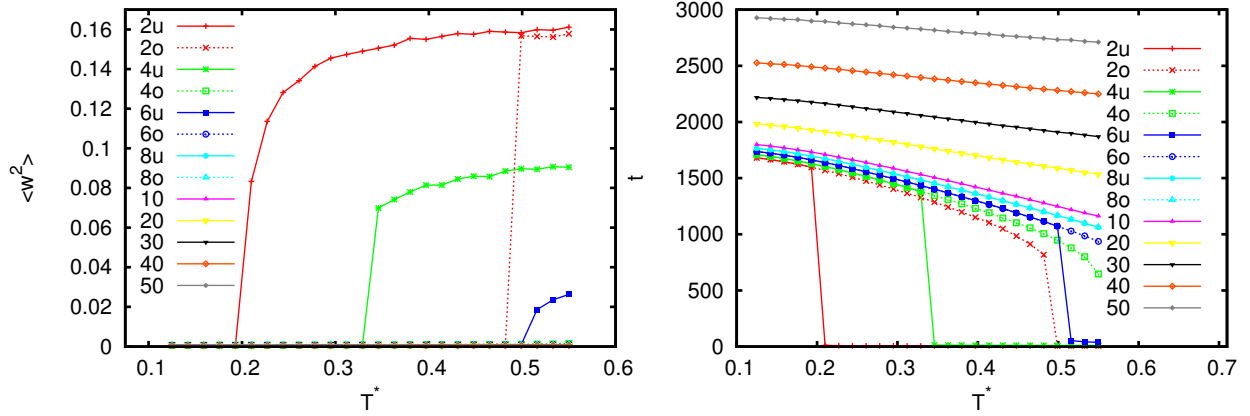


Figure 14: Translational mean square displacement  $\langle w^2 \rangle$  (left) and corresponding spring constant  $t$  (right) for zigzag crystals formed by Janus particles for different fixed pressures  $p^*$  (as labeled) over the reduced temperature  $T^*$ . 'u' denotes the high density, 'o' the low density starting configuration.

The rotational deviations  $\langle \theta^2 \rangle$  and the corresponding spring constant  $q$  also show discontinuities but are otherwise nearly unchanged by a change of pressure, see Fig. 15.

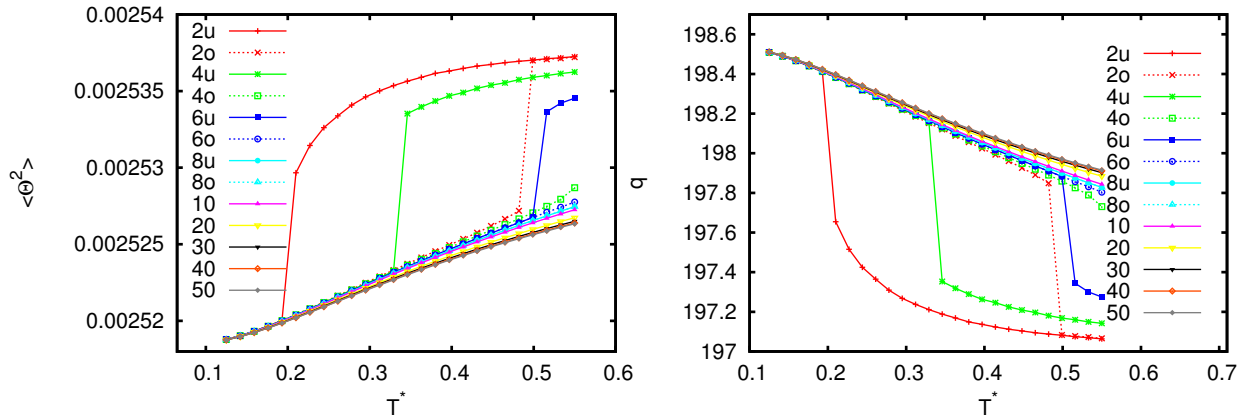


Figure 15: Rotational mean square displacement  $\langle \theta^2 \rangle$  (left) and spring constant  $q$  (right) for zigzag crystals formed by Janus particles for different fixed pressures  $p^*$  (as labeled) over the reduced temperature  $T^*$ . 'u' denotes the high density, 'o' the low density starting configuration.

For the construction of the phase diagram the phase coexistence boundaries where the pressure  $p^*$  and the chemical potential  $\mu$  are equal in both phases need to be evaluated. The chemical

potential is defined via the Gibbs free enthalpy  $G$  as

$$\begin{aligned}
\mu &= \left( \frac{\partial G}{\partial N} \right)_{|T,p} \\
&= \frac{\partial}{\partial N} (fN + pV) = f + p \left( \frac{\partial (NA_i)}{\partial N} \right)_{|T,p} \\
&= f + \eta \left( \frac{\partial f}{\partial \eta} \right)_{|T,p}.
\end{aligned} \tag{55}$$

Here the total area of the crystal,  $V$ , is rewritten in form of the Wigner-Seitz area of one particle:  $V = NA_i$ . The resulting chemical potential  $\mu$  at different constant pressures is shown in Fig. 16. We were not fully able to reproduce the curves from Ref. [5] since we could not calculate the chemical potential independently of the starting density. However it seems that a combination of the curves produced by a low and a high starting density, where always the lower value is taken, produces curves comparable to the results of Ref. [5].

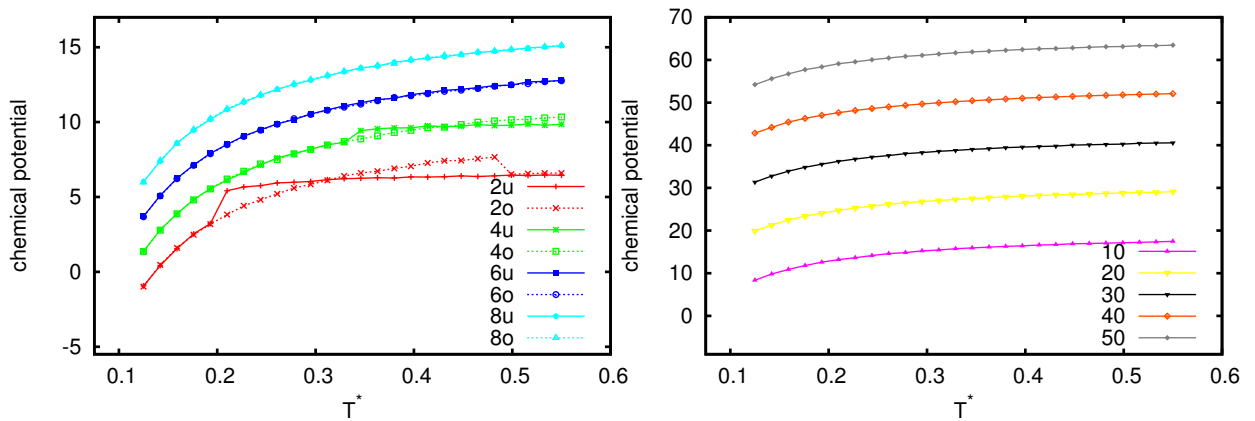


Figure 16: Chemical potential  $\mu$  (in units of  $k_B T^*$ ) over the reduced temperature  $T^*$  in the zigzag structure. The different lines correspond to different reduced pressures  $p^*$  (as labeled). For low pressures (left) the discontinuity in the free energy results in a kink in the chemical potential. High pressures (right) show no such kink. 'u' denotes the high density, 'o' the low density starting configuration.

#### 4.2.2 Trimer structure

In the trimer structure the Janus particles are at the same positions as in the zigzag structure but their orientations are different, they form only two bonds per unit cell (see Fig. 17). The wall potential is less restrictive compared to the wall potential for the zigzag crystal; the maximal angle which the central particle is allowed to rotate from its equilibrium orientation, so that no additional bonds are formed and no existing bonds are broken with respect to the equilibrium orientation, is  $\phi_0 = 35^\circ$ . The central and right panel of Fig. 17 show the trimer structure where the central particle is rotated by  $\pm\phi_0$ .

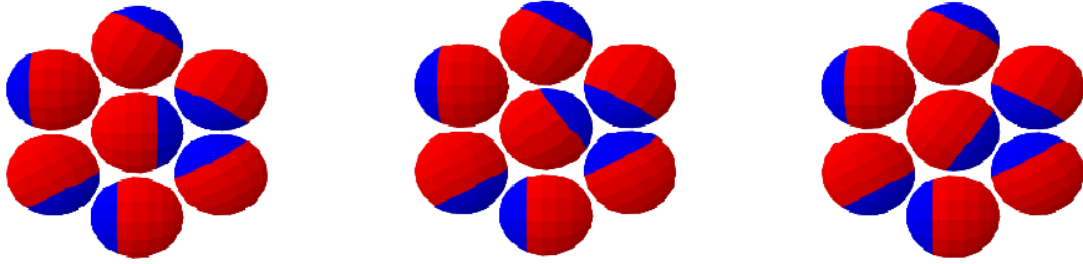


Figure 17: Unit cell of the trimer structure formed by Janus particles at equilibrium (left). A wall potential  $\phi_0$  is introduced to restrict the rotation of the central particle of the structure. This angle is given by the maximal rotation of the central particle from its equilibrium orientation for which no existing bonds are broken or additional ones are formed with respect to the equilibrium orientation. The structure where the central particle is rotated by this maximal rotation angle of  $\phi_0 = 35^\circ$  to the right and to the left is shown in the central and right panel, respectively.

A qualitatively similar behavior for the reduced pressure  $p^*$  as for the zigzag phase is found for the trimer lattice. As can be seen from Fig. 18 and 19 the solution of the pressure search for small pressures does again depend on the density of the starting structure.

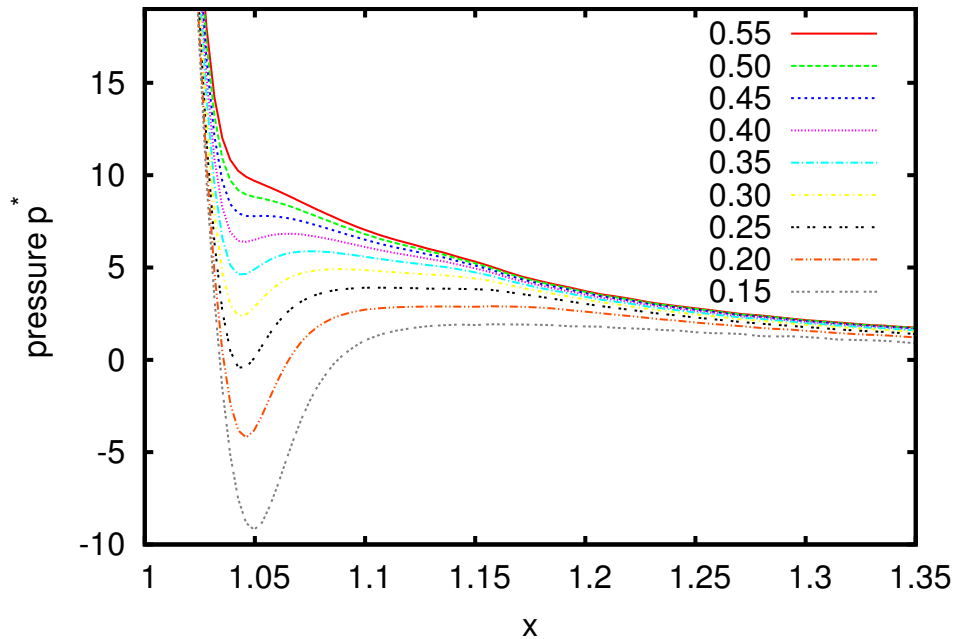


Figure 18: Reduced pressure  $p^*$  over the distance  $x$  between the particles in the trimer structure. The different lines correspond to different reduced temperatures  $T^*$  (as labeled).

For small pressures there seem to be three possible solutions, the free energy is however again only physical at two of these solutions.

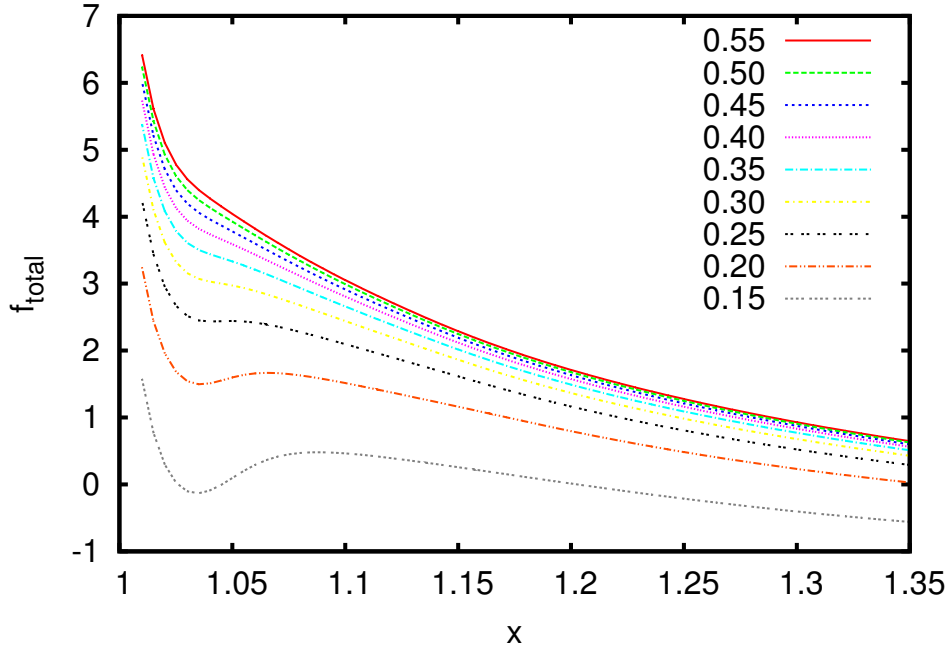


Figure 19: Total free energy per particle,  $f_{\text{total}}$ , over the distance  $x$  between the particles in the trimer structure for different reduced temperatures  $T^*$  (as labeled).

The isobars for the different contributions to the free energy show again discontinuities for small pressures. The actual position of these discontinuities also depends on the starting density of the calculations, as can be seen in Figs. 20 and 21 for the static part of the free energy, in Fig. 22 for the translational part and in Fig. 23 for the rotational part.

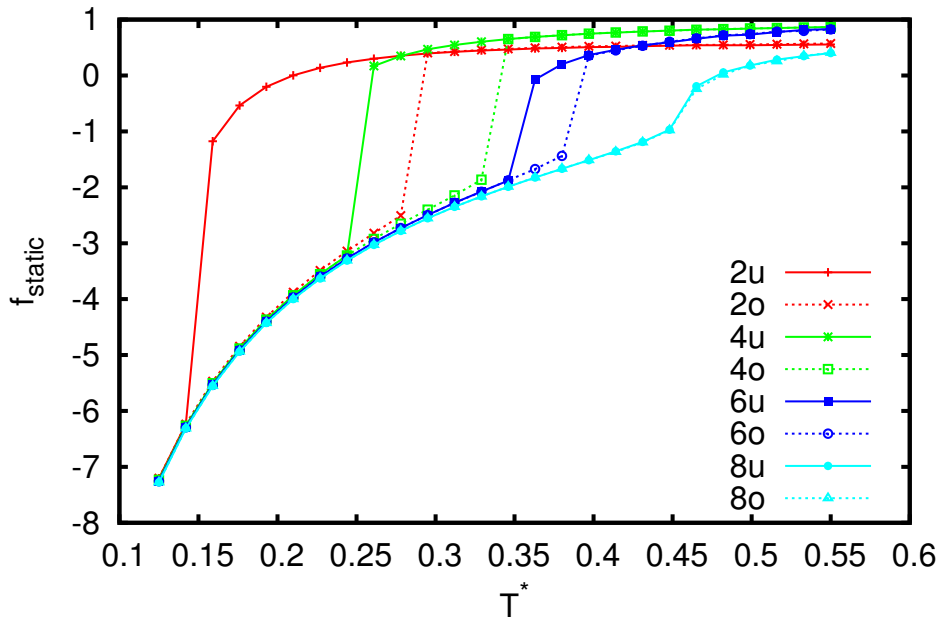


Figure 20: Static free energy per particle,  $f_{\text{static}}$ , over the reduced temperature  $T^*$  between the particles in the trimer structure for low fixed pressures  $p^*$  (as labeled). 'u' denotes the high density, 'o' the low density starting configuration.

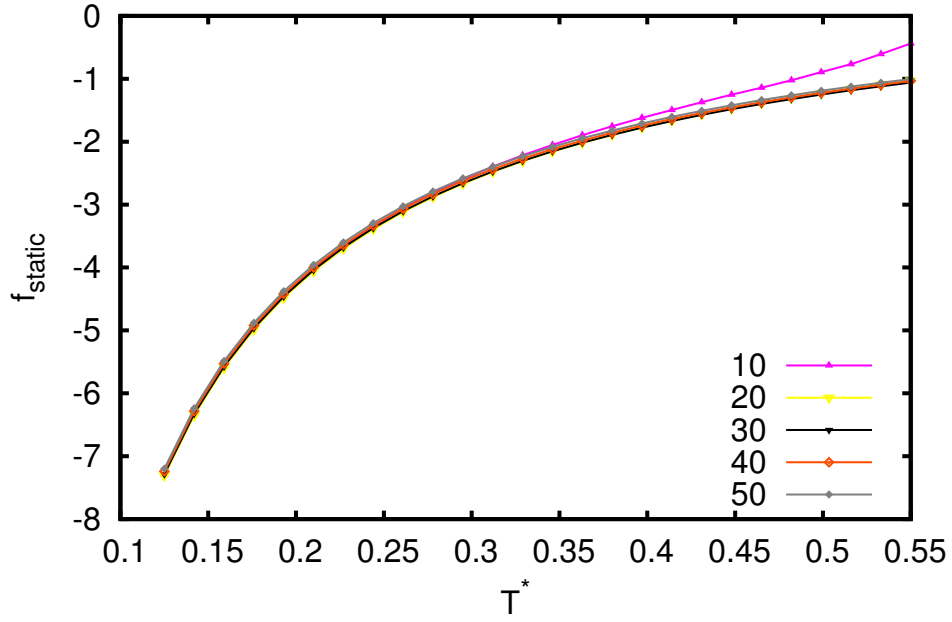


Figure 21: Static free energy per particle,  $f_{\text{static}}$ , over the reduced temperature  $T^*$  in the trimer structure for high fixed pressures  $p^*$  (as labeled). The solution is independent of the density of the starting configuration.

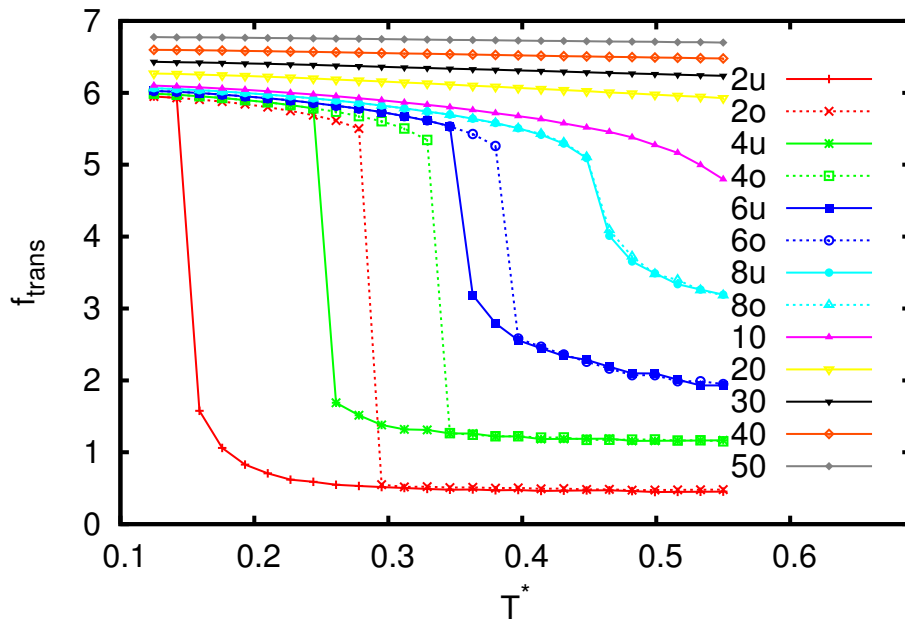


Figure 22: Translational part of the free energy per particle,  $f_{\text{trans}}$ , over the reduced temperature  $T^*$  in the trimer structure for different pressures  $p^*$  (as labeled). 'u' denotes the high density, 'o' the low density starting configuration.

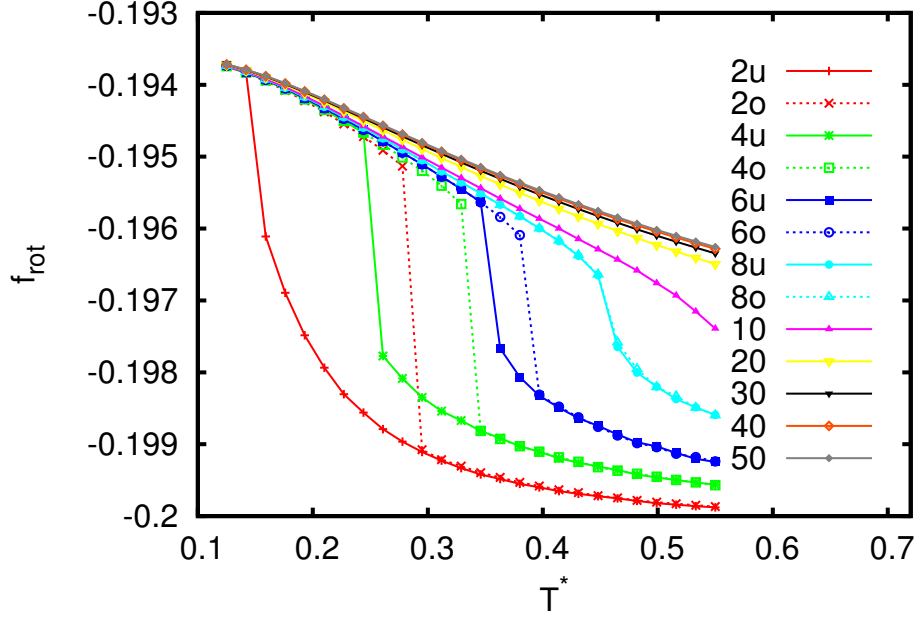


Figure 23: Rotational part of the free energy per particle,  $f_{\text{rot}}$ , over the reduced temperature  $T^*$  in the trimer structure for different pressures  $p^*$  (as labeled). 'u' denotes the high density, 'o' the low density starting configuration.

Since the translational deviations depend mainly on the positions of the particles (which are identical in the zigzag and trimer structures), the temperature dependence of the translational mean squared displacement  $\langle w^2 \rangle$  and the corresponding spring constant  $t$  for the trimer structure show only small differences with respect to the values obtained for the zigzag structure, see Fig. 24. The main difference is the discontinuity at low pressures which is observed at different temperatures for the trimer lattice.

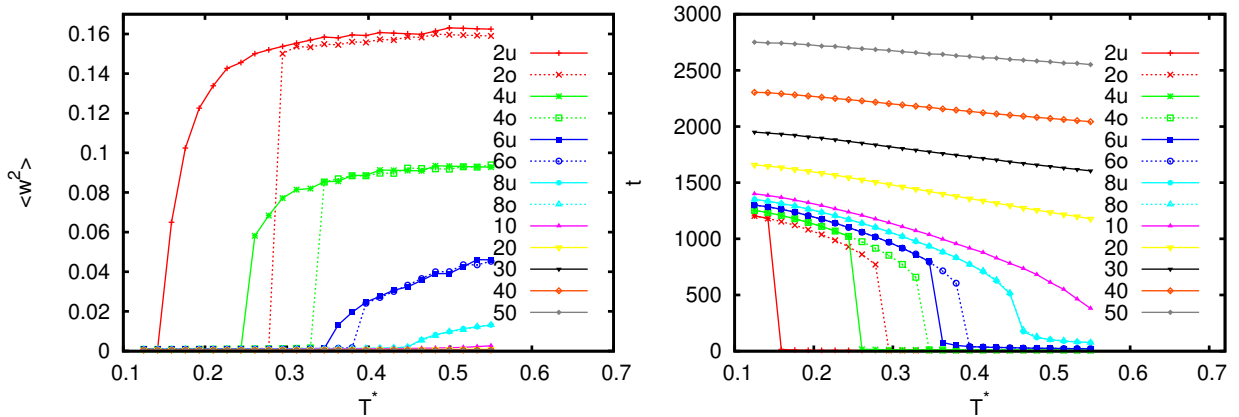


Figure 24: Translational mean square displacement  $\langle w^2 \rangle$  (left) and corresponding spring constant  $t$  (right) for trimer crystals formed by Janus particles for different fixed pressures  $p^*$  (as labeled) over the reduced temperature  $T^*$ . 'u' denotes the high density, 'o' the low density starting configuration.

Since the equilibrium orientations of the particles are different in the zigzag and trimer structure, the values of  $\langle \theta^2 \rangle$  and  $q$  for the trimer structure are significantly different from the values

obtained for the zigzag structure, see Fig 25; the spring constant  $q$  obtained for the trimer lattice is by a factor 50 smaller than the corresponding  $q$  for the zigzag lattice.

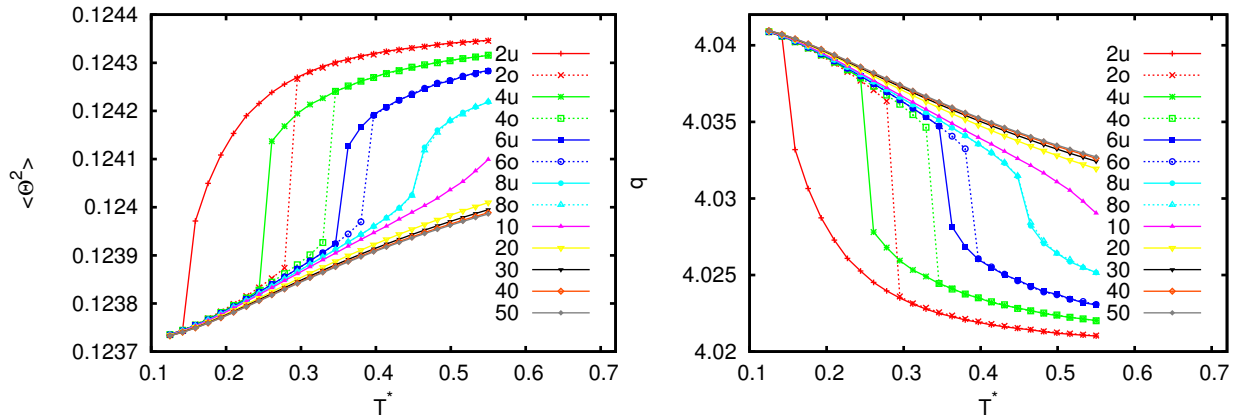


Figure 25: Rotational mean square displacement  $\langle \theta^2 \rangle$  (left) and spring constant  $q$  (right) for trimer crystals formed by Janus particles for different fixed pressures  $p^*$  (as labeled) over the reduced temperature  $T^*$ . 'u' denotes the high density, 'o' the low density starting configuration.

The chemical potential shows again kinks at low pressures while higher pressure isobars are essentially parallel and shifted to higher values with increasing pressure (Fig. 26). The transition from the low to the high pressure range occurs for both zigzag and trimer structure at  $p^* \approx 9$ .

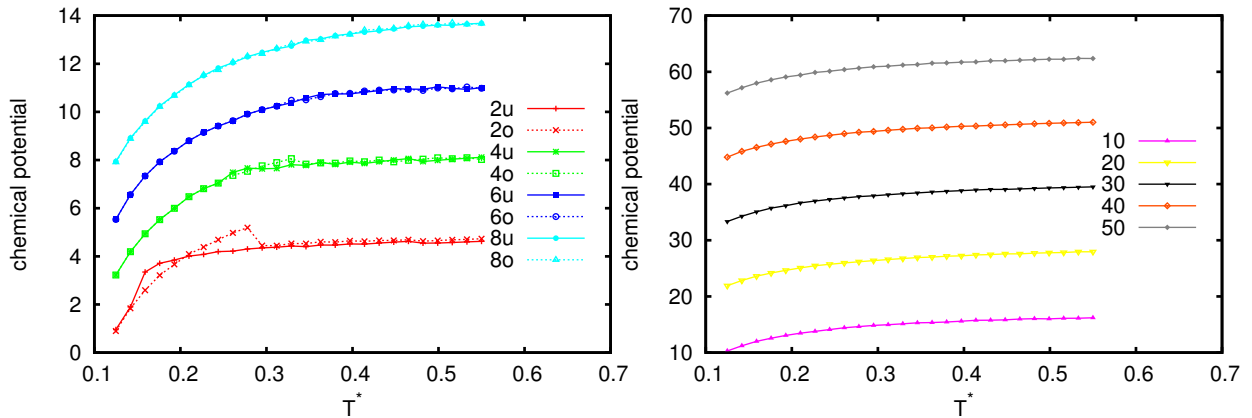


Figure 26: Chemical potential  $\mu$  (in units of  $k_B T^*$ ) over the reduced temperature  $T^*$  in a trimer structure formed by Janus particles. The different lines correspond to different reduced pressures  $p^*$  (as labeled). For low pressures (left) the discontinuity in the free energy results in a kink in the chemical potential. High pressures (right) show no such kink. 'u' denotes the high density, 'o' the low density starting configuration.

### 4.3 Plastic crystals

For the description of plastic crystals which are formed of statistically oriented Janus particles, the angular dependence of the potential is averaged out. Since the particles are three-dimensional objects the potential needs to be averaged over all orientations in  $\mathbb{R}^3$ . In our implementation we restricted the particle rotation to the  $(x, y)$ -plane, thus we only need to average over the planar



angle  $\theta$ . Since for Janus particles the angular part of the potential  $V(\theta, \theta') = \varepsilon$  is constant, the average potential is calculated as the ratio of the surface of the sphere which is covered by a patch with respect to the whole surface. A spherical cap of height  $h$  and radius  $r$  with opening angle  $\theta_0$  has the area  $A = 2\pi r h = 4\pi r^2 \sin^2(\theta_0/2)$ . The average potential is thus

$$\langle \varepsilon \rangle = \frac{\int \int V(\theta, \theta') d\Omega d\Omega'}{\int d\Omega \int d\Omega'} = \varepsilon \cdot \sin^4(\theta_0/2). \quad (56)$$

The  $h(\mathbf{w}_i)$  function for plastic crystals is calculated similar to the case of orientationally dependent crystals, see Equ. (42); however, since the potential does no longer depend on the deviation  $\theta_c$  with respect to the equilibrium orientation, the angular part  $J(\theta_i)$  of Equ. (44) simplifies to

$$J(\theta_i) = \left( e^{\langle \varepsilon \rangle / 2} - 1 \right). \quad (57)$$

Further, since the angular freedom is now completely eliminated no angular wall potential is needed. The Taylor expansion of the effective potential consists only of a constant and a translational part, namely

$$v_e(\mathbf{w}_i) \approx \varepsilon + \gamma w_i^2. \quad (58)$$

For plastic crystals only the self-consistency equation for the translational deviations  $w_i$  of Equ. (45) needs to be met. The static and translational part of the free energy are defined analogously to the case of rotationally ordered particles, see Eqs. (28) and (47), while the rotational contribution is constant [5],

$$f_{\text{rot}} = -\ln\left(\int_0^{2\pi} d\theta_i\right) = -\ln(2\pi). \quad (59)$$

The calculation of the pressure is now nearly independent of the starting pressure, as can be seen in the static free energy,  $f_{\text{static}}$ , shown in Fig. 27 and in its translational part,  $f_{\text{trans}}$ , displayed in Fig. 28.

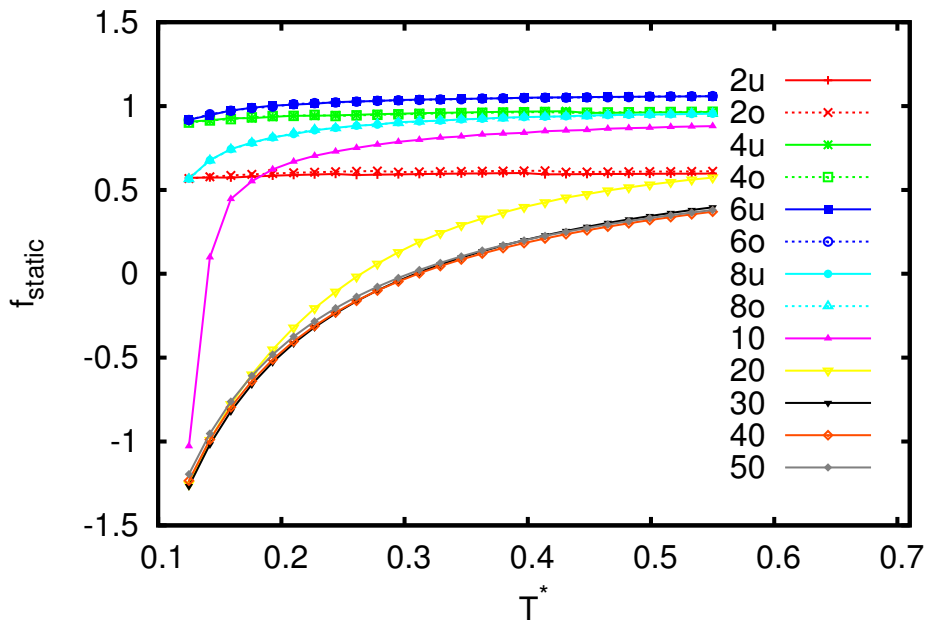


Figure 27: Static free energy per particle,  $f_{\text{static}}$ , over the reduced temperature  $T^*$  for plastic crystals for fixed pressures  $p^*$  (as labeled). 'u' denotes the high density, 'o' the low density starting configuration.

The low and high pressure curves are again distinctly different but for plastic crystals they pass continuously from one to the other as the pressure decreases.

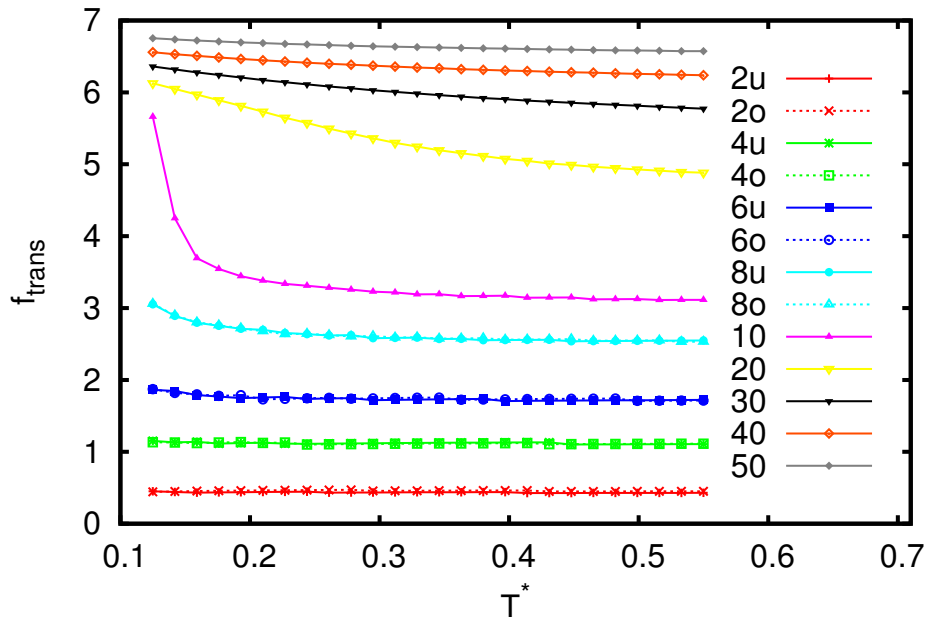


Figure 28: Translational part of the free energy per particle,  $f_{\text{trans}}$ , over the reduced temperature  $T^*$  in plastic structure for different pressures  $p^*$  (as labeled). 'u' denotes the high density, 'o' the low density starting configuration.

The mean squared displacement  $\langle w^2 \rangle$  and the corresponding spring constant  $t$  are shown in Fig. 29. These quantities show no discontinuity as functions of  $T^*$ , they are in the same range as the corresponding values for the trimer and the zigzag structures.

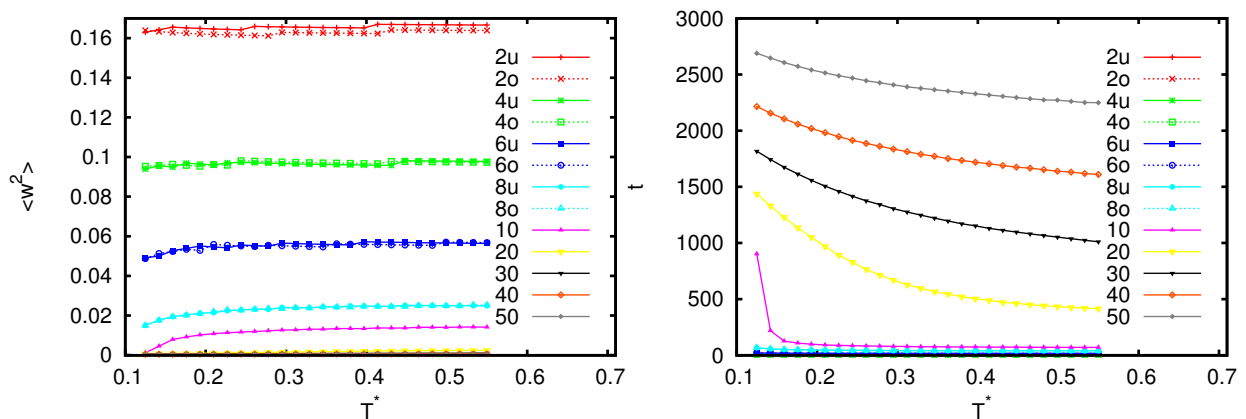


Figure 29: Translational mean square displacement  $\langle w^2 \rangle$  (left) and corresponding spring constant  $t$  (right) for plastic crystals formed by Janus particles for different fixed pressures  $p^*$  (as labeled) over the reduced temperature  $T^*$ . 'u' denotes the high density, 'o' the low density starting configuration.

The chemical potential  $\mu$  for fixed pressures is nearly constant for the temperature range studied here (Fig. 30).

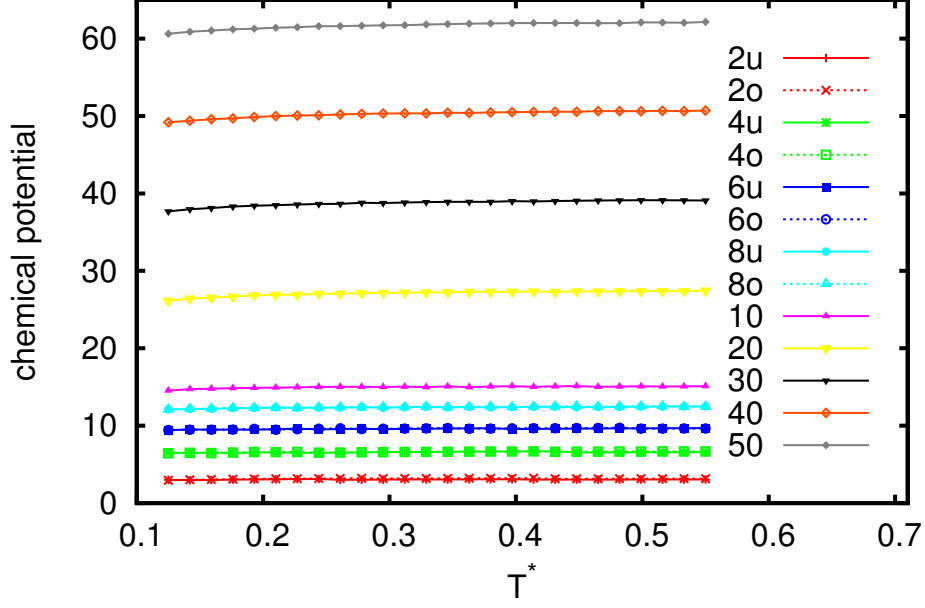


Figure 30: Chemical potential  $\mu$  (in units of  $k_B T^*$ ) over the reduced temperature  $T^*$  for plastic crystals formed by Janus particles. The different lines correspond to different reduced pressures  $p^*$  (as labeled). 'u' denotes the high density, 'o' the low density starting configuration.

#### 4.4 Phase diagram for two dimensional Janus crystals

Equating the chemical potentials at fixed pressures and temperatures of the different structures, points of phase coexistence can be determined. For comparison with the results of Ref. [5] our data is shown for the pressures  $p^* = 2$  and  $p^* = 50$  in Fig. 31.

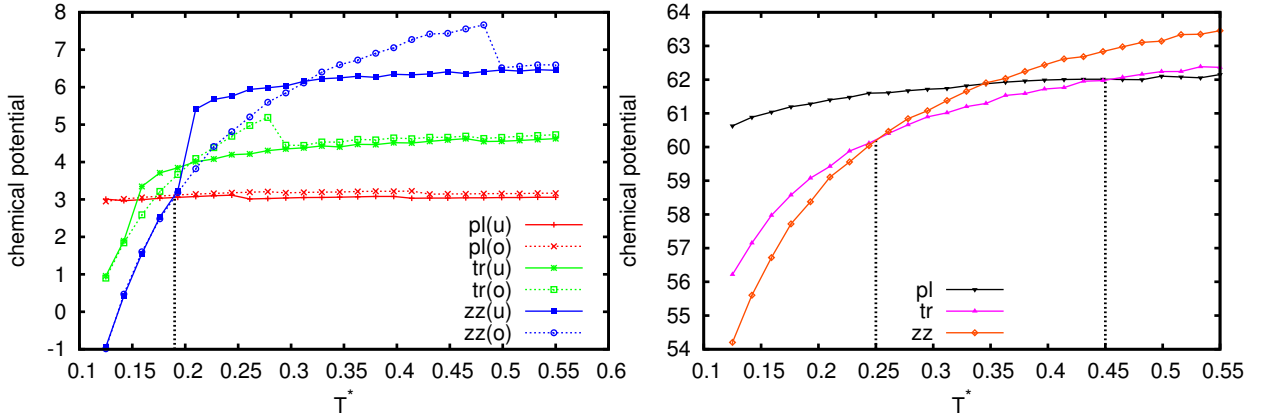


Figure 31: Coexistence points of the zigzag (zz), trimer (tr) and plastic crystals (pl) formed by Janus particles in two dimensions are found at points where the chemical potential and the reduced temperature are equal at both phases at a constant pressure  $p^* = 2$  (left) and  $p^* = 50$  (right). 'u' denotes the high density, 'o' the low density starting configuration.

For pressure  $p^* = 2$  the zigzag phase is stable up to a temperature of  $T^* \approx 0.19$ , where a tran-

sition to the plastic phase occurs. The trimer phase is meta-stable over the whole temperature range investigated. At a pressure of  $p^* = 50$  two transitions are found: for temperatures up to  $T^* \approx 0.25$  the zigzag phase is stable, above this value the trimer structure is found and at high temperatures above  $T^* = 0.45$  the plastic phase occurs.

## 5 SCP for inverse patchy colloids in two dimensions

### 5.1 Ordered crystals

The SCP approach presented in Sec. 4 for Janus colloids can be easily extended to two-dimensional crystals formed by two-patch IPCs, making only minor changes in the formalism necessary. For simplicity we will restrict ourselves to colloids with symmetrical patches. Only the  $h$ -function will change considerably because the IPC potential has an angular and positionally dependent potential within the interaction range  $\sigma < r < \sigma + \delta$ .

Using polar coordinates, the  $h$ -function for ordered two-dimensional structures can be split into a sum of three parts, namely

$$h(\mathbf{R}_i - \mathbf{w}_i, \theta_i) = h_{\text{HS}}(W) - h_{\text{SW}}(W) + h_{2\text{IPC}}(\mathbf{R}_i, \mathbf{w}_i, \theta_i), \quad (60)$$

where  $h_{\text{HS}}(W)$  and  $h_{\text{SW}}(W)$  originate from the hard-sphere and the square well part of the potential and are given by the same integrals as arose for Janus particles, see Eqs. (41) and (43). For  $h_{2\text{IPC}}(\mathbf{R}_i, \mathbf{w}_i, \theta_i)$  the central particle (index 'c') moves in the angular-dependent potential arising from particle  $i$  within the interaction range. The potential is averaged over all possible positions, specified in polar coordinates as  $(a, \varphi)$ , and orientations, corresponding to the planar deviation angle  $\theta_c$  of particle  $c$ . Thus  $h_{2\text{IPC}}(\mathbf{R}_i, \mathbf{w}_i, \theta_i)$  is given by

$$h_{2\text{IPC}}(\mathbf{R}_i, \mathbf{w}_i, \theta_i) = \frac{t\sqrt{q/\pi}}{\pi\text{erf}(\sqrt{q}\pi)} \int_{\sigma}^{\sigma+\delta} da a \int_{-\pi}^{\pi} d\theta_c \int_0^{2\pi} d\varphi e^{-\frac{1}{2}E_{ic}(a, \varphi, \theta_c, \theta_i)} e^{2taW \cos \varphi} e^{-q\theta_c^2} e^{-t(a^2+W^2)} \quad (61)$$

The two particle energy  $E_{ic}(a, \varphi, \theta_c, \theta_i)$  between two IPCs is calculated via the coarse grained model introduced in Sec. 2.2. It depends on the distance  $a$  between particle  $i$  and the central particle, as well as on the  $\varphi$ -coordinate of the spatial integration, which changes the relative orientation of the particles. The rotational deviation of the central particle from its equilibrium orientation is given by the planar rotational angle  $\theta_c$ . The energy  $E_{ic}$  can be written as a sum of overlap volumes  $w_i$  of interaction spheres weighted by the respective energy factors  $u_i$ , see Equ. (9) and Ref. [13]. The contributions of the overlap of the big colloidal spheres, the small patch spheres and the big with the small spheres sum up; therefore they factorize in the averaging factor  $\exp(-\frac{1}{2}E_{ic})$ . The energy  $E_{ic}$  can be divided into a part  $E_a$  which depends only on the actual distance  $a$  between the particles, a part  $E_1$  that depends on the distance  $a$  and the angle  $\varphi$  and a part  $E_2$  that needs to be evaluated anew when the orientation of the central particle  $c$  changes. They are given by

$$E_a(a) = E_{\text{BB}} \quad (62)$$

$$E_1(a, \varphi) = E_{\text{B}_c\text{S}_i} \quad (63)$$

$$E_2(a, \varphi, \theta_c) = E_{\text{B}_i\text{S}_c} + E_{\text{SS}}, \quad (64)$$

where  $E_{\text{BB}}$  is the energy from the overlap of two interacting negatively charged bodies (big spheres) of the central colloid and of particle  $i$ .  $E_{\text{B}_c\text{S}_i}$  and  $E_{\text{B}_i\text{S}_c}$  are both energies emerging from overlaps of the body and one of the patches (small spheres). The first energy stems from an overlap of the body of the central particle and thus the energy does not change under rotations of the central particle; however, the second term stems from the interaction of a patch of the central particle and therefore needs to be evaluated anew each time  $\theta_c$  changes.  $E_{\text{SS}}$  is a sum of energies calculated by the overlap of all possible two patch combinations.

Thus  $h_{2\text{IPC}}(\mathbf{R}_i, \mathbf{w}_i, \theta_i)$  becomes

$$h_{2\text{IPC}}(\mathbf{R}_i, \mathbf{w}_i, \theta_i) = \frac{t\sqrt{q/\pi}}{\pi\text{erf}(\sqrt{q}\pi)} \left[ \int_{\sigma}^{\sigma+\delta} da a e^{-\frac{1}{2}E_a(\mathbf{R}_i, \mathbf{w}_i)} e^{-t(a^2+W^2)} A(\mathbf{R}_i, \mathbf{w}_i, \theta_i) \right], \quad (65)$$

$$A(\mathbf{R}_i, \mathbf{w}_i, \theta_i) = \int_0^{2\pi} d\varphi e^{2taW \cos \varphi} e^{-\frac{1}{2}E_1(\mathbf{R}_i, \mathbf{w}_i)} \int_{-\pi}^{\pi} d\theta_c e^{-q\theta_c^2} e^{-\frac{1}{2}E_2(\mathbf{R}_i, \mathbf{w}_i, \theta_i)}. \quad (66)$$

Since the colloids are decorated by two symmetrical patches the integration range of  $\theta_c$  is symmetrical with respect to 0 and can be rewritten as

$$\int_{-\pi}^{\pi} d\theta_c e^{-q\theta_c^2} e^{-\frac{1}{2}E_2(\mathbf{R}_i, \mathbf{w}_i, \theta_i)} = 2 \cdot \int_0^{\pi} d\theta_c e^{-q\theta_c^2} e^{-\frac{1}{2}E_2(\mathbf{R}_i, \mathbf{w}_i, \theta_i)}. \quad (67)$$

The rest of the integrals leading to the function  $h_{2\text{IPC}}(\mathbf{R}_i, \mathbf{w}_i, \theta_i)$  need to be evaluated numerically.

Since a priori we do not have an estimate for the spring constant  $t$ , we use an approximation of the Bessel function  $I_0(x)$  (where  $t$  occurs in the argument  $x = 2taW$ ) for the evaluation of the functions  $h_{\text{HS}}(W)$  and  $h_{\text{SW}}(W)$  that differs from the one used for Janus particles. Instead of the large argument approximation (see Equ. (49)) we use a polynomial approximation which, according to [16], has an error  $|\varepsilon| \leq 1.9 \cdot 10^{-7}$  for positive arguments.

The remaining steps of the SCP procedure are similar to the ones applied to the Janus colloids. The angular wall potential is again defined via an angle  $\phi_0$ . We define  $\phi_0$  as the angle at which the attractive part of the potential, which stems from an overlap of a colloidal body with one of the patches, becomes zero. For the calculation of this angle, only overlaps of the form big-small which are non-zero in the equilibrium state are used. Actually this angle could depend on the distance of the particles but we choose to always use the value obtained when the particles are in contact.

## 5.2 Plastic crystals

For plastic crystals the potential  $V_{\text{IPC}}(r, \theta, \varphi, \theta', \varphi')$  needs to be averaged over the angular degrees of freedom. In this section we restricted ourselves to two-dimensional structures where deviations in the orientation occur only in the  $(x, y)$ -plane. Those structures are formed by three-dimensional particles so that the averaging is done over all orientations in  $\mathbb{R}^3$ . We study only colloids with two symmetric patches which are aligned along the  $x$ -axis so that the only non-trivial rotations are those around the  $y$ - and  $z$ -axis. The two-particle potential  $V_{\text{IPC}}(r, \theta, \phi, \theta', \phi')$  depends in the interaction range  $\sigma < r < \sigma + \delta$  on the actual distance  $r$  between the center of the particles and on the rotation angle around the  $z$ -axis,  $\varphi$ , and around the  $y$ -axis,  $\theta$ , of both particles.

The averaged potential  $\langle \varepsilon \rangle$  can be calculated via

$$\begin{aligned} \langle \varepsilon \rangle &= \frac{\int d\theta \sin \theta d\varphi \int d\theta' \sin \theta' d\varphi' V_{\text{IPC}}(r, \theta, \varphi, \theta', \varphi')}{\int d\Omega \int d\Omega'} \\ &= E_{\text{BB}} + \frac{1}{2\pi} \int_0^{2\pi} d\varphi \int_0^{\pi} d\theta \sin \theta E_{\text{B'S}}(r, \theta, \varphi) + \\ &+ \frac{1}{(4\pi)^2} \int_0^{2\pi} d\varphi \int_0^{\pi} d\theta \sin \theta \int_0^{2\pi} d\varphi' \int_0^{\pi} d\theta' \sin \theta' E_{\text{SS'}}(r, \theta, \varphi, \theta', \varphi'). \end{aligned} \quad (68)$$

For IPCs the averaged potential depends still on the distance  $r$  of the particles so that the  $h_{2\text{IPC}}$ -function for plastic crystals becomes

$$\begin{aligned} h_{2\text{IPC}}^{\text{pl}}(\mathbf{w}_i) &= \frac{t}{\pi} \int_{r=\sigma}^{\sigma+\delta} dr r e^{-\frac{1}{2}\langle\varepsilon\rangle(r)} e^{-t(r^2+W^2)} \int_0^{2\pi} d\varphi e^{2trW \cos\varphi} \\ &= 2t \int_{r=\sigma}^{\sigma+\delta} dr r e^{-\frac{1}{2}\langle\varepsilon\rangle(r)} e^{-t(r^2+W^2)} I_0(2trW), \end{aligned} \quad (69)$$

where again the modified spherical Bessel function of the first kind  $I_0(x)$ , was used.

### 5.3 Results

In the following we apply the SCP approach to two candidate structures which were previously found in self-assembly studies using Monte Carlo simulations (see Ref. [6]). These investigations showed that a wide variety of two-dimensional structures can occur, depending on the relative charge of the body and the patches of the IPCs. In the Monte Carlo simulation a wall was introduced to enforce quasi two-dimensional structures, this wall could also carry a surface charge. However, the approach presented here is solely two-dimensional so that no wall is required. The colloid particles are chosen in accordance with Ref. [6]; the colloids have an opening angle of  $\theta_0 = 60^\circ$  and an interaction range of  $\delta = 0.4\sigma$  (corresponding to  $\kappa\sigma = 5$ ,  $\kappa\delta = 2$ ).

The two candidate structures are shown in Fig. 32: A triangular structure (labeled 'g-triangles' in [6]) and a square structure, (called 'f-triangles' in [6]) where the particles form squares.



Figure 32: The investigated 2-dimensional crystal structures formed by IPCs: a triangular structure formed by charged colloids (left) and a square structure formed by neutral colloids (right).

The triangular structure is investigated using charged colloids with a total charge of  $Z_{\text{tot}} = -\frac{2}{9}Z_{\text{p}}$ , where  $Z_{\text{p}}$  denotes the charge of a patch. The orientation of the particles was taken from Ref. [6] and is presented in Fig. 33.

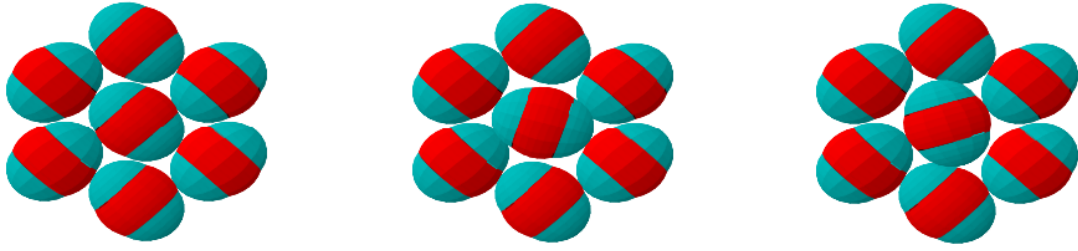


Figure 33: Equilibrium position and orientation of the triangular crystal structure formed by charged IPCs (left). The central and the right panel show the structure when the central particle is rotated by the maximal allowed angle of  $\phi_0 = \pm 27.27^\circ$  with respect to its equilibrium orientation.

The free energy per particle,  $f$ , obtained for different reduced temperatures  $T^*$  for this structure is shown in Fig. 34. The dependence of  $f$  on the distance  $x$  between the particles is as expected, it increases continuously as the density increases.

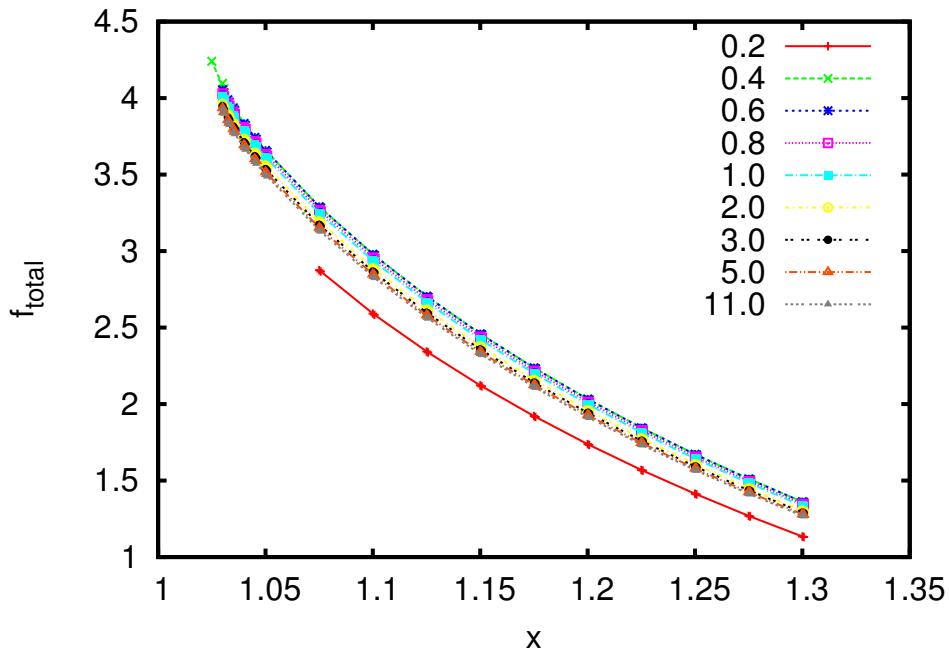


Figure 34: Free energy per particle,  $f_{\text{total}}$ , for a triangular structure formed by IPCs over the distance  $x$  between the particles for different reduced temperatures  $T^*$  (as labeled).

However, we did encounter severe numerical problems for small temperatures since the spring constant  $t$  becomes for very dense structures so large that even calculations using quattro precision could not process the occurring values. For  $T^* = 0.4$  this limit of the program is already reached at particle distances of  $x = 1.05$  while for higher reduced temperatures structures with  $x \approx 1.03$  can still be considered. In the following figures for the free energy  $f$  the smallest possible distance  $x$  between the particles is used as lower boundary of each curve.

For the reduced pressure  $p^*$  we used the definition of Equ. (52). The reduced pressure  $p^*$  for the triangular structure is also quite well-behaved. For large distances between the particles



it changes very slowly and is nearly constant with respect to the temperature. For very dense crystals the reduced pressure  $p^*$  increases rapidly and shows a stronger dependence on the temperature than in the low pressure regime.

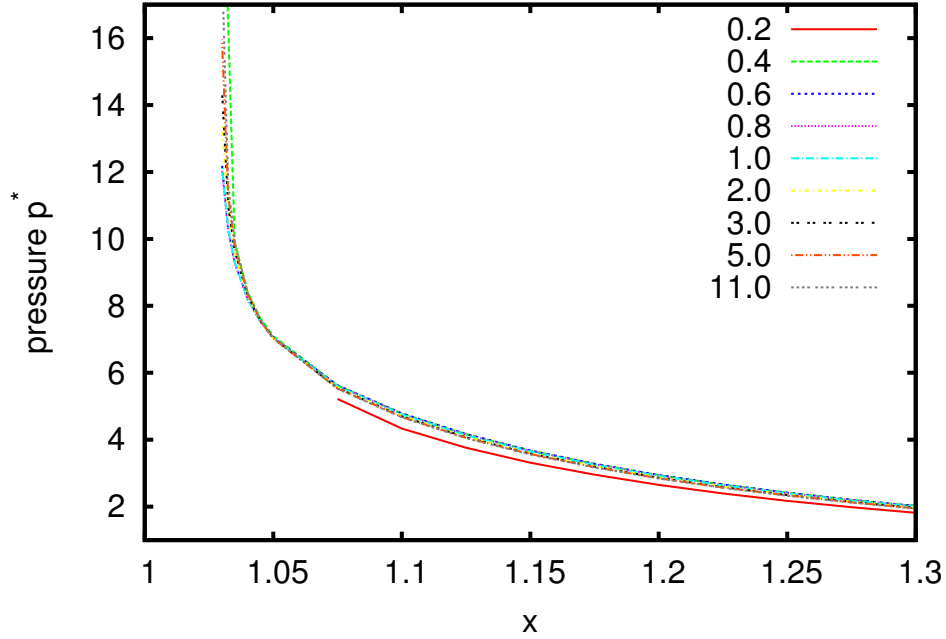


Figure 35: Reduced pressure  $p^*$  for a triangular structure formed by IPCs over the distance  $x$  between the particles for different temperatures  $T^*$  (as labeled).

The second structure investigated is a square structure formed by overall neutral IPCs ( $Z_{\text{tot}} = Z_c + 2Z_p = 0$ ). The equilibrium orientation of the particles is orthogonal, see Fig. 36. The free energy per particle  $f$  (Fig. 37) and the reduced pressure  $p^*$  (Fig. 38) show a similar behavior as compared to the corresponding curves for the triangular structure.

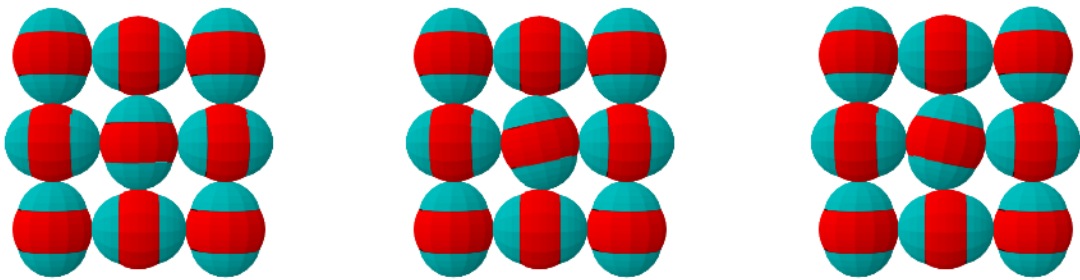


Figure 36: Equilibrium position and orientation of the square crystal structure formed by neutral IPCs (left). The central and the right panel show the structure when the central particle is rotated by the maximally allowed angle of  $\phi_0 = \pm 11.54^\circ$  with respect to its equilibrium orientation.

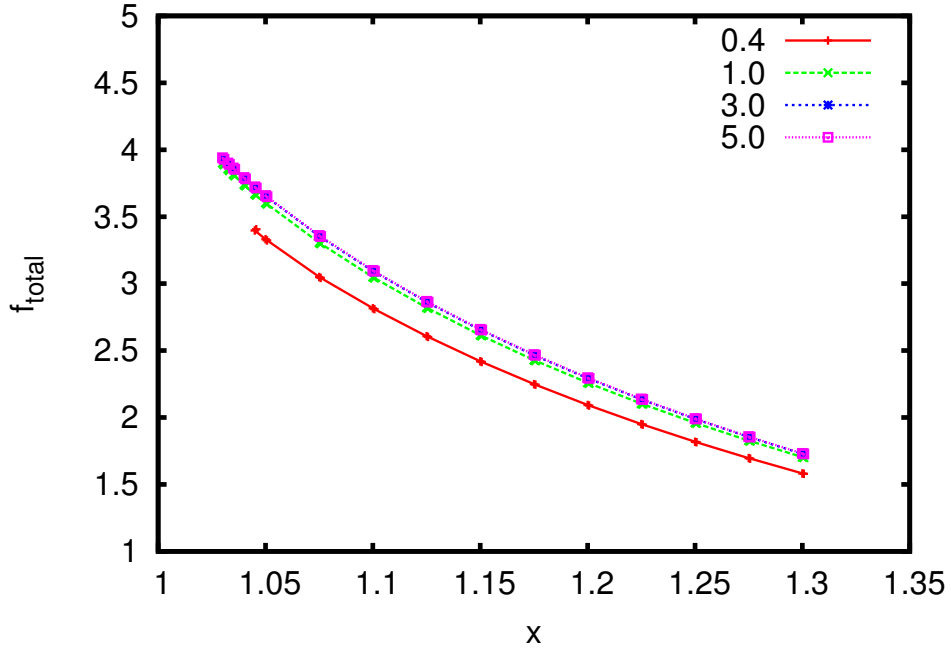


Figure 37: Free energy per particle  $f_{\text{total}}$  for a square structure formed by IPCs over the distance  $x$  between the particles for different reduced temperatures  $T^*$  (as labeled).

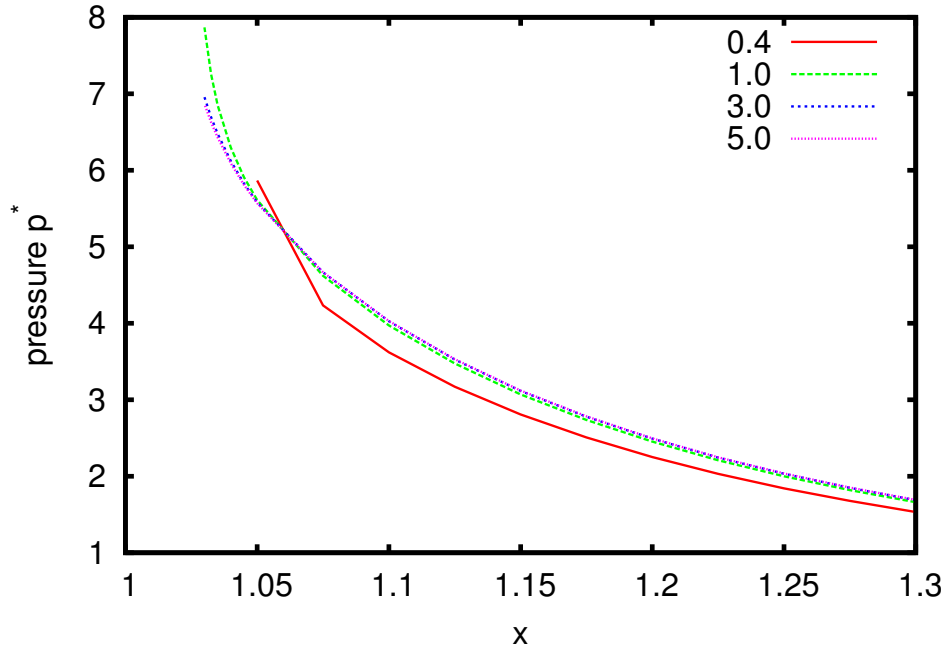


Figure 38: Reduced pressure  $p^*$  for a square structure formed by IPCs over the distance  $x$  between the particles for different temperatures  $T^*$  (as labeled).

Additionally, we considered plastic versions of the triangular and of the square structures shown in Fig. 32, but instead of the patch ordering shown there the particles are now statistically oriented. The averaged potential  $\langle \varepsilon \rangle$ , evaluated via Equ. 68, for both structures is shown in Fig. 39. Since the square structure is build by overall neutral particles, while the triangular structure is formed by colloids with a small overall charge, the average potentials  $\langle \varepsilon \rangle$  of the two plastic structures are slightly different.

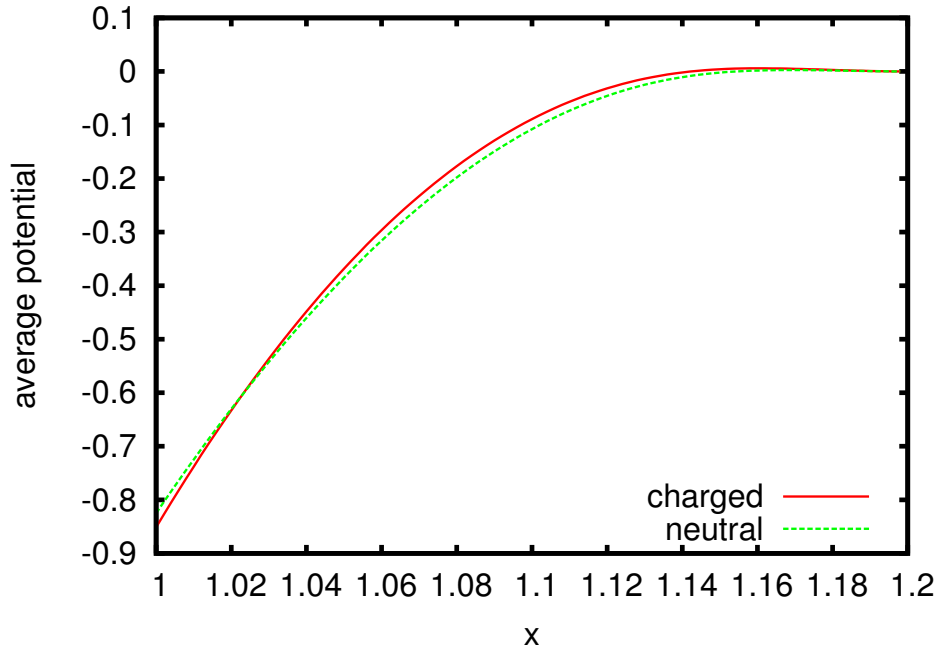


Figure 39: The average potential  $\langle \varepsilon \rangle$  over the distance  $x$  between the particles for overall neutral and charged colloids (for charges see text) as used for the simulation of the square and triangular structure formed by IPCs.

The SCP procedure gives also very reasonable results for the free energy per particle  $f$  for the plastic triangular structure, see Fig. 40. The values of the free energies  $f$  of the plastic and the triangular structures are over a wide distance range comparable. At very low distances, the free energy  $f$  of the plastic structure increases more rapid than the corresponding value of the ordered structure. Note, that the formalism applied to plastic structures works well in a slightly different temperature and distance range than the formalism applied to ordered structures.

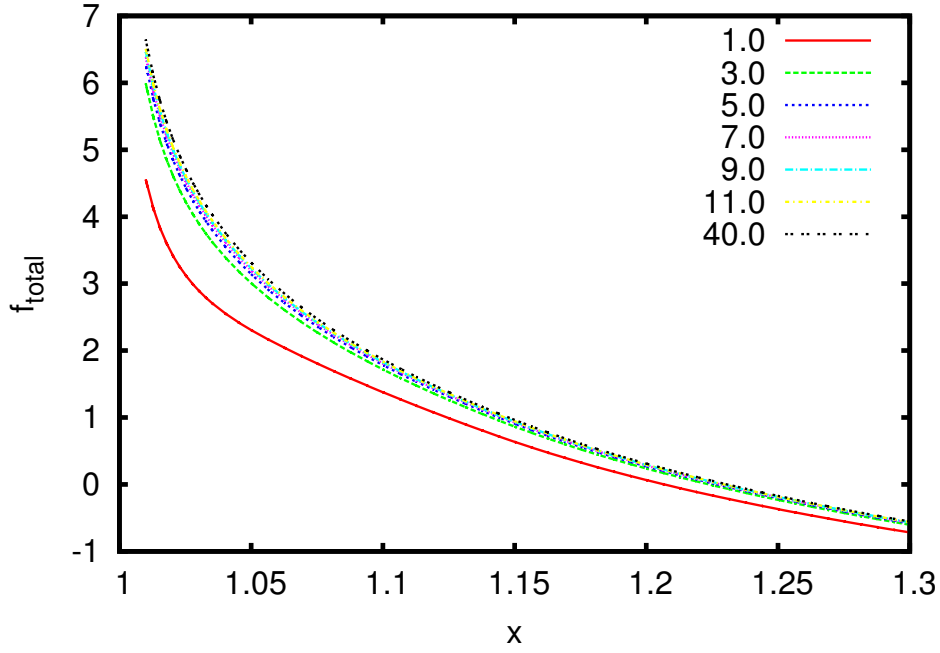


Figure 40: Free energy per particle  $f$  over the distance  $x$  between the particles in the plastic triangular structure formed by IPCs for different temperatures  $T^*$  (as labeled).

The reduced pressure  $p^*$  of the densely packed plastic triangular structure is nearly a magnitude higher than the pressure occurring in the ordered triangular structure, see Fig. 41.

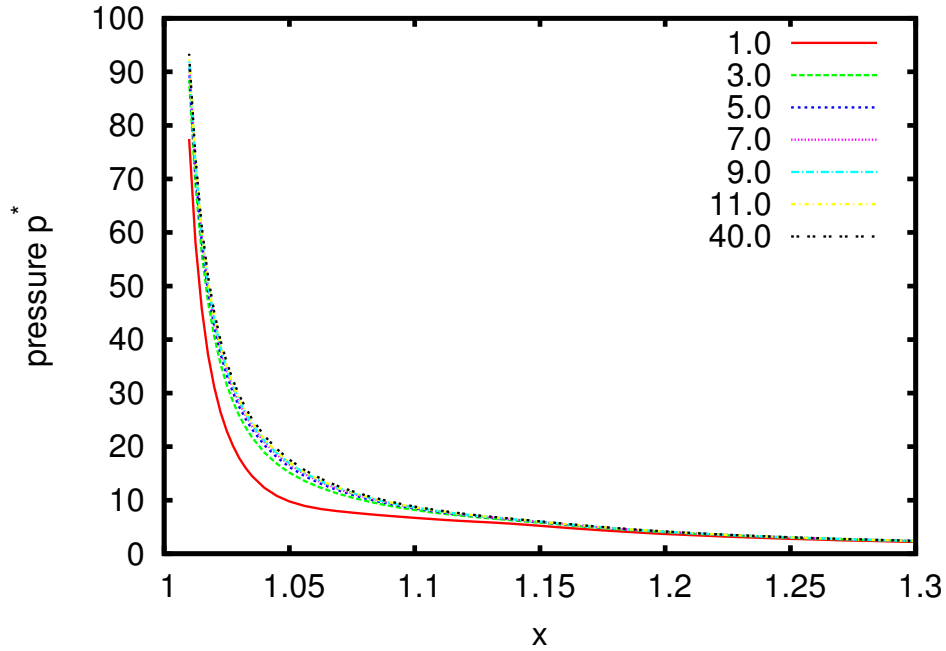


Figure 41: The reduced pressure  $p^*$  of the plastic triangular structure formed by randomly oriented IPCs over the distance between the particles for different temperatures  $T^*$  (as labeled).

For the plastic square structure formed by statistically oriented IPCs the SCP approach results in the free energy curves reported in Fig. 42. In the low density range it decreases slowly with

increasing distance  $x$  between the particles.

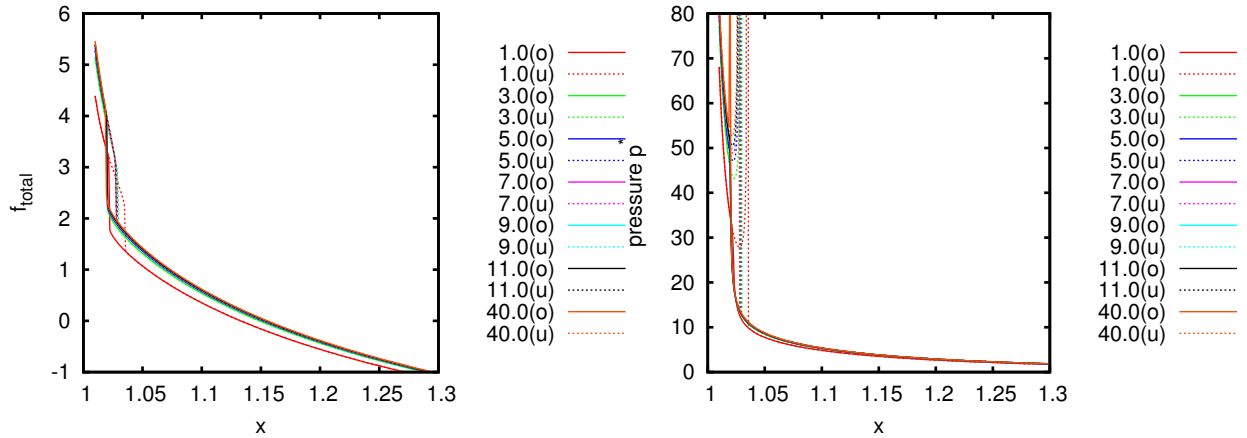


Figure 42: Free energy per particle  $f$  (left) and reduced pressure  $p^*$  for a plastic square structure formed by IPCs over the distance  $x$  between the particles for different temperatures  $T^*$  (as labeled). The singularity in the pressure curve is caused by the numerical discontinuity in the corresponding free energy. 'o' denotes a large starting distance ( $x = 1.4$ ), 'u' a small starting distance ( $x = 1.02$ ).

For smaller distances a discontinuity in the free energy occurs which results in a singularity in the reduced pressure  $p^*$ , see Fig. 43, that is of course unphysical. It is, however, quite probable that the free energy does not show a discontinuity but rather a step kink which cannot easily be distinguished from a discontinuity in numerical results. A kink in the free energy results in a discontinuity in the pressure and thus indicates a first order phase transition.

The position of this kink depends on the direction from which the distance  $x$  is approached: If it is approached from distances larger than  $x$  the kink occurs at  $x \approx 1.02$  (curves labeled 'o' in Fig. 43), if it is approached from distances lower than  $x$  it occurs at  $1.025 \lesssim x \lesssim 1.035$  ('u' in Fig. 43). The position of the kink is shifted to slightly smaller values as the temperature  $T^*$  increases, until, for  $T^* \gtrsim 7$  the position of the kinks does no longer depend on  $T^*$ .

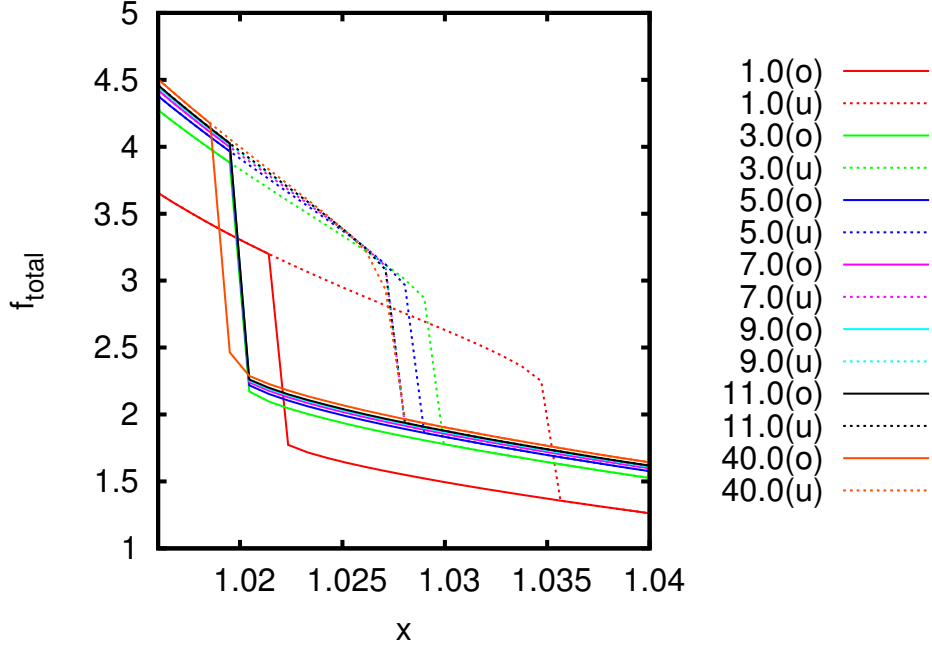


Figure 43: The free energy per particle  $f$  for a plastic square structure formed by IPCs calculated via the SCP procedure shows a steep kink over the distance  $x$  between the particles. The free energy depends on the direction from which the distance  $x$  is approached; 'o' denotes a large starting distance ( $x = 1.4$ ), 'u' a small starting distance ( $x = 1.02$ ).

This steep kink in the total free energy per particle exists in the static contribution,  $f_{\text{static}}$ , as well as in the translational contribution,  $f_{\text{trans}}$ , see Fig. 44.

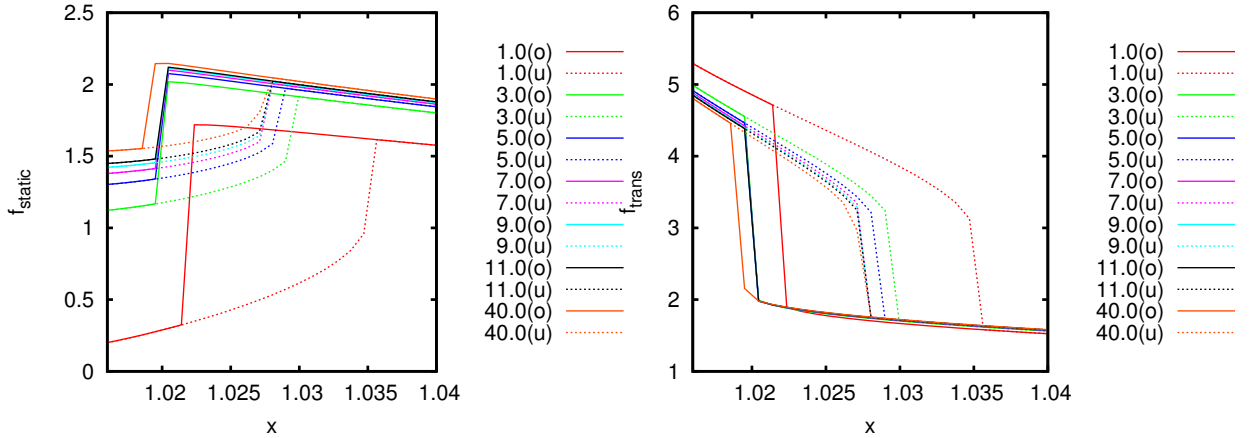


Figure 44: Static (left) and translational (right) contribution to the free energy per particle  $f$  for the plastic square structure formed by randomly oriented IPCs over the distance  $x$  between the particles at different reduced temperatures  $T^*$  (as labeled). For distances  $1.02 \leq x \leq 1.36$  the free energy depends on the direction from which the distance  $x$  is approached; 'o' denotes a large starting distance ( $x = 1.4$ ), 'u' a small starting distance ( $x = 1.02$ ).

The steep kink is also present in the mean squared displacement  $\langle w^2 \rangle$  and the spring constant  $t$  (Fig. 45).

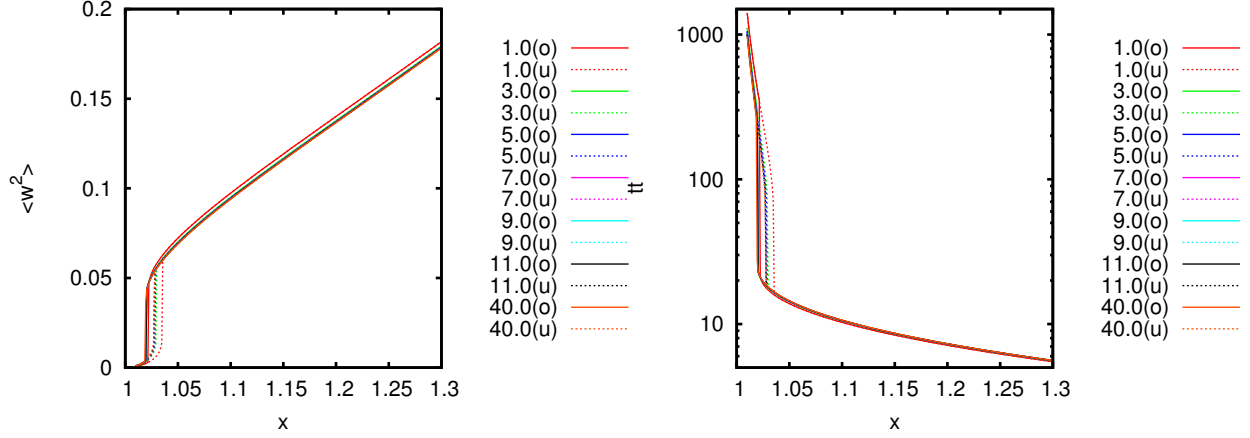


Figure 45: Mean square displacement  $\langle w^2 \rangle$  and corresponding spring constant  $t$  for a plastic square crystal formed by randomly orientated IPCs over the distance  $x$  between the particles for different temperatures  $T^*$  (as labeled). 'o' denotes a large starting distance ( $x = 1.4$ ), 'u' a small starting distance ( $x = 1.02$ ).

A possible reason for this kink is that the averaging of the potential does not fully represent the behavior of the particles in a plastic crystal. Although the particles in a real plastic crystal are randomly oriented, they still interact differently, depending on which areas of the surface overlap. However, in the SCP formalism all areas interact via the same averaged potential.

The kink probably indicates the plastic structure with this averaged potential would not be stable over the whole density range investigated, but rather a transition to a different structure would occur. As soon as the density is low enough for the central particle to interact with the particles at the corner of the unit cell, the particles would form a different structure, a hexagonal or other close packed structure, where a larger number of particles can interact.

When comparing the results for the structures discussed above one has to keep in mind that the behavior of the particles in a real plastic crystal may not be fully represented and thus the results obtained may have considerable errors.

In Fig. 46 the dependence of the free energy per particle  $f$  on the reduced temperature  $T^*$  is shown for the triangular ('gt'), the square structure ('ft') and the corresponding plastic structures ('gp' and 'fp'). The free energy of the structures is nearly constant over the whole temperature range, only at very low temperatures a rapid decrease of the free energy per particle is observed. For the plastic structures a considerably lower free energy is obtained than for the ordered structures.

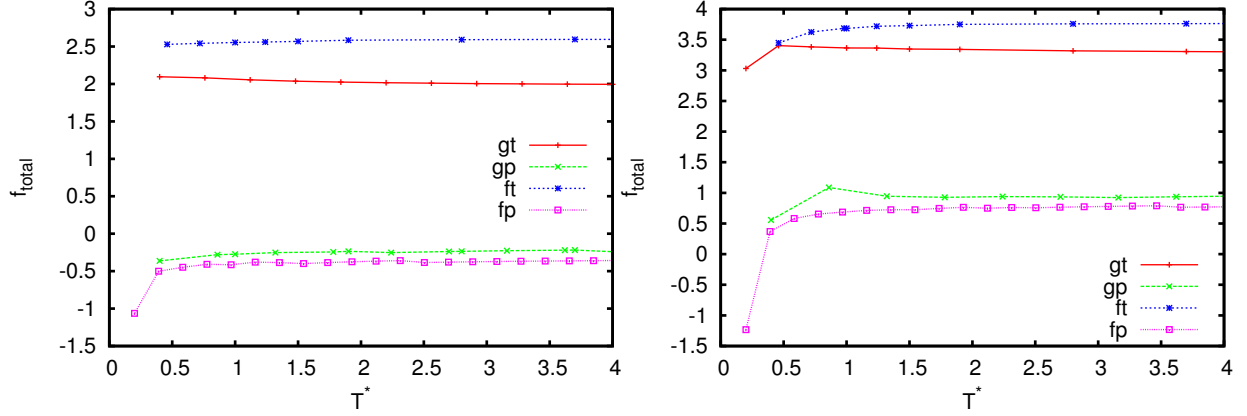


Figure 46: Total free energy per particle  $f$  at constant reduced pressure  $p^* = 3$  (left) and  $p^* = 6$  (right) over the temperature  $T^*$  for the ordered triangular structure ('gt'), the ordered square structure ('ft') and the plastic triangular ('gp') and square structure ('fp').

As discussed, the free energy per particle, consists of a static, a translational and a rotational contribution, which are displayed in Fig. 47, Fig. 48 and Fig. 49 at constant reduced pressures  $p^* = 3$  and  $p^* = 6$ . To a great extent all the contributions are independent of the reduced temperature  $T^*$ , small deviations occur only at very low temperatures.  $f_{\text{static}}$  and  $f_{\text{trans}}$  depend strongly on the reduced pressure  $p^*$ ; the values of the free energy contributions of the different structures assume more comparable values the higher the pressure becomes. The rotational contribution,  $f_{\text{rot}}$ , is independent of the pressure, however, it varies greatly from structure to structure. The different values of the total free energy per particle  $f$  for the plastic and ordered structures result to a great extent from the different rotational contributions  $f_{\text{rot}}$ .

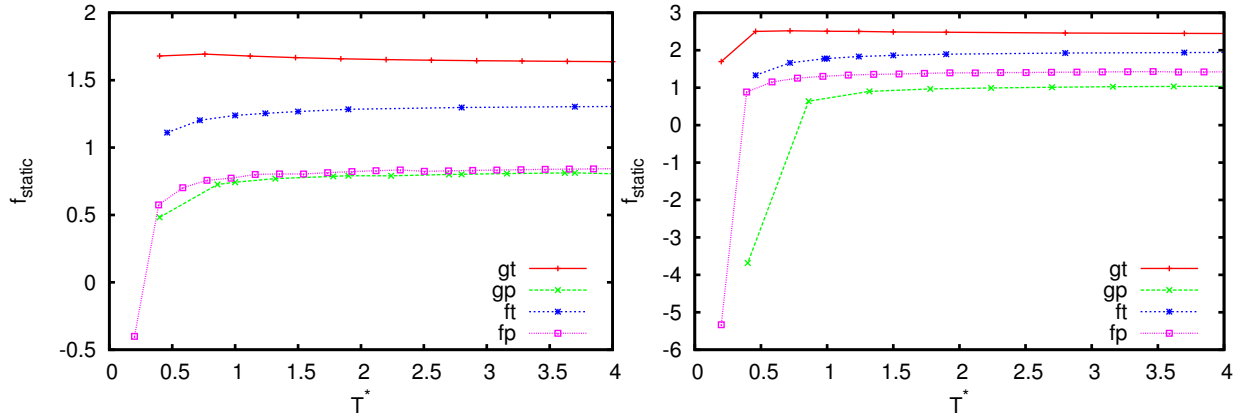


Figure 47: Static contribution  $f_{\text{static}}$  to the free energy per particle at constant reduced pressure  $p^* = 3$  (left) and  $p^* = 6$  (right) over the temperature  $T^*$  for the ordered triangular structure ('gt'), the ordered square structure ('ft') and the plastic triangular ('gp') and square structure ('fp').



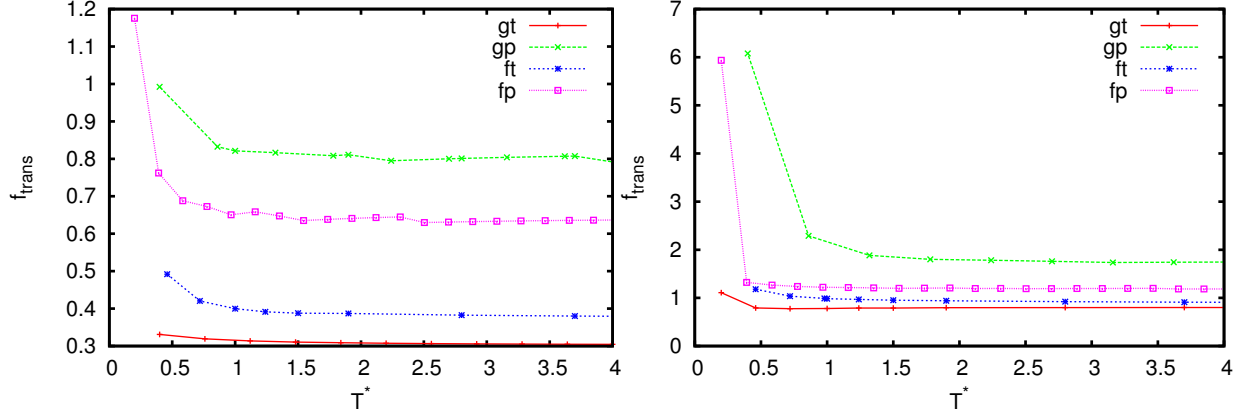


Figure 48: Translational contribution  $f_{\text{trans}}$  to the free energy per particle at constant reduced pressure  $p^* = 3$  (left) and  $p^* = 6$  (right) over the temperature  $T^*$  for the ordered triangular structure ('gt'), the ordered square structure ('ft') and the plastic triangular ('gp') and square structure ('fp').

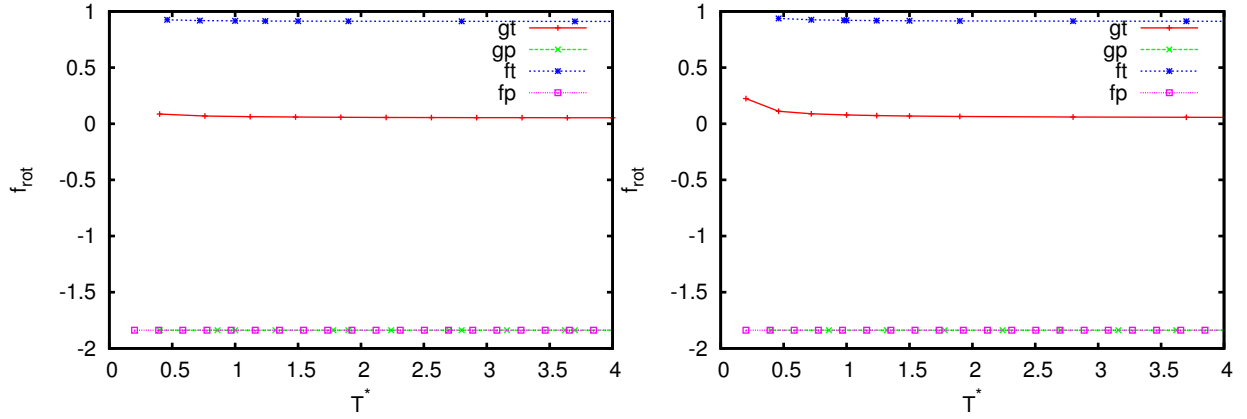


Figure 49: Rotational contribution  $f_{\text{rot}}$  to the free energy per particle at constant reduced pressure  $p^* = 3$  (left) and  $p^* = 6$  (right) over the temperature  $T^*$  for the ordered triangular structure ('gt'), the ordered square structure ('ft') and the plastic triangular ('gp') and square structure ('fp').

The mean square displacement  $\langle w^2 \rangle$  is shown in Fig. 50 for two different reduced pressures  $p^*$ . Naturally, they assume smaller values as the pressure increases. The corresponding spring constants  $t$  are depicted in Fig. 51. Since the spring constant increases strongly as the pressure increases, crystals under high pressures can not be easily considered.

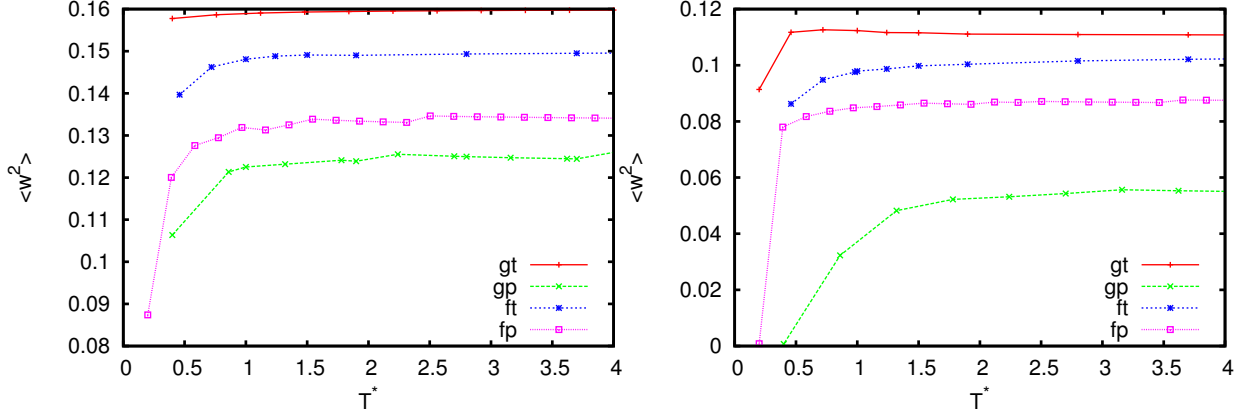


Figure 50: Mean squared displacement  $\langle w^2 \rangle$  at constant reduced pressure  $p^* = 3$  (left) and  $p^* = 6$  (right) over the temperature  $T^*$  for the ordered triangular structure ('gt'), the ordered square structure ('ft') and the plastic triangular ('gp') and square structure ('fp').

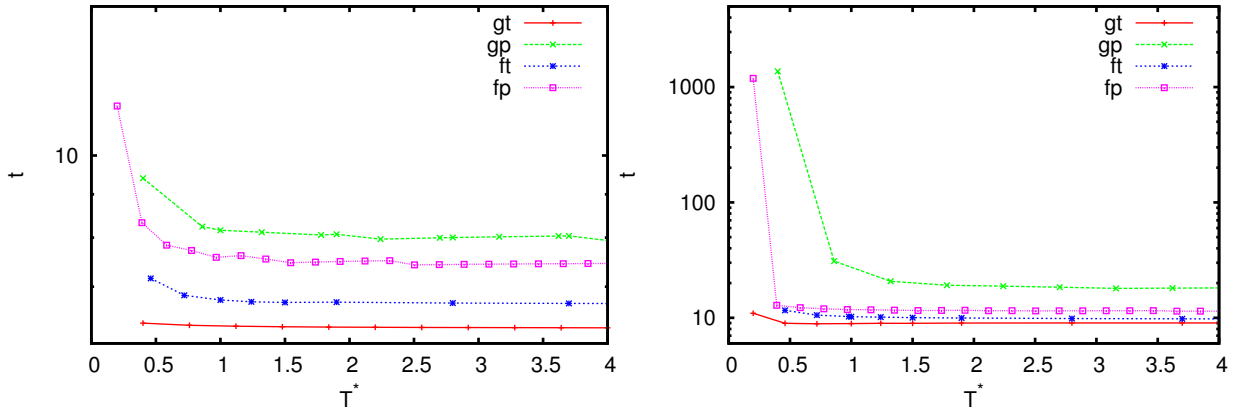


Figure 51: Translational spring constant  $t$  at constant reduced pressure  $p^* = 3$  (left) and  $p^* = 6$  (right) over the temperature  $T^*$  for the ordered triangular structure ('gt'), the ordered square structure ('ft') and the plastic triangular ('gp') and square structure ('fp').

The rotational mean square displacement  $\langle \theta^2 \rangle$  and the corresponding spring constant  $q$  depend mainly on the crystal structure (Fig. 52).

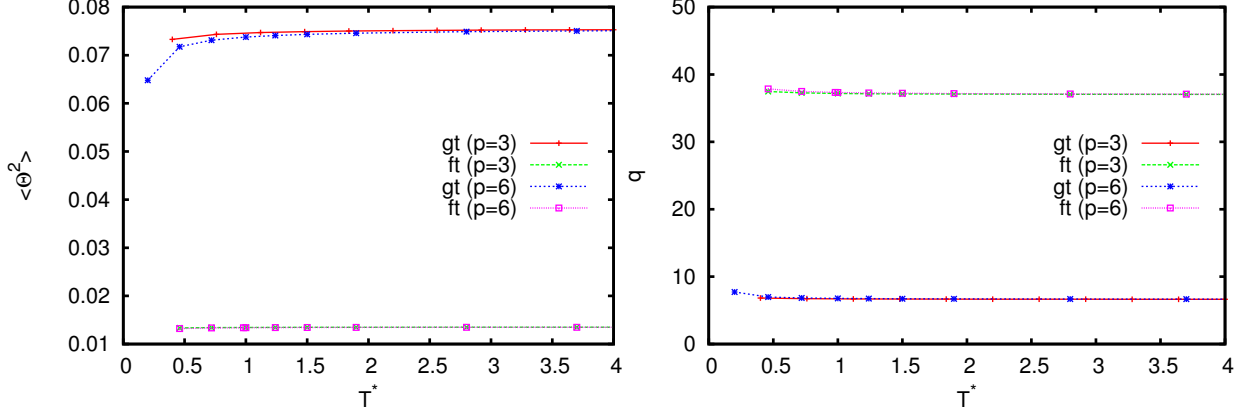


Figure 52: Mean squared displacement  $\langle \theta^2 \rangle$  (left) and corresponding spring constant  $q$  at constant reduced pressure  $p^* = 3$  and  $p^* = 6$  over the temperature  $T^*$  for the ordered triangular structure ('gt'), the ordered square structure ('ft') and the plastic triangular ('gp') and square structure ('fp').

For the determination of points of phase coexistence the chemical potential at constant pressure has to be calculated. As can be seen from Fig. 53 no phase transitions are observed for  $p^* = 3$  in the temperature range investigated since the chemical potential for the two plastic crystals is nearly parallel. At low temperatures the two ordered crystals could have a region of coexistence but this region can not be thoroughly investigated because it is very near the point where the formalism breaks down numerically.

At  $p^* = 6$  the plastic square structure is stable at high temperatures. As the temperature decreases below  $T^* \approx 0.5$  a transition to the plastic triangular structure is predicted by the SCP procedure. The chemical potential of the two ordered structures is nearly similar over the whole temperature range and indicates that they are meta-stable over the whole temperature range investigated.

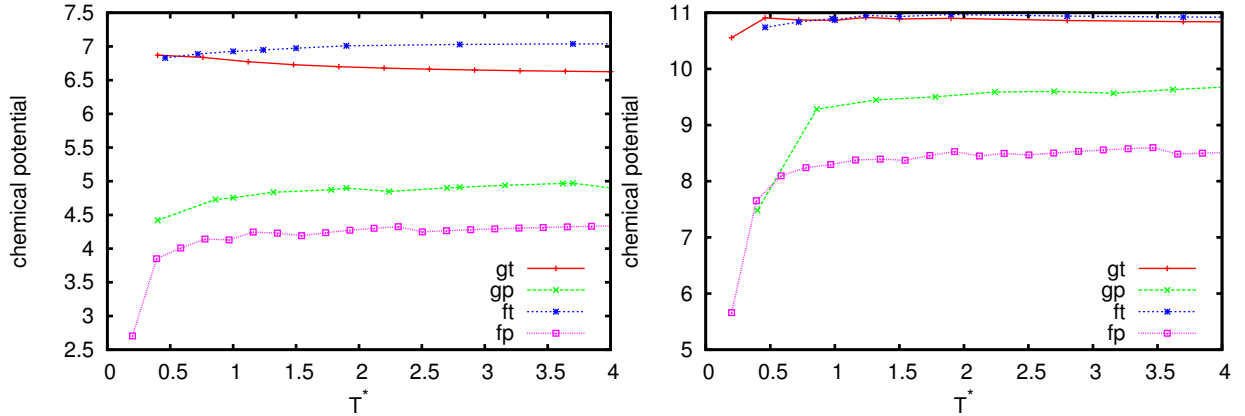


Figure 53: Chemical potential  $\mu$  [ $k_B T^*$ ] at constant reduced pressure  $p^* = 3$  (left) and  $p^* = 6$  (right) over the temperature  $T^*$  for the ordered triangular structure ('gt'), the ordered square structure ('ft') and the plastic triangular ('gp') and square structure ('fp').

## 6 SCP for inverse patchy colloids in three dimensions

The extension of the SCP theory to three dimension is conceptually complicated and numerically intensive. Therefore we restrict the formalism to two types of structures exploiting thereby the symmetry of those systems. In this section we study a face-centered cubic system (fcc) and a layered structure formed by IPCs.

The unit cell of the fcc structure is shown in Fig. 54. Since the distance between all the particles is of similar length only one translational spring constant  $t$  is necessary.



Figure 54: The unit cell of the investigated fcc-structure formed by spatial and orientational ordered IPCs is shown at a typical particle density (left) and at extremely large distances so that the orientation of the particles can be seen (right).

The layered structure consists of planes with a hexagonal structure which are aligned parallel to the  $(x, y)$ -plane (see Fig. 55). The particles in each of these planes are positioned as in the two-dimensional trigonal structure already studied in Sec. 5 (shown in the left panel of Fig. 32). For a regular planar structure two translational spring constants are needed, one within the plane,  $t_p$ , and one in the perpendicular  $z$ -direction,  $t_z$ . For the sake of generality we use two spring constants in the following.

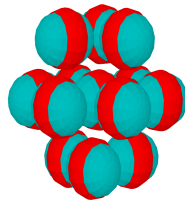


Figure 55: The unit cell of the layered structure formed by spatial and orientational ordered IPCs.

The additional degree of freedom of the spatial deviations can be simply added to the potential as an additional spring constant which is assumed to be independent of all the other spring constants.

Further, an additional degree of freedom for the rotations (for IPCs with two patches) has to be taken into account. Inclusion of this rotational degree is not as easy as for the additional translational degree of freedom due to the fact that the rotation axes of the particles within a given structure are difficult to guess; therefore possible inter-dependencies of the rotational degrees of freedom need to be taken into account.

These features render the method quite complicated; further, together with the translational

degrees of freedom five-dimensional integrals need to be performed which have made a full application of the approach too time-consuming for this thesis. Therefore, instead of investigating all degrees of freedoms at once we first study the translational degrees only, via a plastic structure (Sec. 6.1), then we discuss the influence of the rotational degrees separately (Sec. 6.2).

## 6.1 Plastic structure

The simplest three-dimensional structure formed by IPCs is a face-centered cubic (fcc) lattice with randomly oriented patches. The SCP approach is applied to this structure using the averaged potential  $\langle \varepsilon \rangle$  given in Equ. (68). Since only the translational degrees of freedom need to be included for plastic crystals the reference potential is chosen as

$$V_H(\mathbf{w}_i) = \sum_{i=1}^N [t_p(w_{x,i}^2 + w_{y,i}^2) + t_z w_{z,i}^2], \quad (70)$$

so that the  $h$  function is now defined by

$$\begin{aligned} h(\mathbf{w}_i) &= \frac{\int d\{\mathbf{w}_c\} \left[ e^{-\frac{1}{2}\langle v_{ij}(r) \rangle} - 1 \right] e^{-t_p w_{p,c}^2} e^{-t_z w_{z,c}^2}}{\int d\{\mathbf{w}_c\} e^{-t_p w_{p,c}^2} e^{-t_z w_{z,c}^2}} \\ &= -\frac{2t_p t_z}{\sqrt{\pi}} \int_0^\sigma dr r^2 \int_0^\pi d\theta \sin \theta e^{-t_p (W_p - r \sin \theta)^2} I_0'(2t_p r \sin \theta W_p) e^{-t_z (W_z - r \cos \theta)^2} + \\ &\quad + \frac{t_p t_z}{\sqrt{\pi}} \int_\sigma^{\sigma+\delta} dr r^2 \left[ e^{-\frac{1}{2}\langle \varepsilon \rangle(r)} - 1 \right] \int_0^\pi d\theta \sin \theta e^{-t_p (W_p - r \sin \theta)^2} I_0'(2t_p r \sin \theta W_p) e^{-t_z (W_z - r \cos \theta)^2}. \end{aligned} \quad (71)$$

Here we used spherical coordinates and  $W_p = \sqrt{W_x^2 + W_y^2}$ . Since the spherical Bessel function of the first kind behaves as  $I_0(x) \sim e^{+x}$  for large arguments  $x$ , we introduced the function  $I_0'(x) = I_0(x) \cdot e^{-x}$ .

Using the above  $h$ -function the coefficients of the potential,  $\gamma_p$  and  $\gamma_z$ , are defined analogously to Equ. (22). The self-consistency equation has to reflect the symmetry of the fcc crystal. Thus the coefficients should be equal:  $\gamma_p = \gamma_z = \gamma$  and only one mean squared displacement  $\langle w^2 \rangle$  is needed for the self-consistency equations. The sum of the average displacements  $\langle w^2 \rangle$  can be evaluated via

$$\begin{aligned} \langle w^2 \rangle &= \frac{1}{\mathcal{N}} \int_\nu dw_x dw_y dw_z (w_x^2 + w_y^2 + w_z^2) e^{-\gamma(w_x^2 + w_y^2 + w_z^2)} \\ &= \frac{3\sqrt{\pi} \operatorname{erf}(\sqrt{\gamma}a) - 2e^{-\gamma a^2} \sqrt{\gamma}a(2\gamma a^2 + 3)}{2\gamma(\sqrt{\pi} \operatorname{erf}(\sqrt{\gamma}a) - 2e^{-\gamma a^2} \sqrt{\gamma}a)}. \end{aligned} \quad (72)$$

Since the distances between the atoms are of comparable length in all three orthogonal directions, the Wigner-Seitz cell  $\nu$  was approximated by a sphere with radius  $a$  and the same volume as the actual Wigner-Seitz cell.

The updating of the spring constants,  $t_p$  and  $t_z$ , is realized via the self-consistency equation

$$t_p = t_z = \frac{3}{2\langle w^2 \rangle}. \quad (73)$$

### 6.1.1 Results for fcc structure

We have used the same system of IPCs as discussed in Ref. [7]; the particles have an opening angle of  $\gamma = 38.6^\circ$  and are slightly charged so that the total charge of one colloid is  $Z_{\text{tot}} = Z_c + 2Z_p = Z_c/11$ . The properties of the surrounding solvent are set by  $\kappa\sigma = 2$ . The particles have an interaction range of  $\delta = 0.25$ .

The total free energy  $f$  obtained via the SCP method for the fcc-structure formed by ordered IPCs is shown in Fig. 56 for different distances  $x$  between the particles and at different reduced temperatures  $T^*$ . For sufficiently large distances and high enough temperatures the approach performs well. However, as the temperature and/or the distance between the particles decreases, the spring constants start to oscillate so that no convergence could be achieved. At even smaller distances or lower temperatures the method does not work at all.

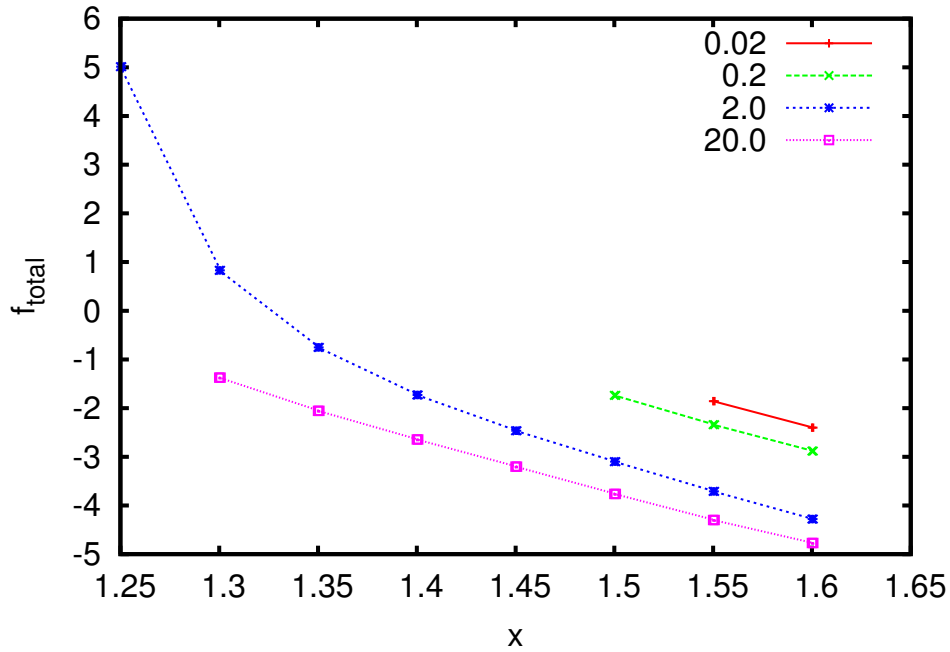


Figure 56: Free energy per particle  $f$  for the fcc crystal formed by IPCs over the distance  $x$  between the particles for different reduced temperatures  $T^*$  (as labeled).

One reason for this failure could be related to the fact that the numerical accuracy is not sufficient as the spring constant increases rapidly (see Fig. 57). As expected the particles become less and less mobile as their equilibrium distance decreases.

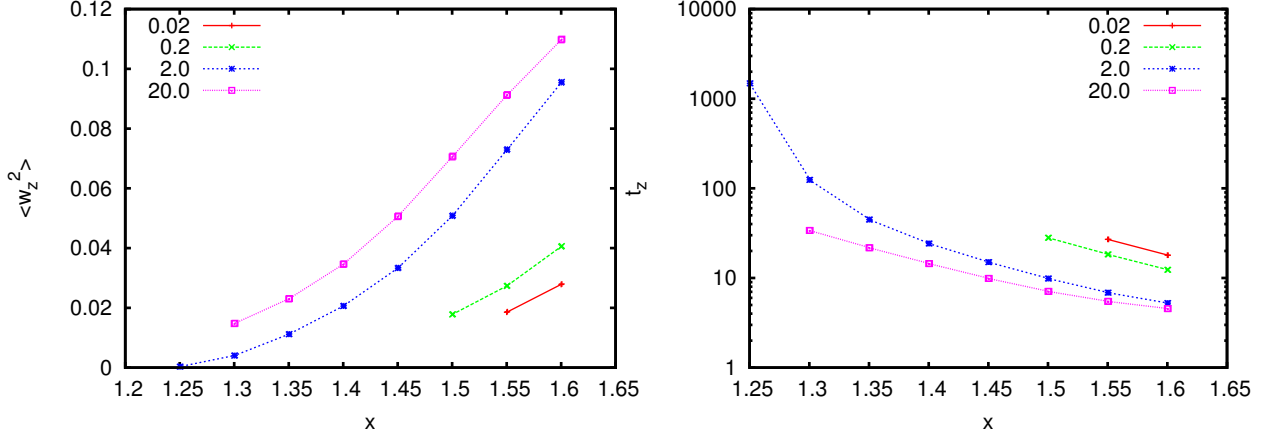


Figure 57: Mean squared displacements in  $z$  direction  $\langle w_z^2 \rangle$  (left) and spring constant  $t_z$  (right) over the distance  $x$  between the particles in a fcc crystal for different temperatures (as labeled). Due to the symmetry of the crystal  $\langle w_p^2 \rangle = 2 \langle w_z^2 \rangle$  and  $t_p = t_z$ .

To clarify the reasons for the numerical instability of the method, the self-consistency equation was further investigated. In Fig. 58 the spring constant,  $t_{\text{new}}$ , that results from an initial spring constant,  $t_{\text{old}}$ , is plotted. The colored curves give the change of the spring constant for different densities of the structure. The solution of the self-consistency equation is given by the intersection of the colored curves with the first median (black line). For  $T^* = 2$  only for distances  $x \gtrsim 1.24$  a solution exists while the positive curvature of the curves for higher densities prevent the convergence of the approach. From the curves at  $T^* = 10$  it becomes obvious why the procedure starts to oscillate between multiple solutions as the density decreases: here curves for distances  $1.20 \gtrsim x \gtrsim 1.19$  have two intersections with the first median (although due to the curvature only the lower intersection should be stable)

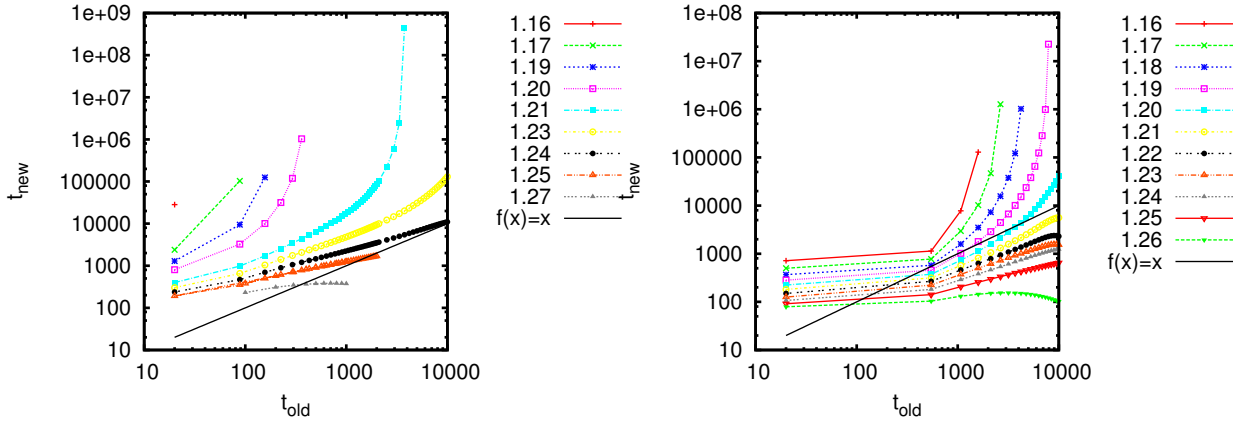


Figure 58: Illustration of the self-consistency equation: the spring constant  $t_{\text{new}}$  as a function of the input spring constant  $t_{\text{old}}$  for different distances  $x$  between the particles in a fcc structure formed by IPCs for  $T^* = 2$  (left) and  $T^* = 10$  (right). The solution of the self-consistency equation is given by the intersection of the colored curves with the first median (black line).

## 6.2 Angular SCP

As indicated by the results for the plastic fcc structure, particles are very immobile at large densities and/or low temperatures and thus very large spring constants occur. Since these large spring constants make the calculations very tricky and numerically instable, we decided to disregard in this Section the translational degrees of freedom and to focus solely on the influence of the angular degrees of freedom found in orientationally ordered crystal structures. We note that the translational and rotational degrees of freedom are coupled via the self-consistency equations, but we expect that the impact of the translational oscillations on the rotations are rather small.

In the following approximation we treat only the angular degrees of freedom of the structures. For the evaluation of the  $h$ -function the coordinate system is orientated so that the patches of the central particle are aligned along the  $x$ -axis. Therefore only rotation around the  $y$ - and  $z$ -axis need to be considered, we term the corresponding rotation angles  $\theta_z$  and  $\theta_p$ , respectively. Although this coordinate system is very handy for the calculation of the  $h$ -function of the system, it is not necessarily the eigensystem of the oscillations.

Thus we include an off-diagonal spring constant  $q_{pz}$  in the reference potential, namely

$$V_H(\theta_p^i, \theta_z^i) = \sum_{i=1}^N [q_p(\theta_p^i)^2 + q_z(\theta_z^i)^2 + 2q_{pz}\theta_p^i\theta_z^i]. \quad (74)$$

The  $h$ -function can be written as

$$h(\theta_p^i, \theta_z^i) = \frac{\int_{-\pi/2}^{\pi/2} d\theta_p \cos \theta_p \int_{-\pi}^{\pi} d\theta_z \left[ e^{-\frac{1}{2}E_{ic}(a, \theta_p, \theta_p^i, \theta_z, \theta_z^i)} - 1 \right] e^{-q_p\theta_p^2} e^{-q_z\theta_z^2} e^{-2q_{pz}\theta_p\theta_z}}{\int_{-\pi/2}^{\pi/2} d\theta_p \cos \theta_p \int_{-\pi}^{\pi} d\theta_z e^{-q_p\theta_p^2} e^{-q_z\theta_z^2} e^{-2q_{pz}\theta_p\theta_z}}. \quad (75)$$

The Taylor expansion of the potential contains also an off-diagonal term,

$$v_e(\theta_p, \theta_z) \approx \varepsilon + \beta_p\theta_p^2 + \beta_z\theta_z^2 + 2\beta_{pz}\theta_p\theta_z, \quad (76)$$

where the coefficients  $\beta_p$ ,  $\beta_z$  and  $\beta_{pz}$  are given by

$$\beta_p = -\frac{1}{2} \sum_i \partial_{\theta_p} \partial_{\theta_p} \ln[1 + h(\theta_p, \theta_z)]|_{\theta_p=0, \theta_z=0} \quad (77)$$

$$\beta_z = -\frac{1}{2} \sum_i \partial_{\theta_z} \partial_{\theta_z} \ln[1 + h(\theta_p, \theta_z)]|_{\theta_p=0, \theta_z=0} \quad (78)$$

$$\beta_{pz} = -\frac{1}{2} \sum_i \partial_{\theta_p} \partial_{\theta_z} \ln[1 + h(\theta_p, \theta_z)]|_{\theta_p=0, \theta_z=0}. \quad (79)$$

Thus the mean squared displacements  $\langle X^2 \rangle$  can be calculated via

$$\langle X^2 \rangle = \frac{\int_{-\phi_1}^{\phi_1} d\theta_p \cos \theta_p \int_{-\phi_2}^{\phi_2} d\theta_z X^2 e^{-\beta_p\theta_p^2} e^{-\beta_z\theta_z^2} e^{-2\beta_{pz}\theta_p\theta_z}}{\int_{-\phi_1}^{\phi_1} d\theta_p \cos \theta_p \int_{-\phi_2}^{\phi_2} d\theta_z e^{-\beta_p\theta_p^2} e^{-\beta_z\theta_z^2} e^{-2\beta_{pz}\theta_p\theta_z}}, \quad (80)$$

where  $X^2$  is either  $\theta_p^2$ ,  $\theta_z^2$  or  $\theta_p\theta_z$ .  $\phi_1$  and  $\phi_2$  are the angular wall factors constraining the rotational deviations within the plane and out of the plane, respectively. These integrals have to be calculated numerically.



For the derivation of the self-consistency equations we first write the spring constants in terms of a real, symmetric matrix  $Q_\theta$ ,

$$Q_\theta = \begin{pmatrix} q_p & q_{pz} \\ q_{pz} & q_z \end{pmatrix}, \quad (81)$$

the subscript  $\theta$  denotes that the matrix is given in the coordinate system described above defined by the vector  $\vec{\theta} = (\theta_p, \theta_z)$ . The matrix  $Q_\theta$  can be diagonalized using the transformation matrix  $U$ ,

$$Q_v = U^T Q_\theta U \quad \text{with} \quad Q_v = \begin{pmatrix} \lambda_1 & 0 \\ 0 & \lambda_2 \end{pmatrix}. \quad (82)$$

The eigenbasis of matrix  $Q$  is called  $v$ . The squares of the deviations are analogously collected into a matrix  $\vec{X}^2$ ,

$$\vec{X}^2 = \vec{\theta} \cdot \vec{\theta}^T = \begin{pmatrix} \theta_p^2 & \theta_p \theta_z \\ \theta_p \theta_z & \theta_z^2 \end{pmatrix}. \quad (83)$$

Using the rotation matrix  $U$  we find that the matrix of the mean squared displacements,  $\langle \vec{X}^2 \rangle$  has the same eigenbasis as the matrix  $Q_\theta$ , since

$$\vec{\theta} = U \vec{v} \rightarrow \langle \vec{X}^2 \rangle = \langle \vec{\theta} \cdot \vec{\theta}^T \rangle = U \langle \vec{v} \cdot \vec{v}^T \rangle U^T. \quad (84)$$

The matrix  $\langle \vec{v} \cdot \vec{v}^T \rangle$  is a diagonal matrix since the off-diagonal terms  $\langle v_1 v_2 \rangle$  are zero:

$$\langle v_1 v_2 \rangle = \frac{1}{\mathcal{N}} \int_{-\pi/2}^{\pi/2} dv_1 \cos v_1 \int_{-\pi}^{\pi} dv_2 (v_1 v_2) e^{-\lambda_1 v_1^2} e^{-\lambda_2 v_2^2} = 0. \quad (85)$$

The diagonal terms are given by

$$\langle v_1^2 \rangle (\lambda_1) = \frac{\int_0^{\pi/2} dv_1 \cos v_1 v_1^2 e^{-\lambda_1 v_1^2}}{\int_0^{\pi/2} dv_1 \cos v_1 e^{-\lambda_1 v_1^2}} = \frac{2\lambda_1 - 1}{4\lambda_1^2} + \frac{e^{-\pi^2 \lambda_1 / 4}}{\sqrt{\lambda_1^3 \pi} e^{-1/(4\lambda_1)} \left( \operatorname{erf}\left(\frac{\pi \lambda_1 - 1}{2\sqrt{\lambda_1}}\right) + \operatorname{erf}\left(\frac{\pi \lambda_1 + 1}{2\sqrt{\lambda_1}}\right) \right)} \quad (86)$$

$$\langle v_2^2 \rangle (\lambda_2) = \frac{\int_0^{\pi/2} dv_2 v_2^2 e^{-\lambda_2 v_2^2}}{\int_0^{\pi/2} dv_2 e^{-\lambda_2 v_2^2}} = \frac{1}{2\lambda_2} - \frac{e^{-\lambda_2 \pi^2} \sqrt{\pi}}{\sqrt{\lambda_2} \operatorname{erf}(\sqrt{\lambda_2} \pi)}. \quad (87)$$

The procedure is now the following: First the  $h$ -function is calculated using Equ. (75), assuming some starting values for  $q_p$ ,  $q_z$  and  $q_{pz}$ . Solving Equ. (77) for the coefficients  $\beta$ , the mean squared displacements  $\langle X^2 \rangle|_{\text{num}}$  are calculated via Equ. (80). In the next step,  $\langle X^2 \rangle|_{\text{num}}$  is diagonalized to obtain the diagonal elements  $\langle X_1^2 \rangle|_{\text{num}}$  and  $\langle X_2^2 \rangle|_{\text{num}}$  and the corresponding transformation matrix  $U$ . Then the new eigenvalues  $\lambda_1$  and  $\lambda_2$  are calculated, so that the  $v_1$  and  $v_2$  of Equ. (86) fulfill the following relations:

$$\langle v_1^2 \rangle (\lambda_1) = \langle X_1^2 \rangle|_{\text{num}} \quad (88)$$

$$\langle v_2^2 \rangle (\lambda_2) = \langle X_2^2 \rangle|_{\text{num}}. \quad (89)$$

The eigenvalues  $\lambda_1$  and  $\lambda_2$  are now the new diagonal values of  $Q_v$  in its eigenbasis. Transforming  $Q_v$  via  $Q_\theta = U^T Q_v U$  we obtain the new values for  $q_p$ ,  $q_z$  and  $q_{pz}$  which are then used to calculate the  $h$ -function anew.

The free energy per particle  $f$  consists only of a static and a rotational contribution, which can be evaluated via

$$f_{\text{static}} = \varepsilon \quad (90)$$

$$f_{\text{trans}} = 0 \quad (91)$$

$$f_{\text{rot}} = -\ln \left( \int_{\varphi_0} d\theta_p \cos \theta_p \int_{\varphi_0} d\theta_z e^{-\beta_p \theta_p^2 - \beta_z \theta_z^2 - 2\beta_{pz} \theta_p \theta_z} \right) - \ln(2\pi). \quad (92)$$

### 6.2.1 Fcc structure

The orientations of the particles in the investigated fcc-structure are chosen according to Ref. [7]; the unit cell used for the calculation is shown in Fig. 54.

In the following we will denote the coordinate system chosen for the orientation of the  $h$ -function ( $p, z$ )-system; the  $x$ -axis is aligned parallel to the orientation of the central particle, the 'plane' ( $p$ ) is formed by the  $x$ - and  $y$ -axis, the  $z$ -axis is orthogonal to this plane.

Since the initial axes chosen for the rotation of the particles are not necessarily the actual rotation axes, the angles  $\phi_0$  setting the angular wall potentials depend also on the direction. Actually, instead of independent restriction angles a rather complex restriction volume would be needed. The wall potential is however primarily introduced to prohibit unreasonably large rotations. Anyhow, the actual form of this integration boundary should not be of relevance since large rotation angles are suppressed exponentially with the weight of the spring constant. Thus the restriction angle is set in the ( $p, z$ )-coordinate system to  $\phi_0 = \pm 65^\circ$  for both directions, representing thereby the hexagonal structure of the fcc crystal (the additional  $5^\circ$  assure that the particles can actually rotate by  $\pm 60^\circ$ ).

The application of the SCP method to the fcc crystal shows that the actual rotation axes differ only slightly from the axes initially chosen for the integration of the  $h$ -function. As can be seen in Fig. 59 the angle  $\alpha$  between the actual and the chosen axes has a maximum of  $\alpha \approx 5^\circ$  in the investigated density and temperature range. Interestingly, the angle has several local maxima and minima as the distance  $x$  between the particles decreases. This is not surprising since the energy is calculated via the overlap volumes, which for 12 two-particle interactions is a quite complicated function of the distance.

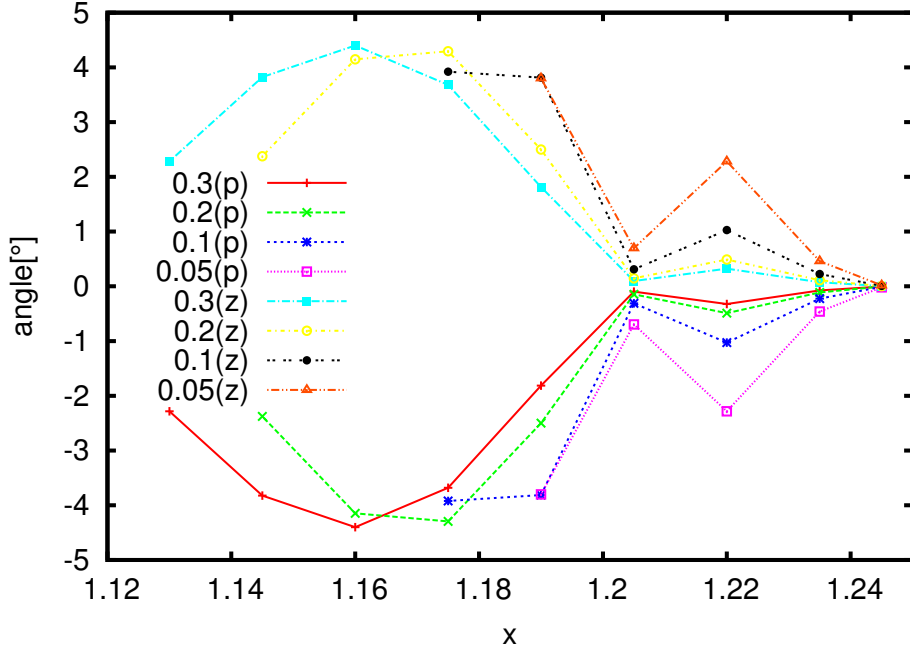


Figure 59: Angle between the actual rotation axes in an ordered fcc-crystal formed by IPCs and the  $(p, z)$ -coordinate system (detailed description in text) chosen due to the symmetry of the IPCs. The location of the minima and maxima with respect to the distance  $x$  between the particles depends on the reduced temperature  $T^*$  (as labeled). 'p' denotes the planar part of the coordinate system (combination of two axes), 'z' denotes the axis orthogonal to the 'p' part.

The mean squared displacements for the rotation  $\langle \theta_p^2 \rangle$ ,  $\langle \theta_z^2 \rangle$  and  $\langle \theta_p \theta_z \rangle$  around the different axes in the  $(p, z)$ -coordinate system are shown in Fig. 60. Since the basis nearly coincides with the eigen directions of the rotation, the off-diagonal oscillations are quite small. While  $\langle \theta_p^2 \rangle$  decreases as the distance between the particles decreases,  $\langle \theta_z^2 \rangle$  increases slightly.

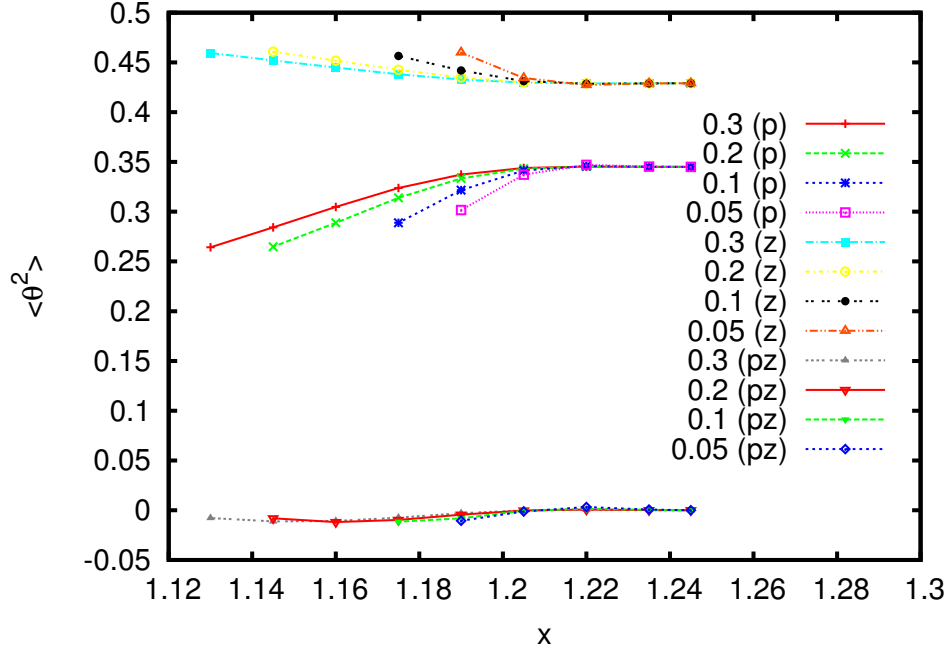


Figure 60: Mean squared displacements for the rotation,  $\langle \theta_p^2 \rangle$ ,  $\langle \theta_z^2 \rangle$  and  $\langle \theta_p \theta_z \rangle$ , with respect to the initial equilibrium system  $(p, z)$  as a function of the distance  $x$  between the particles in the fcc-structure formed by ordered IPCs. The reduced temperatures  $T^*$  are labeled on the right. 'p' denotes the mean squared displacement  $\langle \theta_p^2 \rangle$  which gives the rotation in the plane, 'z' denotes  $\langle \theta_z^2 \rangle$  of the rotation around the  $y$ -axis and 'pz' the off-diagonal rotation  $\langle \theta_p \theta_z \rangle$ .

The corresponding spring constants  $q_p$ ,  $q_z$  and  $q_{pz}$  are depicted in Fig. 61. Note that although the off-diagonal spring constant  $q_{pz}$  lies in the same range as  $q_z$ , the oscillations can be quite different since the off-diagonal spring constant is weighted with an additional factor two in the potential with respect to the diagonal spring constants.

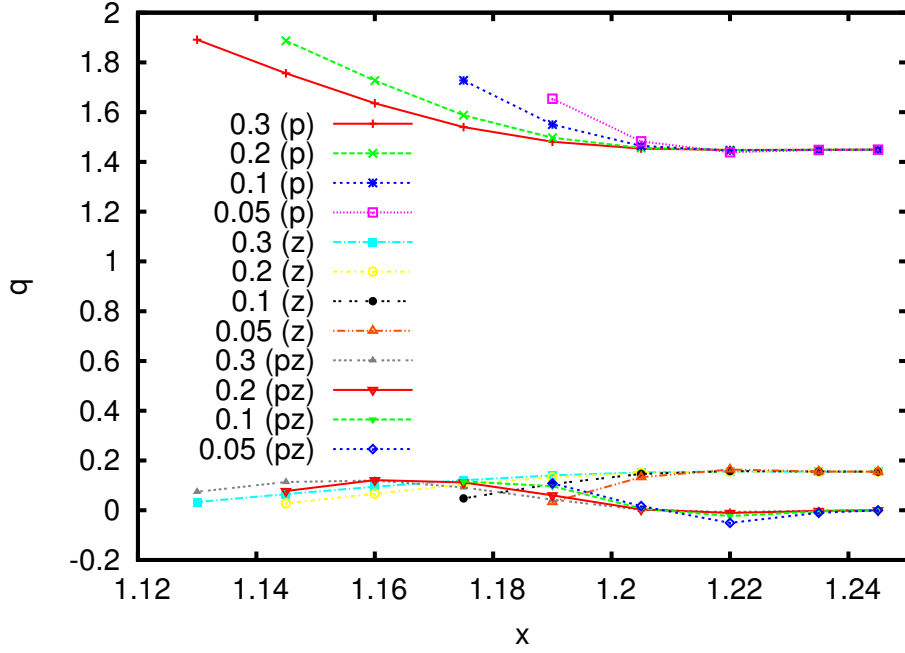


Figure 61: Spring constants for the rotation,  $q_p$ ,  $q_z$  and  $q_{pz}$ , with respect to the initial equilibrium system  $(p, z)$  as functions of the distance  $x$  between the particles in the fcc-structure formed by ordered IPCs. The reduced temperatures  $T^*$  are labeled on the right. 'p' denotes the spring constant  $q_p$  which gives the rotation in the plane, 'z' denotes  $q_z$  of the rotation around the  $y$ -axis and 'pz' the off-diagonal spring constant  $q_{pz}$ .

For completeness, the free energy per particle and its contributions obtained via this angular SCP method are shown in Fig. 62, Fig. 63 and Fig. 64. These functions have a negative curvature over wide parts of the investigated temperature and density range and are thus unphysical. However, this fact is not surprising since in this approach we disregarded the translational degrees of freedom which are responsible for the rapid increase of the free energy as the distance decreases.

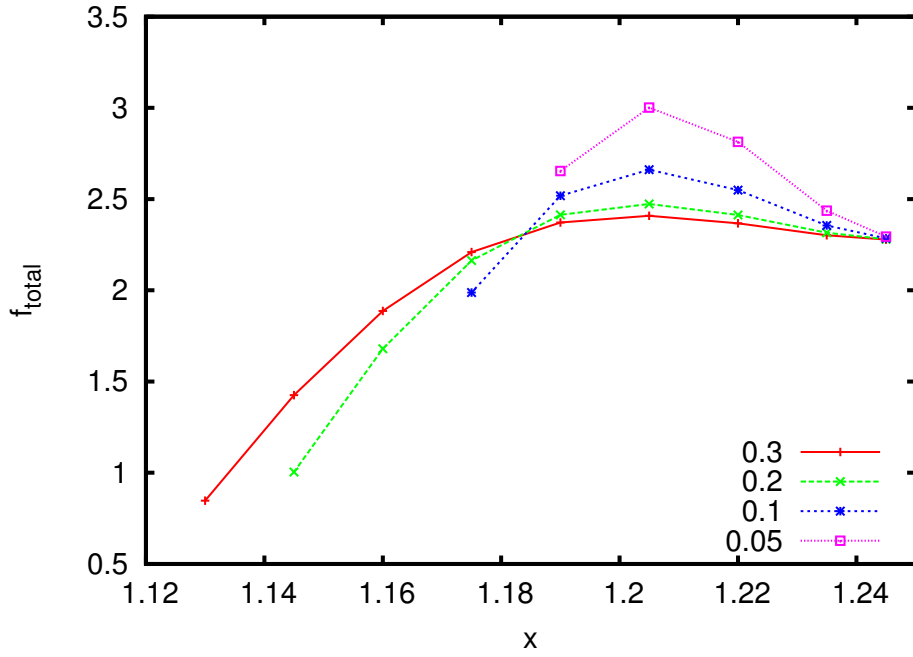


Figure 62: Total free energy per particle,  $f_{\text{total}}$ , over the distance  $x$  between the particles for the fcc-structure formed by ordered IPCs for different reduced temperatures  $T^*$  (as labeled). Note that in this angular SCP approach the translational degrees of freedom are disregarded.

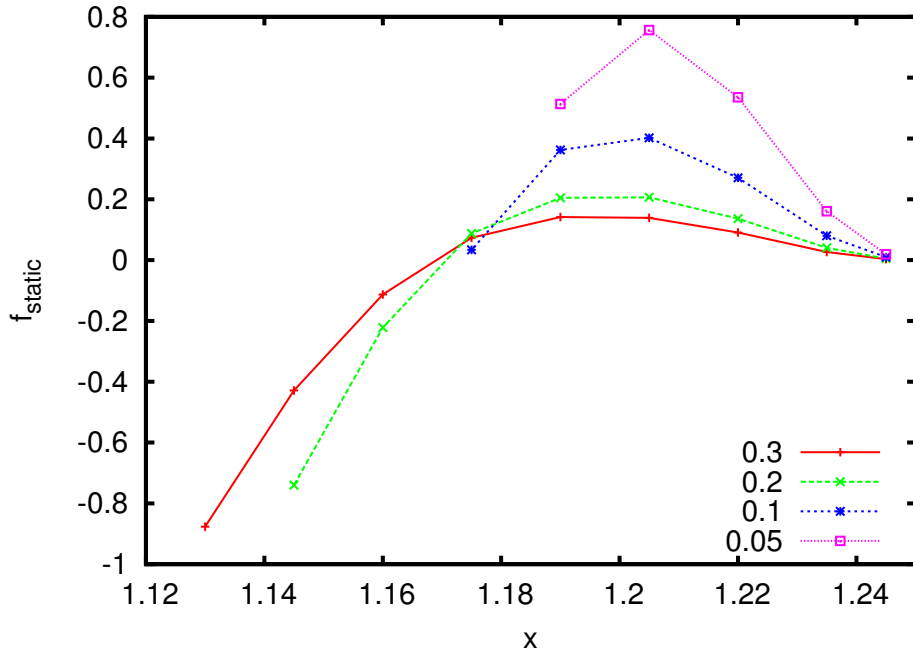


Figure 63: Static contribution,  $f_{\text{static}}$ , to the free energy per particle over the distance  $x$  between the particles for the fcc-structure formed by ordered IPCs for different reduced temperatures  $T^*$  (as labeled). Note that in this angular SCP approach the translational degrees of freedom are disregarded.

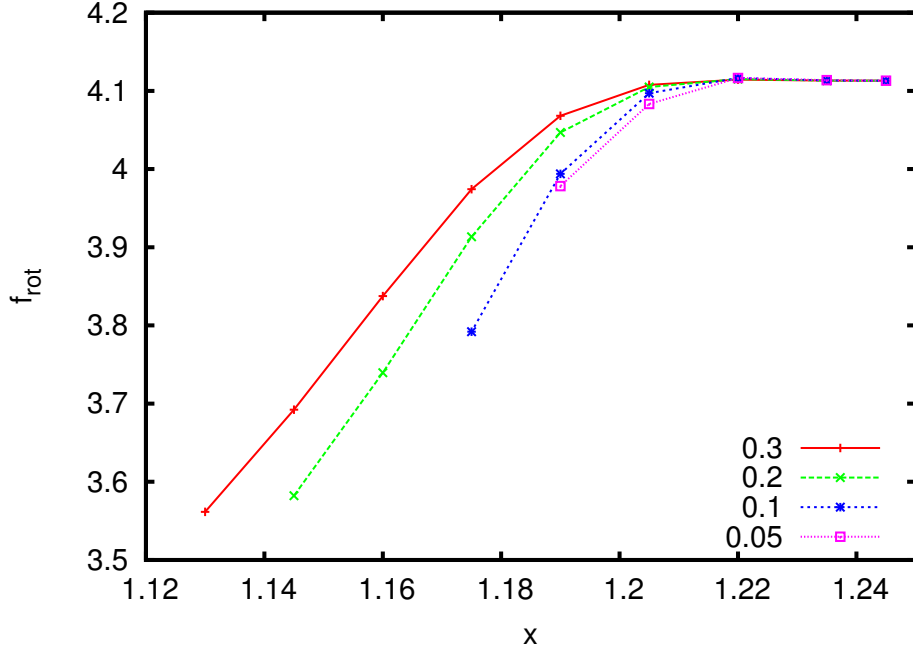
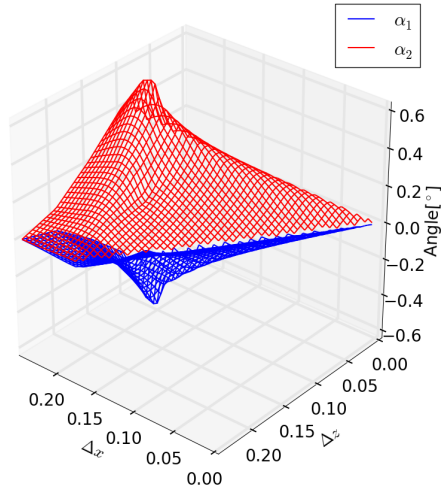


Figure 64: Rotational contribution,  $f_{\text{rot}}$ , to the free energy per particle over the distance  $x$  between the particles for the fcc-structure formed by ordered IPCs for different reduced temperatures  $T^*$  (as labeled). Note that in this angular SCP approach the translational degrees of freedom are disregarded.

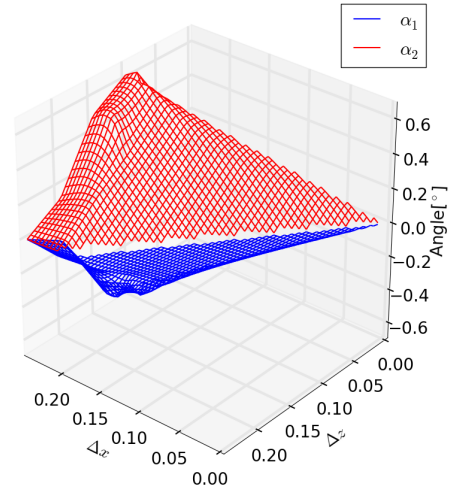
### 6.2.2 Layered structure

In this Section the results obtained for the layered structure with the angular SCP approach are presented. As can be seen from the unit cell (Fig. 55) the layered structure has two different characteristic distances: the distance  $\Delta x$  between two particles located in the same plane and the distance  $\Delta z$  between two particles positioned in different planes.

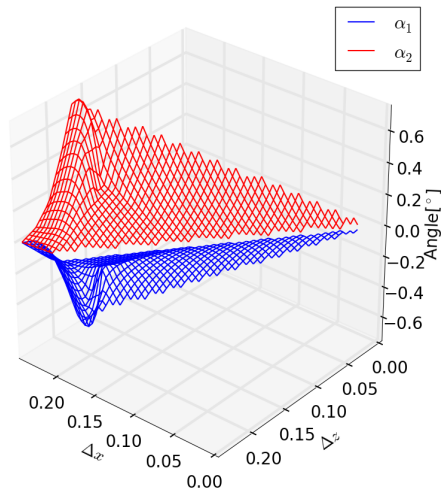
The rotation of the eigenbasis with respect to the  $(p, z)$ -basis used for the integration of the  $h$ -function is shown in Fig. 65.  $\alpha_1$  and  $\alpha_2$  give the rotation angle of the  $p$ -axes and the  $z$ -axis, respectively. Both angles depend strongly on the characteristic distances. As a general trend, we observe that the absolute values of the angles increase as  $\Delta z$  decreases (if  $\Delta x$  is constant). The dependence on  $\Delta x$  is more complicated, this was also observed for the fcc lattice. The absolute value of the rotation angle for the layered structure is nearly a magnitude smaller than the rotations observed for the fcc lattice. We note also, that the maximum of the coordinate rotation is shifted to larger  $\Delta z$  values as  $T^*$  decreases.



(a)  $T^* = 0.2$



(b)  $T^* = 0.1$

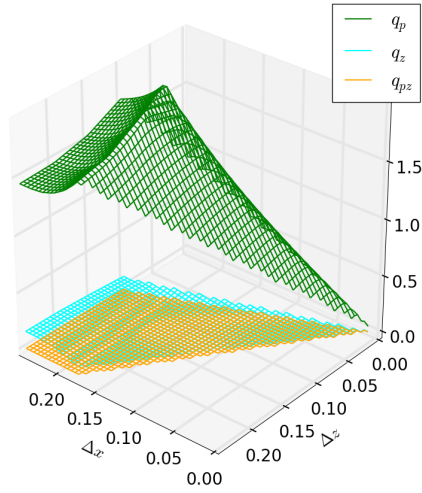


(c)  $T^* = 0.05$

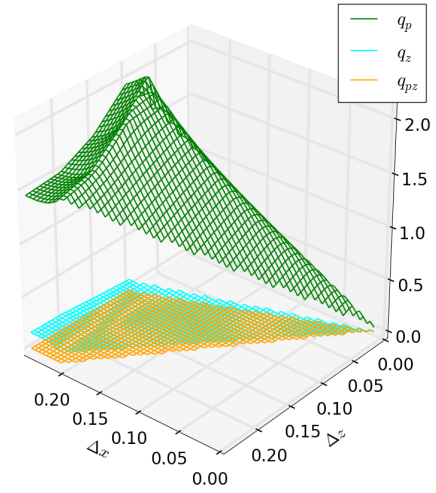
Figure 65: Angle between the actual rotation axes in an layered crystal formed by IPCs and the  $(p, z)$ -coordinate system (detailed description in text) chosen due to the symmetry of the IPCs. The angle depends on the distance of the particles within the plane,  $\Delta x$ , the distance of the planes,  $\Delta z$  and the reduced temperature  $T^*$ ; the panels correspond to (a)  $T^* = 0.2$ , (b)  $T^* = 0.1$ , (c)  $T^* = 0.05$ . 'p' denotes the planar part of the coordinate system (combination of two axes), 'z' denotes the axis orthogonal to the 'p' part.  $(\Delta x, \Delta z) = (0.0, 0.0)$  denotes the density where the particles are in contact.

The spring constants,  $q_p$ ,  $q_z$  and  $q_{pz}$  obtained for the layered structures show parallels to the ones obtained for the fcc lattice (see Fig. 66 and Fig. 61). In both cases,  $q_p$  is much larger than  $q_z$  and  $q_{pz}$  which have comparable values.

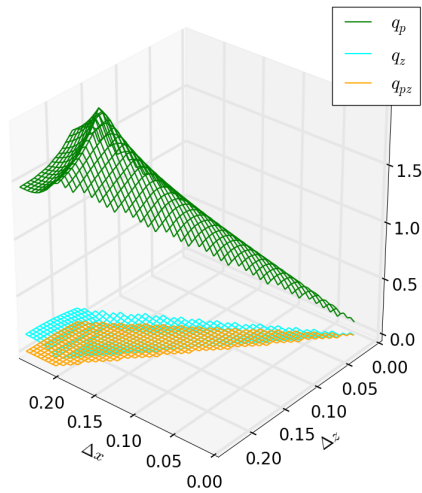




(a)  $T^* = 0.2$



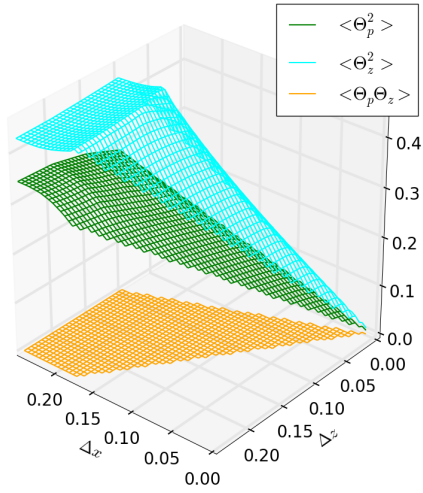
(b)  $T^* = 0.1$



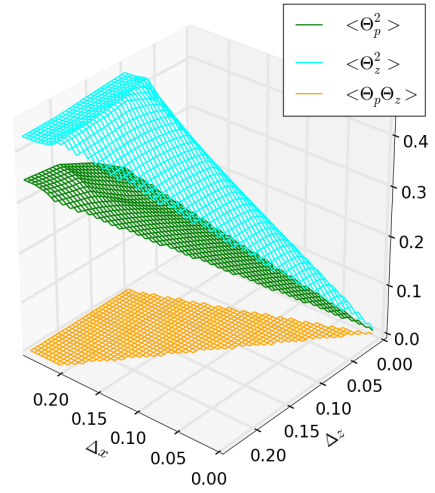
(c)  $T^* = 0.05$

Figure 66: Dependence of the spring constants  $q_p$ ,  $q_z$  and  $q_{pz}$ , on the characteristic distances  $\Delta x$  and  $\Delta z$  for three different reduced temperatures: (a)  $T^* = 0.2$ , (b)  $T^* = 0.1$  and (c)  $T^* = 0.05$ .  $(\Delta x, \Delta z) = (0.0, 0.0)$  denotes the density where the particles are in contact.

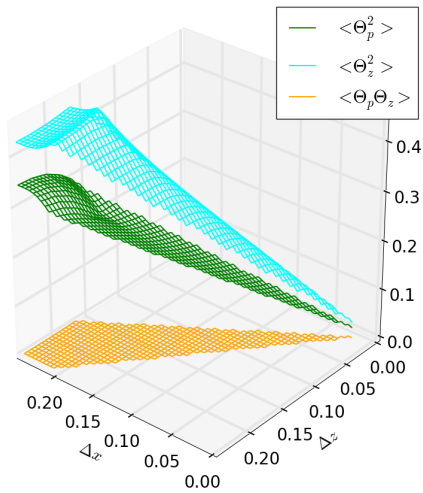
Although the values obtained for  $q_z$  and  $q_{pz}$  are comparable, the mean squared displacements are distinctly different (see Fig. 67). Since the  $(p, z)$ -system nearly coincides with the eigenbasis of the system,  $\langle \theta_p \theta_z \rangle \approx 0$ . Although,  $q_p$  is larger than  $q_z$  the corresponding mean squared displacement  $\langle \theta_p^2 \rangle$  is smaller than  $\langle \theta_z^2 \rangle$ .



(a)  $T^* = 0.2$



(b)  $T^* = 0.1$



(c)  $T^* = 0.05$

Figure 67: Dependence of the mean squared displacements,  $\langle \theta_p^2 \rangle$ ,  $\langle \theta_z^2 \rangle$  and  $\langle \theta_p \theta_z \rangle$ , on the characteristic distances  $\Delta x$  and  $\Delta z$  for three different reduced temperatures: (a)  $T^* = 0.2$ , (b)  $T^* = 0.1$  and (c)  $T^* = 0.05$ .  $(\Delta x, \Delta z) = (0.0, 0.0)$  denotes the density where the particles are in contact.

## 7 Conclusion

In this thesis, the thermodynamic properties of crystal structures formed by two types of patchy particles in two- and three-dimensions were investigated. For this purpose we extended the SCP method introduced in Refs. [4, 5] for hard spheres and Janus particles to inverse patchy particles (ICPs).

First we applied the SCP theory to two-dimensional crystals formed by Janus particles in Sec. 4. Janus particles are simple hard-sphere based particles with an orientationally dependent interaction. They have a heterogeneous surface where a large part of the surface does not interact with other particles and only small regions of the surface ('patches') attract each other. This attraction is modeled via a simple step-function. As already investigated in Ref. [5], particles self-assemble in a wide range of structures depending on the extension of the patch. We investigated a zigzag, a trimer and a plastic structure that are observed for particles with an intermediate patch angle.

The results for Janus particles confirm to a great extent the phase diagram described in Ref. [5]. We obtain the same values for the phase transitions at the two investigated temperatures as in [5]. Only the coexistence of the meta-stable phases is, according to our results, not solely dependent on the structure but also on the numerical implementation.

In the next step, we extended the SCP method to the more complex interactions of IPCs (Sec. 5). The method was tested by applying it to two-dimensional candidate structures described in [6], i.e. a triangular and a square structure. The free energy of the system was obtained via the SCP method for a large temperature and density range and exhibits a reasonable behavior.

The technique was also applied to two plastic structures, which are obtained by assuming the same positions of the particles as for the ordered structures but orienting the particles randomly. Here a possible phase transition was identified in the square plastic structure. We did, however, not investigate this transition any further, since on the one hand not all structures involved in this transition were known and on the other hand we are primarily interested in three-dimensional structures.

The simplest three-dimensional structure formed by IPCs is a plastic face-centered cubic (fcc) lattice, which has already been widely investigated, e.g. in Ref. [7]. In Sec. 6.1 we showed that the SCP method leads in principle to meaningful results. However, a bottle neck of this method is the self-consistency equation which cannot be met for all initial spring constants. For the plastic fcc structure only a certain temperature and density range works fine while at lower temperatures and higher densities no solution can be found using the SCP method with the self-consistency equation used in this thesis.

In Sec. 6.2 the influence of the rotational degrees of freedom on the mean squared displacements was investigated. For this we disregarded the translational degrees of freedom and derived a formalism which includes only the rotational deviations. It was applied to two ordered structures, a fcc lattice formed by ordered IPCs and a layered structure according to Ref. [18]. Since now two axes of rotation exist, which are a priori not known, the theory was extended to allow also self-consistent changes of these axes.

We derived the oscillation frequencies in the different directions and obtained the eigenbasis of the oscillations. Taking the symmetry of the particles into account, the initial rotation axes were chosen in the two directions orthogonal to the patch direction. The simulations showed that only small deviations of about  $5^\circ$  (for the fcc structure) and about  $0.6^\circ$  (for the layered lattice) from the axes around those initial axes directions occur. The free energies of the structure were also obtained, they are however not comparable for different structures since the translational oscillations have not been included.

Calculations including the translational as well as the rotational degrees of freedom would of course be quite interesting. Using the SCP theory, this aim is however not easily achieved since it involves an immense computational effort combined with severe numerical problems since the stability range of this self-consistent theory can be very small for dense structures.

Therefore, it seems more promising to extend this work by either comparing structures with different orientational ordering but the same positions of the particles, or by trying to combine two calculations of the same structure, one where only the spatial and one where only the rotational degrees of freedom are included. This combination is however not straight-forward since the translational and rotational degrees of freedom are by construction linked via the self-consistency equations.

## References

- [1] A. B. Pawar and I. Kretzschmar. *Langmuir*, 24:355, 2008.
- [2] Christina-Maria Niedermayer. Synthesis of inverse patchy particles. Master's thesis, University of Natural Resources and Life Sciences, Vienna, 2014.
- [3] D. Frenkel and B. Smit. *Understanding Molecular Simulations*. Academic Press, 2002.
- [4] M. Fixman. *J. Chem. Phys.*, 54:3270, 1969.
- [5] H. Shin and K. S. Schweizer. *Soft Matter*, 10:262, 2014.
- [6] E. Bianchi, C. N. Likos, and G. Kahl. *NanoLetters*, 14:3412, 2014.
- [7] E. Noya, I. Kolovos, G. Doppelbauer, G. Kahl, and E. Bianchi. *Soft Matter*, 10:8464, 2014.
- [8] C. N. Likos, R. Blaak, and A. Wynveen. *J. Phys.: Condens. Matter*, 20:494221, 2008.
- [9] R. Blaak and C. N. Likos. *J. Phys.: Condens. Matter*, 24:322101, 2012.
- [10] C. N. Likos E. Bianchi and G. Kahl. *ACS Nano*, 7:4647, 2013.
- [11] C. N. Likos E. Bianchi and G. Kahl. *ACS Nano*, 14:3412, 2014.
- [12] P. Debye and E. Hückel. *Physikalische Zeitschrift*, 24:185, 1923.
- [13] E. Bianchi, G. Kahl, and C. N. Likos. *Soft Matter*, 7:8313, 2011.
- [14] H. Shin and K. S. Schweizer. *J. Chem. Phys.*, 138:084510, 2013.
- [15] M. Fixman. *J. Chem. Phys.*, 45:785, 1966.
- [16] M. Abramowitz and I. Stegun. *Handbook of Mathematical Functions with Formulas, Graphs and Mathematical Tables*. Dover Publications, 1964.
- [17] F. Schwabl. *Statistische Mechanik*. Springer, 2006.
- [18] E. Bianchi G. Doppelbauer, E. Noya and G. Kahl. *Soft Matter*, 8:7768, 2012.
- [19] J. D. Hunter. Matplotlib: A 2d graphics environment. *Computing In Science & Engineering*, 9(3):90–95, 2007.

## Acknowledgements

I would like to thank my supervisor Gerhard Kahl for suggesting this highly interesting topic to me and for letting me explore it widely independently while at the same time giving advice whenever I had a problem.

Also, I would like to thank Emanuela Bianchi for her patience in explaining things to me although she herself was short on time.

Of course I would also like to thank the whole soft matter theory group of the TU Vienna for welcoming me; especially to Emanuela Bianchi, Silvano Ferrari, Moritz Antlanger, Marta Montes Saralegui and Dieter Schwanzner for the nice atmosphere (and often delicious pizza scent) in our office.

I acknowledge the use of the python based matplotlib [19] for the generation of some figures.